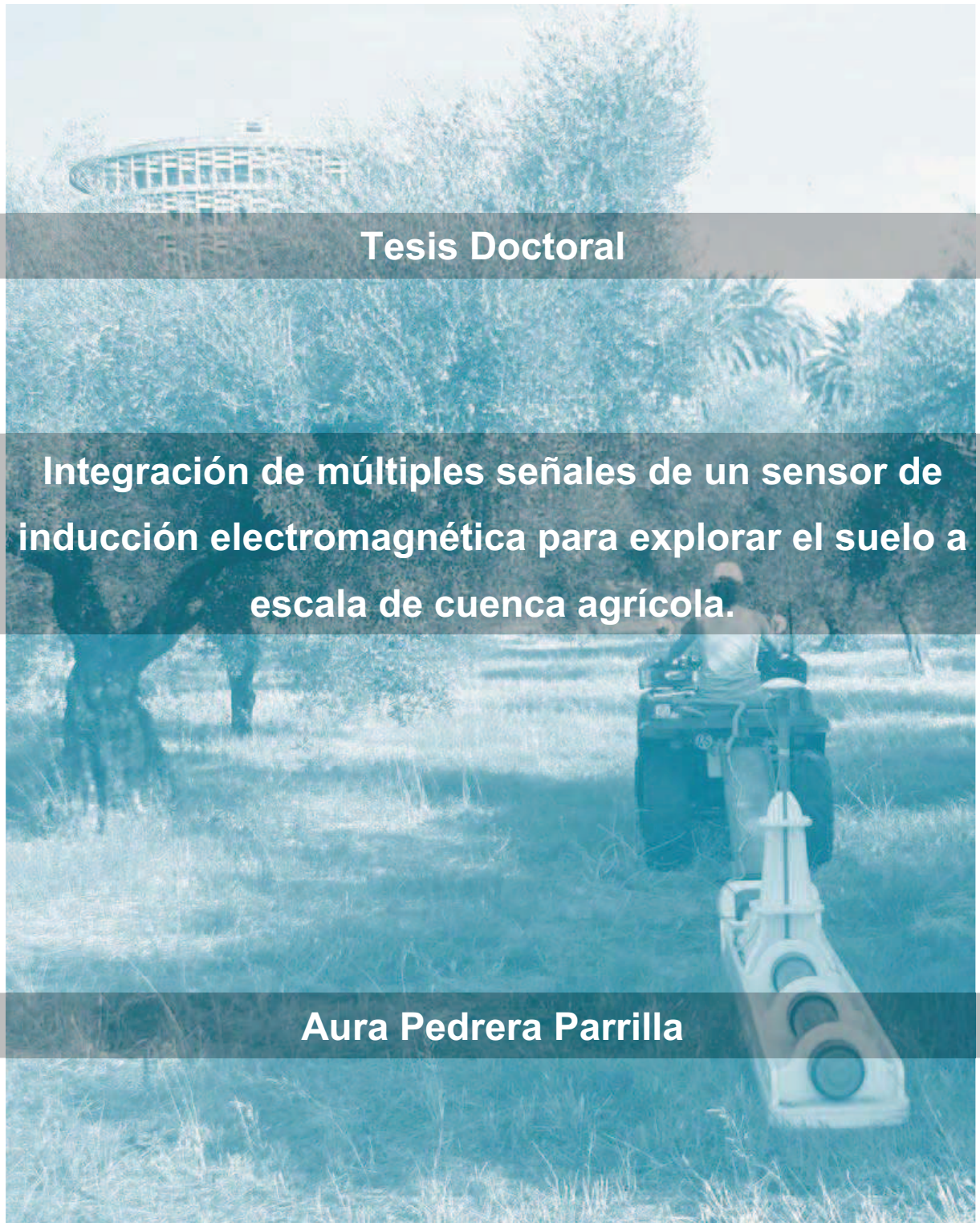

Tesis Doctoral

Integración de múltiples señales de un sensor de inducción electromagnética para explorar el suelo a escala de cuenca agrícola.

Aura Pedrera Parrilla

Octubre 2014

TITULO: *Integración de múltiples señales de un sensor de inducción electromagnética para explorar el suelo a escala de cuenca agrícola*

AUTOR: *Aura Pedrera Parrilla*

Campus de Rabanales
Ctra. Nacional IV, Km. 396 A
14071 Córdoba

www.uco.es/publicaciones
publicaciones@uco.es

Universidad de Córdoba

Departamento de Agronomía

Programa de Doctorado

Dinámica de Flujos Biogeoquímicos y su Aplicación

Línea de Investigación

Análisis de Procesos Hidrológicos e Hidráulicos y sus Aplicaciones Ambientales

Tesis Doctoral

Integración de múltiples señales de sensores geofísicos para explorar el suelo a escala de cuenca agrícola

Autora

Dª. Aura Pedrera Parrilla

Dirigida por

Dr. D. Juan Vicente Giráldez Cervera

Dr. D. Karl Vanderlinden

Córdoba, Octubre de 2014

Universidad de Córdoba

Departamento de Agronomía

UNIVERSIDAD D CÓRDOBA

Programa de Doctorado

Dinámica de Flujos Biogeoquímicos y su Aplicación

Línea de Investigación

Análisis de Procesos Hidrológicos e Hidráulicos y sus Aplicaciones Ambientales

Tesis Doctoral

Integración de múltiples señales de sensores geofísicos para explorar el suelo a escala de cuenca agrícola

Tesis doctoral presentada por D.ª Aura Pedrera Parrilla, en satisfacción de los requisitos necesarios para optar al grado de Doctora Ingeniera Agrónoma con mención internacional y con indicios de calidad, dirigida por los Drs. D. Juan Vicente Giráldez Cervera, de la Universidad de Córdoba, y D. Karl Vanderlinden, del Instituto de Investigación y Formación Agraria y Pesquera de la Junta de Andalucía.

Los directores

La doctoranda

Juan V. Giráldez Cervera

Karl Vanderlinden

Aura Pedrera Parrilla

Córdoba, Octubre de 2014

Título de la tesis: Integración de múltiples señales de sensores geofísicos para explorar el suelo a escala de cuenca agrícola

Doctorando: Aura Pedrera Parrilla

Informe razonado de los directores de la tesis

D. Juan Vicente Giráldez Cervera y D. Karl Vanderlinden, directores de la tesis, informan que la doctoranda ha desarrollado los objetivos previstos compartiendo su formación con la investigación, completándola con dos estancias en un centro extranjero, la Universiteit Gent, Gante (de Agosto a Septiembre de 2011, y en Junio de 2014) y con una publicación en la revista "Plant and Soil" de Springer (DOI 10.1007/s11104-014-2207-5). La tesis se presenta separada en capítulos, los cuales se encuentran en fase de envío o ya publicados en revista indexadas.

Por todo ello, se autoriza la presentación de esta tesis doctoral.

Los directores

Juan V. Giráldez Cervera

Karl Vanderlinden

Córdoba, 14 de Octubre de 2014

"Toda aventura comienza con un sí"

-Autor desconocido-

A Beatriz…

A mis padres, hermana y familia…

A la agricultura…

LIST OF CONTENTS

LIST OF FIGURES

LIST OF TABLES

LIST OF ABBREVIATIONS

Chapter 1

apparent magnetic susceptibility (MSa)
DUALEM-21S (D21S)
apparent electrical conductivity (ECa)
electromagnetic induction (EMI)
frequency domain electromagnetic (FDEM)
global positioning systems (GPS)
ground penetration radar (GPR)
low induction numbers (LIN)
proximal soil sensors (PSS)
soil water content (SWC)

Chapter 2

apparent electrical conductivity (ECa)
bulk density (ρ_b)
cation exchange capacity (CEC)
cumulative response (C)
depth of exploration (DOE)
DUALEM-21S (D21S)
electrical conductivity (EC)
electromagnetic induction (EMI)
horizontal (H)
apparent magnetic susceptibility (MSa)
organic matter (OM)
perpendicular (P)
polyethylene (PE)
polyvinyl chloride (PVC)
primary field (Hp)
receiver coils (Rx)
relative response (R)
secondary field (Hs)
soil water content (SWC)
transmitter coil (Tx)

Chapter 3

analysis of variance (ANOVA)

apparent electrical conductivity (ECa)

coefficient of variation (CV)

depth of exploration (DOE)

electromagnetic induction (EMI)

elevation (Z)

horizontal co-planar coil orientation (H)

kurtosis coefficient (KC)

organic matter (OM)

perpendicular coil orientation (P)

canopy area (CA)

skewness coefficient (SC)

soil water content (SWC)

standard deviation (s)

wetness index (WI)

Chapter 4

apparent electrical conductivity (ECa)

apparent electrical conductivity measured under dry soil conditions (ECa-d)

coefficient of correlation (r)

depth of exploration (DOE)

ECa increment (ΔECa)

electromagnetic induction (EMI)

horizontal co-planar coil orientation (H)

perpendicular coil orientation (P)

apparent electrical conductivity measured under wet soil conditions (ECa-w)

proximal soil sensing (PSS)

relative nugget effect (RNE)

soil water content (SWC)

soil water content measured under dry soil conditions (SWC-d)

soil water content measured under wet soil conditions (SWC-w)

SWC increment (ΔSWC)

Chapter 5

all-terrain vehicle (ATV)

analysis of variance (ANOVA)
apparent electrical conductivity (ECa)
bulk density (ρ_b)
coefficient of determination (R^2)
coefficient of variation (CV)
correlation coefficient (R)
depth of exploration (DOE)
electrical conductivity ($EC_{1:5}$)
electromagnetic induction (EMI)
first principal component (PC1)
horizontal-coplanar coil orientation (H)
intercoil distance (*ID*, m)
mean temperature (Tm)
organic matter (OM)
perpendicular coil orientation (P)
precipitation (P,mm)
principal component analysis (PCA)
root mean squared error (RMSE)
soil water content (SWC)

Chapter 6

apparent electrical conductivity (ECa)
coefficients of determination (R^2)
correlation coefficient (R)
depth of exploration (DOE)
horizontal co-planar coil orientation (H)
mean absolute bias error (MABE)
mean relative difference (MRD)
mean temperature (Tm, ºC)
perpendicular coil orientation (P)
polyvinyl chloride (PVC)
precipitation (P, mm)
root mean squared error (RMSE)
soil water content (SWC)
standard deviation of the relative differences (SDRD)
temporal stability analysis (TSA)

AGRADECIMIENTOS

Los trabajos incluidos en esta Tesis Doctoral han sido subvencionados por el IFAPA (Consejería de Agricultura, Pesca y Desarrollo Rural de la Junta de Andalucía) y financiados por el Programa Operativo del Fondo Social Europeo 2007-2013 de Andalucía, en el ámbito de actuación prioritario del Eje 3 (Aumento y mejora del capital humano), en un 80%.

Quiero agradecer en primer lugar a mis directores de tesis, Dr. Karl Vanderlinden y Dr. Juan Vicente Giráldez Cervera, por su dedicación y paciencia. Junto a ellos me he adentrado en la investigación y gracias a ellos ahora dispongo de numerosas herramientas para desenvolverme en este ámbito.

Gracias al IFAPA por concederme la beca que me ha permitido desarrollar esta tesis doctoral, y gracias al IFAPA Centro Las Torres-Tomejil por haberme proporcionado medios para realizar mi trabajo.

Gracias a mis compañeros (Alberto Jardúo, Esther Rodríguez, Jorge García, Manuel Morón y Miguel Ángel Fernández) por su esfuerzo y voluntad de realizar un gran trabajo de campo y laboratorio, y conseguir además amenizar esas largas jornadas en tierras de olivares. Gracias también a los dueños de las parcelas por ponerlas a nuestros servicios para realizar los diferentes estudios.
Gracias al Orbit Group de la Universidad de Gante por esos tres meses de estancia, no sólo por los conocimientos que me transmitieron sino por su grata acogida, especialmente a Dr. Marc Van Meirvenne (Head of department), Ellen Van De Vijver y Philippe De Smedt.
Gracias a Dr. Eric C. Brevik y a Dr. Yakov A. Pachesky por su revisión y valoración de la tesis.

Gracias a mis compañeros de máster, especialmente a Rafael Pimentel, por estar ahí ya sea desde Granada, Holanda o China. Agradecer también a mis compañeros de tesis por su ayuda incondicional, Antonio Espejo y Javier Arriaga, y gracias a mis compañeros de departamento, en especial a Almudena Hernández, María Antonia Molina y María Luisa Prados. Y cómo no, agradecer al grupo “Precarios Las Torres” y al grupo “The Koalas” por

Y gracias a mi gran familia por seguir acompañándome durante estos cuatro años a pesar de encontrarme lejos de Córdoba, gracias también a Mati y Ale, y gracias a Beatriz Tudela por su paciencia y por su incalculable apoyo en el período final de la tesis que es el más difícil.

A todos vosotros y a muchos otros que no por no nombrarlos dejan de ocupar un espacio en mis recuerdos, gracias porque sin vosotros esta tesis no hubiese sido posible.

RESUMEN

La caracterización de las propiedades físico-químicas del suelo y de su variabilidad espacio-temporal a escala de parcela o micro-cuenca es de gran importancia para numerosas aplicaciones agrícolas y ambientales que persiguen un mejor uso de los recursos suelo y agua. El carácter no destructivo de la medición y la posibilidad de realizar un gran número de mediciones abarcando grandes superficies hacen que los métodos geofísicos, tales como la inducción electromagnética (IE), sean una herramienta muy útil para llevar a cabo dicha caracterización a escala de parcela o cuenca agrícola. Para estudios con mayor detalle y con una extensión espacial más reducida se cuenta con técnicas como el geo-radar y la tomografía de resistividad eléctrica.

Las técnicas geofísicas tienen en común que sus respuestas dependen de las características electromagnéticas del subsuelo sobre el que se realizan mediciones. Dichas características, tales como la conductividad eléctrica aparente (CEa) o su inverso, la resistividad eléctrica, dependen directamente de las propiedades del suelo, entre los que se pueden destacar la conductividad eléctrica de la solución del suelo (salinidad), el contenido de arcilla (textura), la fracción gruesa, el contenido de agua, la profundidad del suelo y la temperatura.

El objetivo general de esta tesis es explorar los posibles usos y la integración de múltiples señales de un sensor geofísico para estimar propiedades del suelo así como para interpretar y explicar procesos relacionados con el manejo de suelo y agua en olivar tradicional, utilizando medidas intensivas de CEa, humedad y propiedades del suelo en varias cuencas de olivar de secano.

La tesis se divide en 7 capítulos. El capítulo 1 incluye la motivación, el objetivo general y los objetivos específicos. El capítulo 2 describe las cuencas de estudio, el procedimiento de muestreo de la humedad y las propiedades del suelo, además de la configuración móvil diseñada para medir CEa en parcelas de olivar tradicional, así como el post-procesado y análisis de los datos de CEa. Los capítulos 3-6 se centran en conocer la influencia de la humedad y las propiedades del suelo en las medidas de CEa. En el capítulo 3 se delimitan áreas que presentan diferente desarrollo arbóreo en base a la CEa y se identifican las relaciones subyacentes entre las propiedades del suelo en la CEa que ocasionan ese desarrollo irregular de los árboles. En el capítulo 4 se caracteriza y compara la variabilidad espacial de la CEa en condiciones de suelo seco y húmedo, además dicha variabilidad se interpreta en términos de la humedad y el contenido en arcilla del suelo. El capítulo 5 se basa en las relaciones espaciales y temporales de la humedad y las propiedades del suelo (*p.e.* contenido en arcilla) con la CEa medidas en varias ocasiones dentro de un mismo año hidrológico. El capítulo 6 ofrece un paso más en el estudio

de estabilidad temporal dado que delimita en términos de CEa diferentes zonas en la parcela, en lugar de localizaciones puntuales, que presentan la propiedad de representar el contenido medio de humedad de la parcela. Por último, el capítulo 7 presenta las conclusiones y las futuras líneas de investigación.

Esta tesis pone de manifiesto la utilidad de realizar muestreos intensivos de CEa en campo (*p.e.* olivar tradicional), los cuales tras los procesos de filtrado e interpolación, permiten mejorar el conocimiento sobre la variabilidad espacial del suelo a escala de parcela. El análisis conjunto de los datos de CEa, humedad y de las propiedades del suelo, permiten entender de forma más precisa dicha variabilidad, así como determinar aquellos factores que influyen en mayor medida a la señal de CEa. Además de la posibilidad de diferenciar zonas de la parcela con diferentes comportamientos, y de ofrecer la posibilidad de conocer la dinámica de la humedad del suelo. Todo esto permite desarrollar estrategias de manejo del suelo y los recursos hídricos más sostenibles. Los capítulos 3 y 5 delimitan varias áreas con comportamientos diferenciados, en cada una de las dos cuencas de olivar estudiadas. En ambos casos se observó que la variabilidad espacial de la CEa está relacionada con la variación espacial de las propiedades del suelo. En el capítulo 4 se observa una estructura espacial de la CEa muy similar en condiciones tanto de suelo seco como húmedo, y una mejor relación entre la CEa y la arcilla en condiciones húmedas. Por último en el capítulo 6 se delimitan aquellas zonas de la parcela que incluyen relaciones lineales entre los valores puntuales de CEa y los valores medios espaciales de CEa de diferentes muestreos, que son representativas de aquellas zonas que presentan estabilidad temporal de la humedad del suelo.

SUMMARY

The characterization of soil physical and chemical properties and their spatio-temporal variability at the field or micro-catchment scale is of prime importance for many agricultural and environmental applications that seek a better use of soil and water resources. The non-destructive nature of the measurements and the possibility to survey large areas in short time intervals make geophysical methods, such as electromagnetic induction (EMI), a useful tool to perform this characterization. For more detailed studies and at smaller spatial extents, other techniques such as geo-radar and electrical resistivity tomography exist.
The response of geophysical sensors depends on the electromagnetic characteristics of the soil on which measurements are made. Geophysical measurements, such as apparent electrical conductivity (ECa) or its inverse, electrical resistivity, depend directly on soil properties such as electrical conductivity of the soil solution (salinity), clay content (texture), stone content, soil water content, soil depth and soil temperature.

The general aim of this thesis was to explore the use and integration of multiple geophysical signals to estimate soil properties and interpret and explain related processes within the context of applications related with soil and water management in olive orchards.

The thesis is organized in 7 chapters. Chapter 1 includes the motivation, and the overall and specific objectives. Chapter 2 describes the study catchments, the sampling procedures for soil moisture and soil properties, the mobile platform designed to measure ECa in traditional olive orchards, and the post-processing and analysis methods of the measured ECa data. Chapters 3-6 focus on the influence of soil moisture and soil properties on ECa measurements. In Chapter 3 areas with differing tree development could be delimited based on ECa data, and the underlying relationships between soil properties and ECa causing this irregular development were identified. In Chapter 4 the spatial variability of ECa under dry and wet soil conditions was characterized and compared, and interpreted in terms of soil moisture and clay content. Chapter 5 is based on the spatial and temporal relationships between soil moisture and soil properties (eg clay content) and ECa, which was repeatedly measured during a hydrological year. Chapter 6 provides a next step in the temporal stability analysis of soil moisture, using CEa to identify representative areas, rather than point locations, for estimating the average moisture content of the field. Finally, Chapter 7 presents the conclusions and future lines of research.

This thesis demonstrates the usefulness of intensive field CEa measurements in traditional olive orchards, providing a better understanding of the soil spatial variability at the field scale. The combined information of spatially distributed ECa, soil moisture and soil properties, is

necessary to understand more precisely this variability, and to determine the factors that most influence ECa. Furthermore, it offers the possibility to delineate areas in the field with a differing hydrological behavior and contrasting soil moisture dynamics. This knowledge allows us to develop better soil and water management strategies. In chapters 3 to 5 several areas were identified the studied olive orchards. The spatial variability of ECa was related with the spatial variation of soil properties. In chapter 4 the spatial structure of ECa was very similar under, both, dry and wet soil conditions. A better relationship between ECa and clay content under wet conditions was observed. Finally, in chapter 6, areas with linear relationships between point ECa values and their spatial average were delimited. These areas showed better temporal soil moisture stability characteristics and were found to be representative for the estimation of the filed-average soil moisture.

Chapter 1. Introduction

The characterization of the physico-chemical soil properties and their spatio-temporal variability at field or micro-catchment scale is of prime importance for many agricultural and environmental applications that seek a better use of soil and water resources. In the Mediterranean regions, the scarcity of water prevents the potential development of olive trees, which is the most representative agricultural system in the region, resulting in suboptimal olive yields. This problem is often aggravated by the need to implement soil conserving management systems in order to reduce erosion and other threats for soil quality and health. Knowledge of soil water content patterns at the field scale, and soil water variability at basin scales, allows the implementation of more efficient agricultural techniques in terms of water and soil management, and crop yield.

The non-destructive nature of geophysical measurement methods and the possibility to achieve large numbers of measurements over large areas make electromagnetic induction (EMI) a useful technique to characterize soils and related processes at field or agricultural catchment scales. For detailed studies, with a smaller spatial extent, techniques such as ground penetrating radar (GPR) or electrical resistivity tomography are available. The response from geophysical techniques generally depends on the electromagnetic characteristics of the soil on which measurements are made. These characteristics, such as electrical apparent conductivity (ECa) or its inverse, electrical resistivity, directly depend on soil properties, among which we can highlight the electrical conductivity of the soil solution (salinity), clay content, the water content, and temperature.

1.1 Proximal Soil Sensors (PSS)

Soil is a complex medium produced by rock weathering, in which micro- and macro-organisms interact with the underlying partially decomposed inorganic material conditioned by the climate and surface topography. Under such circumstances soil shows a strong spatial variability (Sommer, 2006). Soil physical, chemical and biological properties affect crop production, which demands a complete understanding of their variability. Soils have been traditionally characterized by field sampling and posterior laboratory analysis. This procedure is generally expensive and time consuming and can therefore only provide a limited coverage of the studied area. Advanced technologies, such as remote and proximal sensors, allows the acquisition of

data in real time, at larger scales, with better resolution and lower costs than those of classical or conventional methods. Proximal sensors operating close to the soil surface were developed to quantify soil mechanical, chemical and physical properties with a high resolution and frequency of measurement, as well as with lower cost. These sensors can be classified either into: 1) active or passive methods, depending on whether a signal is emitted or not; 2) invasive, contact or non-contact methods; or 3) according to the measured physical property, *e.g*. apparent electrical conductivity estimated by electromagnetic induction, electrical resistivity evaluated by direct current injection, soil magnetic properties detected by magnetometers, and dielectric permittivity discontinuities measured by GPR. There is a large variety of PSS, from which the fittest one for specific purposes can be chosen. Adamchuck et al. (2004) summarized the measurement methods for the most used soil sensor systems mounted in a mobile configuration ("on-the-go sensors"): 1) Electrical and electromagnetic sensors, 2) Optical and radiometric sensors, 3) Mechanical sensors, 4) Acoustic sensors, 5) Pneumatic sensors, and 6) Electrochemical sensors. Electrical resistivity and electrical conductivity sensors are the most widely used on-the-go sensors.

1.1.1 Electromagnetic Induction Sensors

During the last decades, the most popular proximal soil sensing technique is probably electromagnetic induction (Adamchuk et al. 2004; Doolittle et al. 2014). With the introduction of global positioning systems (GPS) in agriculture during the nineties EMI sensors have been integrated into mobile configurations which enable "on-the-go" measurement of ECa. Electrical conductivity based sensors are preferred for such configurations because they do not need physical contact between the soil and the sensor. Viscarra-Rossel et al. (2011) reviewed the different proximal soil sensing techniques, in particular the electromagnetic induction which is used in this work. EMI sensors work in the time or frequency domain. Frequency domain electromagnetic (FDEM) sensors operate at low frequencies (9 KHz) and are considered active geophysical methods that dissipate energy "volumetrically", where the physical property is measured over a bulk soil volume. They do not require direct soil contact, operate at low induction numbers (LIN), and measure the apparent electrical conductivity or the apparent magnetic susceptibility (MSa).The measured electrical conductivity is called "apparent" because it is the integrated electrical conductivity of all the soil constituents within in certain soil volume (Friedman, 2005).

Operation at LIN implies that the charge of any loop of the magnetic field is completely independent of the charge flowing in another loop as they are not magnetically coupled. The induction number (β) is defined as the ratio between the inter-coil spacing (*s*, m) and the skin

depth (ς) (McNeill, 1980), at which the magnetic field has been attenuated to 1/*e* from its original value at the soil surface.

$$\beta = \frac{s}{\varsigma} = \frac{s}{\sqrt{2/(\sigma \cdot \omega \cdot \mu_0)}} \tag{1.1}$$

Where σ is the soil electrical conductivity, $\omega = 2\pi f$, f the frequency and μ_0 the permeability of the free space ($4\pi \cdot 10^{(-7)}$ H^{-1})

Since EMI sensors are designed to ensure an induction number much lower than unity, σ becomes proportional to the ratio of the induced secondary magnetic field (*Hs*, H m^{-1}) to the primary magnetic field (*Hp*, H m^{-1}).

$$\sigma = \frac{4}{\omega \mu_0 s^2} \cdot \frac{H_s}{H_p} \tag{1.2}$$

The main disadvantage of the EMI sensors is that the value of the electrical parameter is affected by the overall physical and chemical soil properties. Therefore it is necessary to determine which soil property affects most the sensor's response to correctly interpret the measured data. One of main advantages of EMI is that it does not require direct soil contact, improving the easiness of operation, the relatively low cost of operation and the high surveying speed in relation to other methods such as electrical resistivity, which needs direct soil-electrode contact. In addition, EMI sensors enable data collection under dry and wet soil conditions, and even when vegetation is present. EMI sensors also allow high resolution surveys by adding a GPS, a data logger and a sled, made of non-metallic components and are designed to operate the sensor as close as possible to soil surface while preventing lateral rotation of the sensor, towed by an all-terrain vehicle. On rough terrain the sensor can tilt laterally. This movement can add noise to the measurements, although only the magnetic susceptibility (MSa) signal was observed to be very sensitive to this movement (Simpson, 2009). Such mobile configurations are capable of providing several thousands of geo-referenced measurements in one hour, from which ECa maps can be produced using geo-statistical interpolation techniques.

1.2 Soil Apparent Electrical conductivity

EMI sensors such as is the DUALEM-21S (D21S) use electrical circuits to determine the ability of soil to conduct electrical charge. As soil becomes part of a circuit, measured electrical parameters will be influenced by soil physical and chemical properties. The differences in these soil properties allow soil-variability to be measured (Mc Neill, 1980). Rhoades et al. (1989) and Rhoades and Corwin (1991) modeled the apparent electrical conductivity of soils considering three parallel and alternatives pathways to conduct charge: 1) through alternant layers of soil

particles and solution via exchangeable cations associated with clay minerals, 2) through continuous liquid solutions (soil water and salts), and 3) through solid soil particles (made of quartz, feldspars, mica…) on direct contact. In the absence of dissolved salts in the second pathway, soil conductivity, texture and water content are correlated. Most of the elements of soils and rocks have a low electrical conductivity, and the conduction of electric charge will mostly be electrolytic and will take place in the pores and cracks of soils and rocks. Under non-saline conditions ECa depends only on soil water content and temperature (Keller and Frischknecht, 1966). However, it is indirectly affected also by other factors such as porosity, concentration of dissolved electrolytes, amount and composition of colloids, and rock type. Spatial variations of MSa are usually seen in the first few centimeters of soil and can be caused by microbial action during soil forming processes, excavation or soil movement, fire or long flooding periods. Moist soil conditions are generally considered the most suitable for data acquisition with an EMI sensor. In water limited environments, such as those of the Mediterranean climate, these conditions are not met during long periods along the hydrological year, apparently limiting the potential use of the method in these regions to specific periods.

1.2.1 Soil properties affecting ECa

ECa measurements depend on several soil properties such as soil water content, soil temperature, soil salinity and soil texture. Vitharana et al. (2006) classified the factors that influence electrolytic conduction in four categories: the nature and arrangement of the soil constituents (characterized by clay content and pore geometry), soil water content (SWC), pore fluid composition (characterized by the dissolved ions) and soil temperature. Clay particles usually have negative charges at their surface, due to isomorphic substitution within its structure caused by weathering processes. Therefore higher clay contents are associated with higher ECa values. Pore geometry is also important. Macro-pores are less conductive than meso-or micro-pores, while better pore connectivity increases electrical conductivity. Given that one of the pathways (Rhoades et al. 1989) is entirely related to soil water, an increase in soil water content will increase conductivity, but under saline conditions, ions dissolved in the soil are clearly the most related variable to soil conductivity. The more ions move into the soil solution the higher the current flow is. Also temperature affects conductivity. Higher temperatures cause higher ECa, as a result of the increased viscosity of the liquid and the increased ion mobility. Sheets and Hendrickx (1995) proposed an equation to refer ECa measurements to a standard temperature of 25 ºC, ECa_{25}:

$$ECa_{25} = ECa \cdot \left[0.447 + 1.403 \cdot e^{-T/26.815} \right] \tag{1.3}$$

where T is temperature in ºC.

Rhoades et al. (1976) and Nadler and Frenkel (1980) found that soils with higher water contents showed greater ECa, possibly hampering the straightforward use of ECa data to delimit homogeneous soil units. In low conductive environments with a small variation in soil ECa, a general understanding of the soil water content in surveyed areas is advisable, because soil moisture can have potentially a significant effect on soil ECa (Brevik et al. 2006). Usefulness of soil ECa measurements to map soil properties is elusive due to complex interactions between ECa and soil physical and chemical properties (clay content, SWC, temperature, organic matter (OM)...) (Sheets and Hendrickx, 1995). Therefore, the relationship between ECa and a stable soil property (*e.g*. clay content) is determined by the status of the soil transient properties (*e.g*. SWC). The transient nature of soil water can complicate the interpretation of the ECa variability, altering the relationship between ECa and a soil property, even during a single survey. This is one of the reasons why it is generally recommended to perform ECa surveys under wet soil conditions, preferably near field capacity. Due to the contribution of SWC and other transient soil properties it is generally not possible to establish general calibration equations that relate ECa to time-invariant properties such as clay or sand contents.

1.2.2 ECa as auxiliary information

Historically ECa was first used to evaluate soil salinity (Rhoades et al. 1976). Nowadays it has emerged as an effective and rapid indicator of soil variability and soil productivity (Kitchen et al. 1999), to support decisions on soil management. In the context of precision agriculture many authors discriminated different management zones based on EMI surveys (Johnson et al. 2003; Corwin and Lesch, 2003; Vitharana et al. 2006). Hydrological subsurface patterns (moisture content, soil texture, water holding capacity, …) in watersheds have been shown to be related with the spatial distribution of vegetation (Robinson et al. 2008, 2010; Atwell et al. 2013, Pedrera-Parrilla et al. 2014) and could be identified using EMI sensors (Abdu et al. 2008; Martinez et al. 2010, 2012; Robinson et al. 2012). Given that soil water content and soil texture are two properties affecting agricultural production, from all the emergent technologies, ECa measuring devices allows, in a simple and economic way, to measure soil variability (James et al. 2003).

From high resolution geophysical explorations carried out with a D21S in conjunction with direct topsoil observations at a limited number of control points, Saey (2008) reconstructed the paleo-topography of an area within the loess belt in Belgium. In addition the sensor has been used to detect metal archaeological structures and war remnants such as unexploded bombs and bomb shells (De Smedt et al. 2011). Geophysical explorations are useful to map the spatial

distribution of sub-superficial textural soil properties and to identify subtle changes of these properties in small watersheds. Abdu et al. (2008) explored the identification of hydrologically active locations and mapped the subsurface textural pattern and the soil water holding capacity in a 38-ha watershed. Field measured ECa is useful, as auxiliary information, to characterize the spatial distribution of time-invariant soil properties such as the OM (Martínez et al. 2009), but also transient properties such as SWC (Martínez et al. 2012).

1.3 Aim and objectives

The general aim of this thesis was to explore the use and integration of multiple geophysical signals to estimate soil properties and interpret and explain related processes within the context of applications related with soil and water management in olive orchards.

To reach this general objective, the following specific objectives were put forward:

1) Develop a rugged mobile platform to perform surveys with the Dualem-21S on rough and sloping terrain in traditional olive orchards.

2) Characterize and compare the spatial variability of ECa surveys under dry and wet soil conditions, and interpret this variability in terms of clay and soil water content.

3) Analyze and explain the observed spatial relationship between ECa and tree development in an olive orchard, and identify the causal relationships between ECa and soil properties.

4) Characterize the effect of soil water content on the relationship between ECa and time-invariant soil properties.

5) Identify representative areas for field-average soil water content estimation using ECa surveys in an olive orchard.

REFERENCES

Abdu H., Robinson D.A., Seyfried M., Jones S.B. 2008. Geophysical imaging of watershed subsurface patterns and prediction of soil texture and water holding capacity. Water Resour. Res., doi:10.1029/2008WR007043.

Adamchuk V.I., Hummel J.W., Morgan M.T., Upadhyaya S.K. 2004. On-the-go soil sensors for precision agriculture. Comp. Electron. Agric. 44:71-91.

Atwell M.M., Wuddivira M., Gobin J., Robinson D.A. 2013. Edaphic controls on Sedge invasion in a tropical wetland assessed with electromagnetic induction. Soil Sci Soc Am. J 77:1865-1874.

Brevik E.C., Fenton T.E., Lazari A. 2006. Soil electrical conductivity as a function of soil water content and implications for soil mapping. Prec. Agric. 7:393-404.

Corwin D.L., Lesch S.M. 2003. Application of soil electrical conductivity to precision agriculture: Theory, principle and guidelines. Agron. J. 95:455-471.

De Smedt P., Van Meirvenne M., Davies N.S., Bats M., Saey T., De Reu J., Meerschman E., Gelorini V., Zwertvaegher A, Antrop M., Bourgeois J., De Maeyer P, Finke P.A., Verniers J., Crombé P. 2013. A multidisciplinary approach to reconstructing Late Glacial and Early Holocene landscapes. J Archaeol Sci 40:1260-1267.

Doolittle J.A., Brevik C. 2014. The use of electromagnetic induction techniques in soils studies. Geoderma 223-225, 33-45.

Friedman S.P. 2005. Soil properties influencing apparent electrical conductivity: a review. Comput. Electron. Agric. 46:45–70.

James I.T., Waine T.W., Bradley R.I., Taylor J.C., Godwin R.J. 2003. Determination of soil type boundaries using electromagnetic induction scanning techniques. Biosyst Eng 86:421–430.

Johnson C.K., Mortensen D.A., Wienhold B.J., Shanahan J.F., Doran J.W. 2003. Site-specific management zones based on soil electrical conductivity in a semiarid cropping system. Agron. J. 95:303-315.

Keller G.V., Frischknecht F.C. 1966. Electrical Mehotds in Geophysical Prospection. International Series of Monographs in Electromagnetic Waves Volume 10. Pergamon Press, London.

Kitchen N.R., Sudduth K.A., Drummond S.T. 1999. Soil electrical conductivity as a crop productivity measure for claypan soils. J. Prod. Agric. 12:607-617.

Martínez G., Vanderlinden K., Espejo A.J., Giráldez J.V., Muriel J.L. 2010. Field-scale soil moisture pattern mapping using electromagnetic induction. Vadose Zone J. 9:871-881.

Martínez G., Vanderlinden K., Pachepsky Y., Espejo A.J., Giráldez J.V. 2012. Estimating topsoil water content of clay soils with data from time-lapse electrical conductivity surveys. Soil Sci. 177:369-376.

Martinez G., Vanderlinden K., Ordoñez R., Muriel J.L. 2009. Can apparent electrical conductivity improve the spatial characterization of soil organic carbon? Vadose Zone J., 8:586-593.

McNeill J.D. 1980. Electromagnetic terrain conductivity measurement at low induction numbers.Technical Note TN-6.Geonics Limited, Missisauga, Ontario, Canada.

Nadler A., Frenkel H. 1980. Determination of soil solution electrical conductivity from bulk soil electrical conductivity measurements by the four electrode method. Soil Sci. Soc. Am. J. 44:1216-1221.

Pedrera-Parrilla A., Martínez G, Espejo-Pérez A.J., Gómez J.A., Giráldez JV, Vanderlinden K., 2014. Mapping impaired olive tree development using electromagnetic induction surveys. Plant and Soil, DOI: 10.1007/s11104-014-2207-5.

Rhoades J.D., Manteghi N.A., Shouse P.J., Alves W.J. 1989. Soil electrical-conductivity and soil-salinity – new formulations and calibrations. Soil Sci. Soc. Am. J. 53:433:439.

Rhoades J.D., Raats P.C.A., Prather R.J. 1976. Effects of liquid-phase electrical conductivity, water content, and surface conductivity on bulk soil electrical conductivity. Soil Sci. Soc. Am. J. 40:652-655.

Rhoades J.D., Corwin D.L. 1991 Determining soil electrical conductivity-depth relations using an inductive electromagnetic soil conductivity meter. Soil Sci. Soc. Am. J. 45: 255-260.

Robinson D.A., Abdu H., Jones S.B., Seyfried M., Lebron I., Knight R. 2008. Ecogeophysical imaging of watershed-scale soil patterns links with plant community spatial patterns. Vadose Zone J. 7:1132–1138.

Robinson D.A., Abdu H., Lebron I., Scott J. 2012. Imaging of hill-slope soil moisture wetting patterns in a semi-arid oak savanna catchment using time-lapse electromagnetic induction. J. Hydrol. 416-417:39-49.

Robinson D.A., Lebron I., Quejereta J.I. 2010. Determining soil-tree-grass relationships in a California oak savanna using eco-geophysics. Vadose Zone J. 9:528–536.

Saey T., Simpson D., Vitharana U.W.A., Vermeersch H., Vermang J., van Meirvenne M. 2008. Reconstructing the paleotopography beneath the loess cover with the aid of an electromagnetic sensor. Catena 74:58-64.

Sheets K.R., Hendrickx J.M.H., 1995. Noninvasive soil water content measurement using electromagnetic induction. Water Resour. Res. 31:2401-2409.

Simpson D. 2009. Geoarchaeological prospection with multi-coil electromagnetic induction sensors. Ph.D. thesis, Dept. soil spatial inventory techniques. Ghent University.

Sommer M. 2006. Influence of soil pattern on matter transportation in and from terrestrial biogeosystems – a new concept for landscape pedology. Geoderma, 133: 107-123.

Viscarra-Rossel R.A., Adamchuk V.I., Sudduth K.A., McKenzie N.J., Lobsey C. 2011. Proximal Soil Sensing: An Effective Approach for Soil Measurements in Space and Time. Adv. Agron. 113:243-291.

Vitharana U.W.A., van Meirvenne M., Cockx L., Bourgeois J. 2006. Identifying potential management zones in a layered soil using several sources of ancillary information. Soil Use Manag. 22:405-413.

Chapter 2. Materials and Methods

2.1 Electromagnetic Induction Sensors: DUALEM-21S

Geophysical surveys in this work were mainly focus on high density and spatially distributed surveys of soil apparent electrical conductivity (ECa). ECa data were measured using a DUALEM-21S (D21S) sensor (DUALEM, Milton, Canada), which is an electromagnetic induction (EMI) sensor that works at a fixed frequency of 9 KHz. Doolittle and Brevik (2014) reviewed other EMI sensors. This D21S comes pre-calibrated from the factory and auto-calibrates on the field. Therefore it is recommended to power the sensor away from sources of electromagnetic interferences. The D21S consists of a 2.41-m long tube that contains the transmitter coil (Tx) at one end of the tube and four receiver coils (Rx) which are located at 1, 1.1, 2, 2.1 m from the Tx. The Tx transmits multiple signals at the same time and the coil spatial orientation between Rx and Tx can be horizontal (H) or perpendicular (P) (Figure 2. 1). It measures simultaneously ECa and magnetic susceptibility (MSa) on different soil volumes. The high measurement frequency allows us to measure with the required in-line spacing.

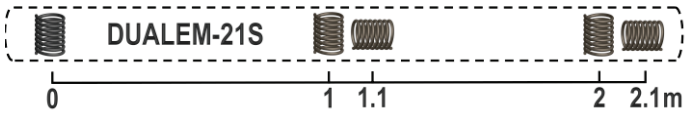

Figure 2. 1 Coil configurations of the DUALEM-21S. The coil at the left is the transmitter, while the four remaining coils are receivers. After Simpson (2009).

The working principle of the EMI sensors consists in the transmission of a primary electromagnetic field that induces electric currents in the soil. These currents generate a secondary electromagnetic field that is received by the Rx of the sensor. The sensor is designed to operate under low induction numbers conditions, therefore the ratio between the secondary field (Hs) and the primary field (Hp) is linearly proportional to the electrical conductivity of the explored soil volume.

The depth sensitivity distributions of the D21S signals depend on the inter-coil spacing and the coil orientation. Under LIN conditions, the sensor's relative response (R) to a soil layer depends on the frequency of the magnetic field, which is constant in this case, on the distance between the transmitter and receiver coils and on their orientation. R can be expressed as a function of depth, (z, m), and the sensor cumulative response (C) can be calculated by integrating the

relative weights of all soil layers from an infinite depth to the instrument on the soil surface. The sensor's cumulative response (C) as a function of depth *(z,* m) is expressed as:

$$C(H,z,s)=\left[4\left(\frac{z}{s}\right)^{2}+1\right]^{-1/2} \tag{2.1}$$

$$C(P,z,s)=1-\left[1+\left(\frac{2z}{s}\right)^{-2}\right]^{-1}, \tag{2.2}$$

with s (m) being the intercoil spacing. H and P refer to the horizontal and perpendicular coil orientation, respectively (De Smedt, 2013). Given the non-linear response of neither R nor C, the depth of exploration (DOE) of each signal is defined as the depth at which 70% of the response is obtained from the soil volume above (Figure 2.2).

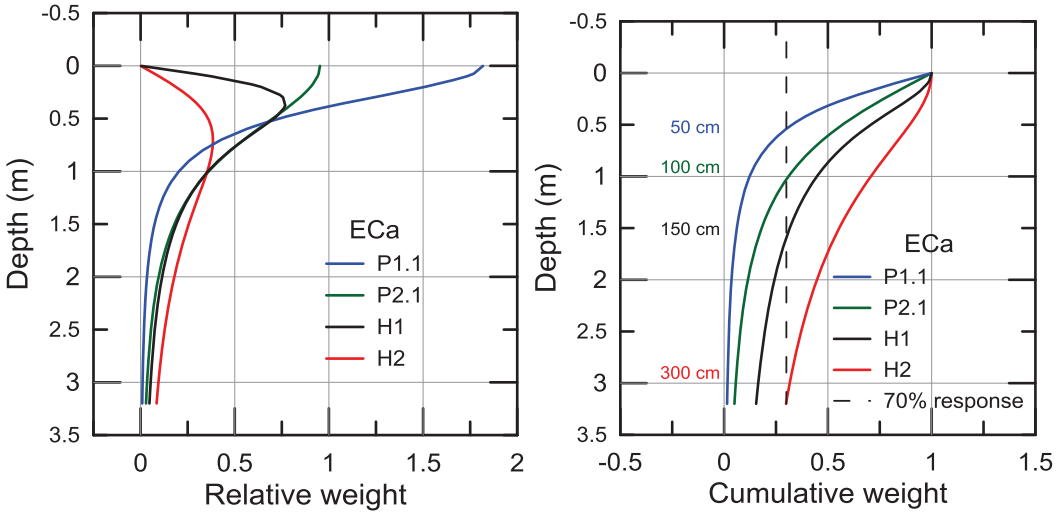

Figure 2. 2 Relative and cumulative response of the DUALEM-21S. The approximate depth of exploration of each signal is shown in cm.

2.2 The "La Manga" Catchment

2.2.1 Site Description

The experimental catchment "La Manga" (36° 52' 21" N, 5° 7' 44" W), located in Setenil de las Bodegas in the SW of Spain covers 6.7 ha of a rainfed olive orchard (Figure 2.3). The trees were planted in 1995 on a 7 × 7-m grid, with an average tree density of about 200 trees ha^{-1}. The mean elevation is 740 m a.m.s.l. and the mean slope is 10 %. The orchard is under minimum tillage and weeds are controlled with herbicides. The soil subgroup is an intergrade between

Lithic and Typic Rhodoxeralf (Soil Survey Staff, 1999, pp. 269-270; García del Barrio et al. 1971) with a loamy sandy texture and a maximum depth of 1.2 m to the calcarenite bedrock. The climate is Mediterranean, with a mean annual precipitation of 1100 mm and a mean annual temperature of 16 ºC. On average, 75% of the rainfall occurs from October to May, while 25% occurs between June and September as intense and brief rain showers. An area of 1.2 ha in the south-east of the catchment was transformed from cereal to olives in 2006 (Figure 2.4). A gully intersects the catchment from the SE towards the catchment outlet in the NW and separates the two main subareas and slopes of the catchment (Figure 2.5 y 2.6).

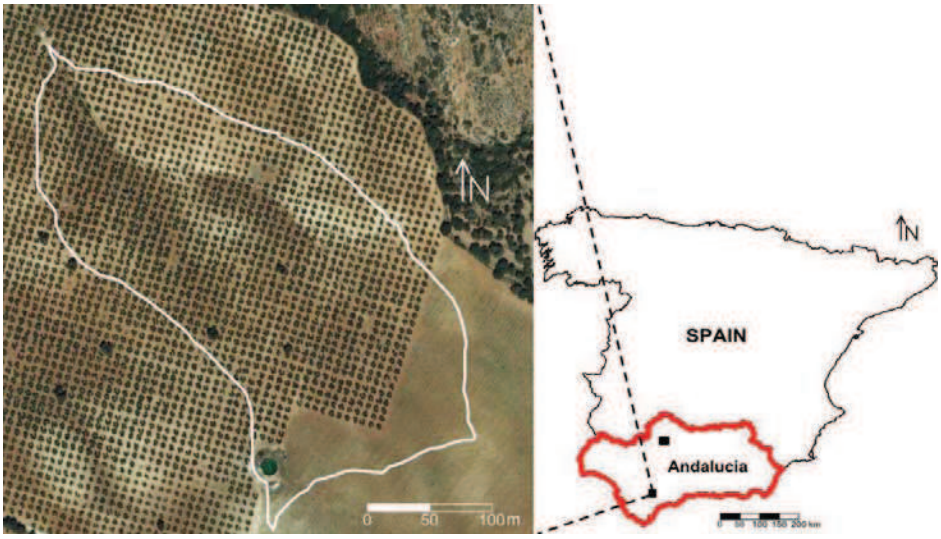

Figure 2. 3 Aerial photograph of the study field La Manga and catchment boundaries.


Figure 2. 4 Actual view of the 1.4-ha area in the south-east of the catchment which was transformed from cereal to olives in 2006.

Figure 2. 5 View of the two main subareas and slopes of the catchment.

Figure 2. 6 The gully that intersects the catchment from the SE towards the catchment outlet in the NW, showing the bedrock uncovered by the erosion.

2.2.2 Field Measurements

Exhaustive soil surveys were performed in 2012 at La Manga. Soil profile samples were collected on a pseudo regular grid at 48 locations, using a 0.093-m diameter cylinder auger (Eijkelkamp Agrisearch Equipment, Giesbeek, The Netherlands) and a percussion drill (Figure 2.7). Soil samples were taken at 0.1 m depth intervals, from the soil surface down to the bedrock (maximum reached soil depth = 1.2 m). The samples were analyzed in the laboratory for soil organic matter content following the Walkley-Black procedure, pH in a 1/2.5 dilution, texture

according to the hydrometer method (Grossman and Reinsch, 2002), electrical conductivity (1:5) (EC), bulk density (ρ_b), and stone content by conventional methods (e.g. Dane and Topp 2002). Stones retained with a 2 mm sieve were first washed and then the volume of stones per soil sample was calculated by water displacement, finally stones were dried and weighed.

The "La Manga" catchment was sampled for gravimetric soil water content (SWC) at the same 48 locations and on 18 occasions during the hydrological years 2010/11 and 2011/12 (Figure 2.8). As a result of excessive soil hardness under dry soil conditions and the calcarenite bedrock, samples were only taken down to a depth of 0.2 m, with 0.1-m intervals. At certain locations, only topsoil samples could be taken as a result of excessive soil hardness.

ECa surveys were performed using the D21S with a mobile configuration (Figure 2.9). The surveys were conducted at a speed range of 5-10 km/h, along parallel measurement lines along the alleys in-between the tree rows with an approximate separation of 7 m. Inline measurements were recorded every second. At La Manga field, ECa surveys started few months later than the gravimetric soil water surveys. A total of ten ECa surveys were performed from October 2011 to November 2012, simultaneously with the gravimetric water content and point ECa measurements at the 48 locations. Summary descriptive of the measured soil properties are mentioned on Chapters 4, 5 and 6.

Figure 2. 7 Cylinder auger and percussion drill (left) used to collect soil samples (right).

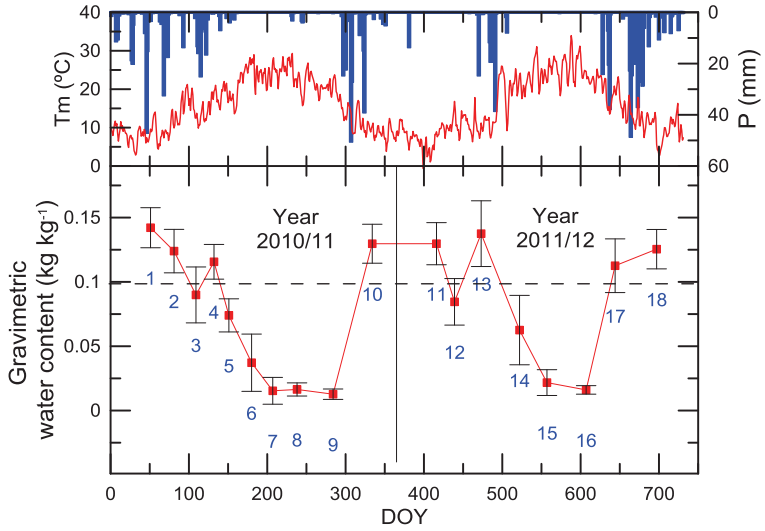

Figure 2. 8 Temporal evolution at La Manga of temperature, precipitation and mean gravimetric soil water content for hydrological years 2011 and 2012. Error bars represent standard deviations.

Figure 2. 9 View of the mobile configuration surveying the catchment "La Manga".

2.3 The "La Conchuela" Catchment.

2.3.1 Site Description

This experimental catchment is located at the "La Conchuela" farm (37° 48' 54" N, 4° 53' 53" W), 10 km west of Córdoba, Spain (Figure 2.10). The mean elevation is 93 m a.m.s.l. and the mean slope is 9%. The soil is a deep Vertisol formed on Miocene marls, characterized by Soil Survey Staff (1999) as a Chromic Haploxerert. For similar clay soils in the region, water retention at field capacity and wilting point was near 0.30 and 0.15 kg kg^{-1}, respectively. The catchment is intersected by a gully from south-east to north-east (Figure 2.11). The catchment covers approximately 8 ha of an irrigated olive orchard which was planted in 1993 with a tree

density of 240 trees ha^{-1} (Figure 2.12). Approximately 40% of the trees were replanted as a result of water logging and a subsequent severe infestation by *Verticillium dahliae* and possibly other soil borne pathogens during the wet spring of 1996 (Gomez et al. 2009). Generally, in these soils, diseases and root asphyxia appear during extremely wet winters, throughout which the soil remains in near saturated conditions for prolonged periods. The climate is Mediterranean, with a monthly average daily temperature of 9.3ºC for January and 28ºC for July. The mean annual precipitation is 650 mm, of which 75% occurs from October to March. Testi et al. (2006) found modeled average annual evapotranspiration for a 300 trees ha^{-1} mature orchard in Córdoba of 1025 mm. Earlier experimental work by Palomo et al. (2002) showed that water supplies near 400 mm during the irrigation seasons of 1997 and 1998 were adequate.

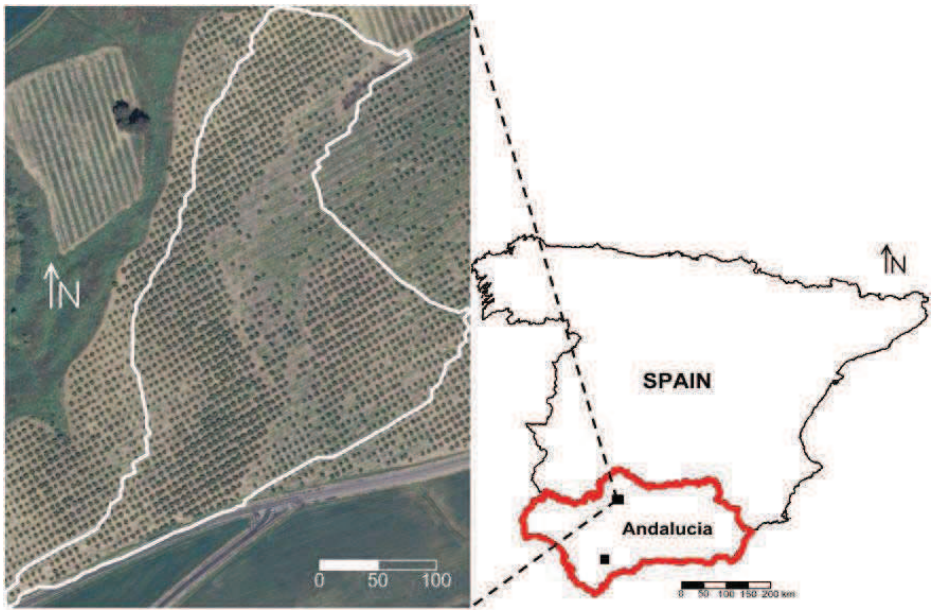

Figure 2. 10 Aerial photograph of the study field La Conchuela and catchment boundaries.

Figure 2. 11 The gully that intersects the catchment from the SE towards the catchment outlet in the NE.

Figure 2. 12 View of the main subarea and slope of the catchment.

2.3.2 Field Measurements

Exhaustive soil surveys were performed in 2010 at La Conchuela. Soil profile samples were collected on a pseudo regular grid at 45 locations, using a 0.093-m diameter cylinder auger (Eijkelkamp Agrisearch Equipment, Giesbeek, The Netherlands) and a percussion drill (Figure 2.7). Soil samples were taken at 0.1 m depth intervals, from the soil surface down to 1 m. The

samples were analyzed in the laboratory for soil organic matter content following the Walkley-Black procedure, pH in a 1/2.5 dilution, texture according to the hydrometer method (Grossman and Reinsch, 2002), $EC_{1:5}$, ρ_b, and stone content by conventional methods (e.g. Dane and Topp 2002). Stones retained with a 2 mm sieve were first washed and then the volume of stones per soil sample was calculated by water displacement, finally stones were dried and weighed.

The "La Conchuela" catchment was sampled at the same 45 locations for gravimetric SWC, under dry (September 2011) and wet (October 2012) soil conditions, using a 0.05-m diameter Edelman hand auger to a depth of 0.3 m. As a result of excessive soil hardness under dry soil conditions, samples were only taken down to a depth of 0.3 m, with 0.1-m intervals.

Based on a preceding EMI survey at La Conchuela , seven locations were selected where soil profile pits were dug to a depth of 2 meters. The soil profile was described according to Soil Survey Staff (1999). Soil samples were collected from the center of each horizon and later analyzed in the laboratory for soil texture, cation exchange capacity (CEC), exchangeable Na, carbonates (CO_3), and organic matter (OM).

ECa surveys were performed using the D21S with a mobile configuration (Figure 2.9). The surveys were conducted at a speed range of 5-10 km/h, along parallel measurement lines along the alleys in-between the tree rows with an approximate separation of 7 m. Inline measurements were recorded every second. Two ECa surveys were performed at La Conchuela field under dry (September 2011) and wet soil conditions (October 2012), simultaneously with the gravimetric water content and point ECa measurements at the 45 locations. Summary descriptive of the measured soil properties are mentioned on Chapter 3.

2.4 Mobile ECa Measurement Configuration

The D21S was operated using a rugged and custom-made mobile measurement configuration for operation in rugged landscapes. Such measurement configurations enable fast surveying of entire fields or catchments with data densities up to $1/m^2$. The sensor was firstly embedded within a sled made of high density polyvinyl chloride (PVC) and surrounded by thermal isolation and shock absorbing material. At the beginning of the summer season, the grey PVC was painted in white to increase the albedo and prevent excessive heating of the equipment during operation. As a result of the high weight (>100 kg) of this sled and the low abrasion resistance of the used PVC a new sled was designed and manufactured of white low density polyethylene (PE) (Figure 2.13).

Figure 2. 13 Pictures of the two designed and manufactured sleds.

A Real Time Kinematic (AgGPS 432, Trimble Navigation Ltd., Sunnyvale, CA, USA) GPS (Trimble Ag RTK Base 430) system was used, with the antenna mounted on the sled for accurate geo-referencing, including elevation, of the ECa measurements. As a result of the sloping and rough terrain that often characterizes olive orchards, the sled does not necessarily follow the path of the towing vehicle. Therefore the antenna has to be mounted on the sled and cannot be positioned on the towing vehicle. RTK operation is based on the use of a mobile GPS measurement, which is corrected in real time by a reference station, enabling centimeter precision. The sled is pulled by an all-terrain vehicle, which is equipped with a guidance system and an TK 6000 (Juniper Systems, Logan, UT) field computer that runs HGIS9 software (HGIS – Starpal Inc, CO) to log measurements and coordinates. In order to avoid interference of the metal pieces of the towing vehicle, the sensor was operated at approximately 2 m from the latter, using a rigid articulated arm which provided stability to the sled and prevented overturning (Figure 2.14). The D21S was positioned inside the sled at a total height of 0.075 m above the soil surface, as a result of a wear-and-tear plate which was mounted underneath the sled to protect it from abrasion by dry soil and stones.

With this mobile configuration the surveying speed can be significantly increased as compared to manual operation. In addition, high amounts of data can be collected with high spatial densities, reducing the uncertainty associated with the spatial interpolation (Goovaerts, 1997).

Figure 2. 14 Detailed view of the complementary electronic devices arranged and fixed on the quad (left) and the low density sled manufactured for the DUALEM-21S (right).

2.5 Sensor drift

Frequency domain EMI sensors suffer often from drift of the absolute values caused by temperature variations which can alter the resistance or capacitance of the electronic components. According to the manufacturer the D21S compensates internally for temperature drift. However, in order to avoid extreme temperature effects measurements started early in the morning. In addition, the sensor was isolated with foam/polystyrene and the PVC sled was first painted in white and then replaced by white PE sled. For the conductivity data, the effect of temperature changes are generally negligible (Simpson, 2009), while for susceptibility more significant effects have been observed. Diurnal changes in soil temperature have no significant effect on the absolute values of ECa (Brevick et al. 2004; Cockx, 2010). Sudduth et al. (2001) were unable to relate changes in air temperature and drift on a frequency domain EMI sensor (EM38 (Geonics Inc. Ontario, Canadá)), and Robinson et al. (2004) showed that at temperatures lower than 40 ºC the drift effect is minimal on a frequency domain EMI sensor.

2.6 Post-processing ECa data

After a geophysical survey with the described mobile configuration, a text file with the ECa and MSa measurements and the geodesic coordinates is obtained. Also internal parameters of the sensor operation such as temperature and inclination are logged along with the measurements.
The post-processing of these data takes place in several stages. First the geodesic coordinates are transformed to UTM coordinates (x, y, z), second the ECa data are filtered, and third the ECa data are corrected for the temperature deviation from 25ºC. The coordinate transformation is performed using the geodesic calculator Utm9e- 200803 (Núñez-Maderal, 2008) given zone 31, hemisphere N and length E, since the GPS output is in WGS84 geodetic coordinates.

In order to filter erroneous or inconsistent measurements a statistical procedure is used. Within a circular search neighborhood centered on each measurement location the mean, *m*, and standard deviation, σ, of the ECa measurements are calculated. The corresponding measurement is then standardized according to $z = |x - m| / \sigma$. If $z < 2$ then the measurement is considered valid, otherwise it is removed (Simpson, 2009).

During the field surveys a temperature probe is inserted into the soil at 5 cm depth, temperature data recorded will be used when processing ECa data, in order to reference the different surveys to a temperature of 25 °C (Equation 1.3).

2.7 Data interpolation

Interpolation through geo-statistical techniques (Goovaerts, 1997) is a further step in the post-processing of the data. This procedure allows the estimation of values at locations where a variable has not been measured. Ordinary Kriging is a geo-statistical interpolation method which is based on the principle that "closer points in space tend to have more similar values than distant points". Based on that principle, a weighted average is calculated at each grid point using the measurements found within a search neighborhood centered on the grid point to be interpolated. Computer generated maps are useful to quantify *z* and ECa values over continuous soil surfaces, which improve understanding of soil variability and landscape relationships (Corwin and Lesch, 2003). In this thesis interpolated maps on a 1x1-m grid were computed using Vesper 1.6 (Whelan et al. 2002) and Surfer 11(Golden Software Inc., Golden, Colorado, USA).

REFERENCES

Brevik E.C., Fenton T.E., Horton R. 2004. Effect of daily soil temperature fluctuations on soil electrical conductivity as measured with the Geonics EM-38. Precis. Agric., 5:145–152.

Cockx L. 2010. High resolution soil inventory using a dual signal electromagnetic induction sensor. Ph.D. thesis, Dept. soil spatial inventory techniques. Ghent University.

Corwin D.L., Lesch S.M. 2003. Application of soil electrical conductivity to precision agriculture: Theory, principle and guidelines. Agron. J., 95:455-471.

De Smedt P., van Meirvenne M., Davies N.S., Bats M., Saey T., De Reu J., Meerschman E., Gelorini V., Zwertvaegher A., Antrop M., Bourgeois J., De Maeyer P, Finke P.A., Verniers J., Crombé P. 2013. A multidisciplinary approach to reconstructing Late Glacial and Early Holocene landscapes. J.Archaeol. Sci. 40:1260-1267.

Doolittle J.A., Brevik C. 2014. The use of electromagnetic induction techniques in soils studies. Geoderma 223-225:33-45.

Dualem Inc. 2007. DUALEM-21S user's manual. Dualem Inc., Milton. Canada.

García del Barrio I., Malvárez L., González J.I. 1971. Mapas provinciales de suelos. Cádiz. Ministerio de Agricultura. Madrid.

Gómez J.A., Sobrinho T.A., Giráldez J.V., Fereres E. 2009.Soil management effects on runoff, erosion and soil properties in an olive grove of southern Spain. Soil Till. Res. 102:5-13.

Goovaerts P. 1997. Geostatistics for natural resources evaluation. Oxford University Press, Oxford, UK.

Grossman R.B., Reinsch, T.G. 2002. The solid phase, in: Dane, J. H., Topp, G. C. (Eds.), SSSA Book Series: 5. Methods of Soil Analysis. Part 4 – Physical Methods. Soil Science Society of America, Madison, Wisconsin, USA, pp. 201-415.

Núñez-Maderal E. 2008. Calculadora Geodésica edición especial para la Península Ibérica, Cartesia.org, Spain.http://www.cartesia.org/download.php?op=viewdownloaddetails&lid=172&ttitle=Calculadora_UTM-Geogr%E1ficas_Espa%F1a. Accessed 11 July 2014.

Palomo M.J., Moreno F., Fernández J.E., Dıaz-Espejo A., Girón I.F. 2002.Determining water consumption in olive orchards using the water balance approach. Agr. Water Manage. 55:15-35.

Robinson D.A., Lebron I., Lesch S.M., Shouse P. 2004. Minimizing drift in electrical conductivity measurements in high temperature environments using the EM-38. Soil Sci. Soc. Am. J. 68:339–345.

Simpson D. 2009. Geoarchaeological prospection with multi-coil electromagnetic induction sensors. Ph.D. thesis, Dept. soil spatial inventory techniques. Ghent University.

Soil Survey Staff. 1999. Soil Survey Manual. Soil Conservation Service. USDA Ag. Hbk. 18, Washington

Soil Survey Staff. 1999. Soil taxonomy: A basic system of soil classification for making and interpreting soil surveys. 2nd ed. NRCS USDA Hbk 436

Sudduth K.A., Drummond S., Kitchen N.R. 2001. Accuracy issues in electromagnetic induction sensing of soil electrical conductivity for precision agriculture. Comput. Electron. Agr., 31:239–264.

Testi L., Villalobos F.J., Orgaz F., Fereres E. 2006. Water requirements of olive orchards: I simulation of daily evapotranspiration for scenario analysis. Irrig. Sci 24:69-76.

Whelan B.M., McBratney A.B., Minasny B. 2002. Vesper 1.5 – spatial prediction software for precision agriculture. In: Robert PC, Rust RH, Larson WE. (eds.) Precision Agriculture, Proceedings of the 6th International Conference on Precision Agriculture, ASA/CSSA/SSSA, Madison, Wisconsin.

Chapter 3. Mapping impaired olive tree development using electromagnetic induction surveys

3.1. Introduction

Olives (*Olea europaea* L.) have supported Mediterranean civilizations for thousands of years. Nowadays olives remain important for their social and economic implications, e.g. in sustaining rural communities (Loumou and Giourga 2003) and for the health benefits of olive oil (de Backer et al. 1997; Clodoveo et al. 2014). Today, a total area of about 2.6 Mha is dedicated to olive cultivation in Spain, representing more than one fourth of the total world acreage of this crop (FAOSTAT 2012, MAGRAMA 2012). Spanish olive oil production represents 62% of the total EU production (European Commission 2012). The largest olive cultivation area is situated in Andalusia, with approximately 60% of the national acreage and 82% of the national olive production (CAP 2012). Olive cultivation and associated industries contribute for 40% to the rural employment in Andalusia and for almost one third of the region´s agricultural production value.

Olives were traditionally cultivated on marginal, often sloping land, and poor soils (e.g., Semple 1931 chapter XIV). The increasing market demand and the introduction of drip irrigation improved the crop's profitability and promoted olive cultivation in the more fertile soils in the valleys. More olive production coincided with the adoption of high plantation densities and the development of high yield varieties, but resulted in an increasing appearance of soil borne diseases, such as Verticillium wilt, caused by the fungus *Verticillium dahliae* Kleb. (Sánchez-Hernández et al. 1998, Navas-Cortés et al. 2008, López-Escudero and Mercado-Blanco 2011). During four cropping seasons Navas-Cortés et al. (2008) found the largest infection rates from late winter to early spring, corresponding roughly to the wettest period of the year. Propagation within the field is possibly caused by the transport of infested plant material (e.g. leafs or fruits) or soil particles by runoff water, wind or tillage. Diseases are often associated with temporary waterlogging conditions, and both soil properties and tree age and cultivar contribute to the risk of infestation (López-Escudero and Mercado-Blanco 2011). Despite recent advances in remote-sensing techniques for the early detection of *Verticillium* wilt (Calderón et al. 2013), the disease causes important losses to the farmers who need to reestablish their plantations. Other fungi such as *Phytophtora* spp cause root rot, and are often associated with deficient drainage and soil aeration conditions, which if persisting in time cause also to root asphyxia. Optimal growing conditions for olive trees are generally found in non-stratified, moderately fine textured soils, with good aeration and permeability, and high water-holding capacity. Such conditions are often not found in the generally more clayey valley soils. Despite

the obvious effects of terrain and soil characteristics on olive growth and susceptibility to soil-borne diseases, little attention is generally paid to the within-field variability of these factors when establishing new plantations.

Conventional soil surveying to determine spatial patterns of soil properties is in general prohibitive at commercial farms. Soil sampling is time consuming, expensive and provides only a limited spatial coverage. Electromagnetic induction (EMI) sensors provide a suitable alternative (Minasny et al. 2013; Doolittle and Brevik 2014; and references therein), providing simultaneously apparent electrical conductivity (ECa) values of different soil volumes with varying depths. Under non-saline conditions ECa depends in theory only on soil water content and temperature (Keller and Frischknecht, 1966). However, it is indirectly also affected by other factors. Therefore, Friedman (2005) suggested to group the factors that affect ECa into three categories, corresponding to the bulk soil (e.g. porositiy, water content, structure), the solid particles (e.g. particle shape and orientation, particle-size distribution), and the soil solution (e.g. conductivity of the aqueous solution, cation composition, temperature).

Traditionally, EMI surveys have been used to identify management zones in the context of precision agriculture (Johnson et al. 2003; Corwin and Lesch 2003; Corwin and Plant 2005; Vitharana et al. 2006; 2008). The inference of the horizontal and vertical distribution of clay from EMI surveys has received considerable attention (Triantafilis et al. 2005; Kitchen et al. 2005; Jung et al. 2005; Saey et al. 2008, 2009; Rodriguez-Perez et al. 2011) as a result of its relevance for water dynamics across fields or catchments.

Periodical surveys with EMI sensors under contrasting soil moisture conditions can be used to identify hydrological patterns in watersheds (Sherlock and McDonnell 2003; Abdu et al. 2008; Martinez et al. 2010, 2012; Robinson et al. 2012). Such patterns (e.g. soil water content, water table depth) have been shown to be related to the spatial distribution of vegetation (Robinson et al. 2008, 2010; Atwell et al. 2013). Robinson et al. (2010) studied the adequacy of EMI surveys for assessing soil spatial resource heterogeneity in a savanna tree-grass ecosystem. In order to evaluate the dominance of trees over grasses and vice versa, the ECa histogram was divided into four sections. Higher ECa values occurred under grass dominance while lower ECa values were found in zones with tree dominance, corresponding to lower clay contents.

The objectives of this work were (1) to delimit areas with impaired tree development using electromagnetic induction surveys, and (2) to identify the underlying relationships between ECa and soil properties causing the spatial patterns in the tree development.

3.2 Materials and methods

3.2.1 Site description

The study was performed in an experimental catchment at the "La Conchuela" farm (37º48'54'' N, 4º53'53''W), 10 km west of Córdoba, Spain (Figure 3.1). The mean elevation is 93 m a.m.s.l. and the mean slope is 9%. The soil is a deep Vertisol formed on Miocene marls, characterized by Soil Survey Staff (1999) as a Chromic Haploxerert. For similar clay soils in the region, water retention at field capacity and wilting point was near 0.3 and 0.15 gg^{-1}. The catchment is intersected by a gully from south-east to north-east (Fig. 3.1). The catchment covers approximately 8 ha of an irrigated olive orchard which was planted in 1993 with a tree density of 240 trees ha^{-1}. Approximately 40% of the trees were replanted as a result of water logging and a subsequent severe infestation by *Verticillium dahliae* and possibly other soil borne pathogens during the wet spring of 1996 (Gomez et al., 2009). Generally, in these soils, diseases and root asphyxia appear during extremely wet winters, throughout which the soil remains in near saturated conditions for prolonged periods. The climate is Mediterranean, with a monthly average daily temperature of January of 9.3ºC and 28ºC for July. The mean annual precipitation is 650 mm, of which 75% occurs from October to March, and occasional precipitation between June and September. Testi et al. (2006) found modeled average annual evapotranspiration for a 300 trees ha^{-1} mature orchard in Córdoba of 1025 mm. Earlier experimental work by Palomo et al. (2002) showed that water supplies near 400 mm during the irrigation seasons of 1997 and 1998 were adequate.

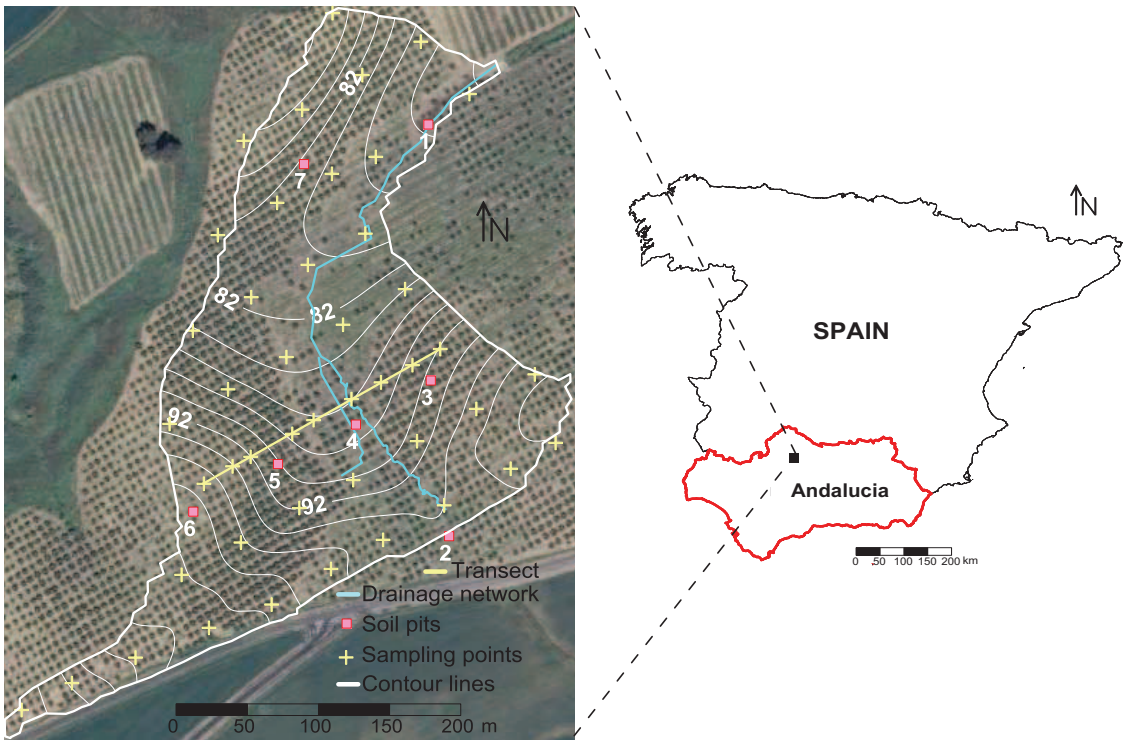

Figure 3. 1 Location and orthophotograph of the experimental catchment, with topography, catchment boundaries, and position of soil sampling points and pits superposed

3.2.2 Soil profile description and soil sampling strategy

Based on a preceding EMI survey, seven locations were selected (Fig. 3.1) where soil profile pits were dug to a depth of 2 meters. The soil profile was described according to Soil Survey Staff (1999). Soil samples were collected from the center of each horizon and later analyzed in the laboratory for soil texture, cation exchange capacity (CEC), exchangeable Na, carbonates (CO_3), and organic matter (OM).

During the spring of 2010 soil profile samples were collected down to 0.9 m at 45 locations on a pseudo-regular grid using a 0.093-m diameter cylinder auger (Eijkelkamp Agrisearch Equipment, Giesbeek, The Netherlands)[1] and a percussion drill. The profile samples were divided in three 0.3-m long subsamples and analyzed in the laboratory for soil OM, pH, texture, electrical conductivity of the saturated paste (5:1) filtrate (EC), bulk density (ρ_b) and stone content. In order to obtain more detailed information, at nine locations along a SW-NE-oriented transect (see Fig. 3.1) profile samples down to a depth of 1 m were divided in five 0.2-m long subsamples and analyzed in the laboratory for the same properties. The transect was chosen to cover the entire range of measured ECa values.

In 2011 and 2012 (under dry and wetter soil conditions, respectively) the catchment was sampled at the same 45 locations for gravimetric soil water content. As a result of excessive soil hardness in 2011, samples were only taken down to a depth of 0.3 m, with 0.1-m intervals. At certain locations, only topsoil samples could be taken as a result of excessive soil hardness. In 2012, several days after the first rainfall event in autumn, after the prolonged dry summer period, samples were taken down to a depth of 0.6 m, with increments of 0.2 m. A larger sampling interval was chosen in 2012 to reduce the number of samples and associated workload. Samples were taken using a 0.05-m diameter Edelman hand auger. Fresh sample weight was approximately 300 g.

3.2.3 Apparent electrical conductivity surveys and post-processing

Catchment-wide apparent electrical conductivity surveys were conducted in-between the tree lines in September 2011 and October 2012, simultaneously with the gravimetric water content and point ECa measurements at the 45 locations. Catchment-wide ECa data were used to delimit areas with different tree development, while point ECa measurements and measured soil properties were used to infer relationships among the studied variables.

ECa measurements were made using a DUALEM-21S (DUALEM, Milton, Canada) sensor, accommodated in a customized polyvinyl chloride sled and pulled by an all-terrain vehicle, equipped with a real time kinematic-differential global positioning system (Trimble, Sunnyvale, CA) and a rugged Allegro-TK6000 field computer (Juniper Systems, Logan, UT) to log measurements, coordinates, and elevation (Z). The GPS antenna was positioned on the sled, 1.5 m above the center of the inter-coil

spacing corresponding to the H1 signal. As a result of the sled configuration, the sensor was operated at a height of 0.075 m above the soil surface.

The sensor works at a fixed frequency of 9 kHz and consists of a transmitter coil at one end and four receiver coils separated 1, 1.1, 2, and 2.1 m from the transmitter coil. Receiver coils are oriented, with respect to the transmitter coil, in a perpendicular (P) or in a horizontal co-planar (H) configuration. Each transmitter-receiver combination provides integrated ECa values for the corresponding explored soil volumes (Table 1). Traditionally a varying sensitivity with depth has been considered (McNeill 1980; Rhoades and Corwin, 1981; Saey et al., 2009). The effective depth of exploration (DOE) is the depth at which 70% of the sensor response is obtained. However, work by Callegary et al. (2007) showed that the depth of exploration depends strongly on the soil's ECa. In addition, Callegary et al. (2012) found that variations of the electrical conductivity within the explored soil volume can compromise the measurements and lead to irregular explored soil volumes.

The ECa data were filtered and interpolated (Whelan et al. 2002) on a 1x1-m grid to create maps for the four ECa signals. Also elevation was interpolated on a 1x1-m grid to provide a digital elevation model from which topographic indices, (Vitharana et al. 2008) a slope map, the stream network and the watershed limits were derived.

Table 3. 1 Intercoil distance (ID, m), coil configuration and depth of exploration (DOE, m) for each signal measured by the DUALEM-21S.

Signal	ID	Coil configuration	DOE
P1.1	1.1	Perpendicular	0.5
P2.1	2.1	Perpendicular	1
H1	1	Horizontal co-planar	1.5
H2	2	Horizontal co-planar	3

3.2.4 Data analysis

Analysis of variance (ANOVA) and Pearson correlation coefficients were calculated using point ECa and soil profile data, measured at exactly the same position. Although the explored soil volumes by the ECa and soil measurements differ in several orders of magnitude and no strong correlations are expected, the significance of potential relationships can be tested. Also differences in point ECa and SWC for both surveys were analyzed.

3.2.5 Canopy coverage and projected canopy area of individual trees

The fraction of canopy coverage was calculated by evaluating the color range of the orthophotograph (in bit map protocol) for each delimited zone. First the color range of the canopies was determined, then the total area occupied by canopies was calculated as the sum of the number of pixels with values within that color range, and, finally, the total area covered by canopy was calculated as the sum of pixels, from which the percentage of canopy coverage was calculated. Projected canopy area (CA) of each olive was

calculated after transforming the raster to polygons for the selected canopy color range, and filtering canopy areas automatically (CA≤ 3m^2) and manually where necessary. The projected canopy area of each olive tree and the mean ECa for the same area were calculated and analyzed.

3.3 Results

3.3.1 Soil properties

Profile pits

Four horizons (A, B, BC and C) were distinguished at pits 1, 2, 3, 5 and 7 (see Fig. 3.1). Pit 4 showed no BC horizon, while only an A and a C horizon were found at pit 6 (Table 2). In general, depth to the C horizon increased downslope (pits 3-6). The C horizon (marl) appeared in most pits at 1-1.5 m depth, except for pit 5 where the C horizon was found at 1.9 m depth and pit 4 where no C horizon was found. The relatively shallow C horizons found at pits 2 and 6 (at 1.1 and 0.8 m, respectively) were possibly a result of soil loss from the overlaying soil horizons towards the lower elevation positions, e.g. pit 4 where the C horizon was not reached at 2 m depth.

Clay content decreased with depth at pits 1, 3 and 5, and remained approximately constant throughout the profile at the other locations. Pits 5 and 7, located within the area with the best tree development (Fig. 3.1) showed substantially lower clay contents in the C horizon as compared to the other soil profiles. The highest clay content was observed at pit 4, which was located in the area with significant tree growth and die-off problems. Organic matter content decreased with depth at all pits. Carbonate content increased with depth at pits 1, 3, 5 and 7, and remained constant at the other pits, while Na increased only at pits 1, 2, 4 and 6.

Table 3. 2 Summary of the profile description of the seven soil pits shown in Fig. 1 and values of selected soil properties. Indexes refer to subdivisions of the same horizon. CEC: Cation exchange capacity and OM: Organic matter content.

Soil properties	Soil pit						
	1	2	3	4	5	6	7
A Horizon							
Layer extent (m)	0–0.39	0–0.30	0–0.30[1] 0.30–0.65[2]	0–0.40[1] 0.40–0.80[2] 0.80–1.15[3]	0–0.32[1] 0.32–0.87[2]	0–0.80	0–0.10[1] 0.10–0.32[2] 0.32–0.60[3]
Clay (%)	50.2	50.0	50.3[1] 54.3[2]	55.6[1] 57.1[2] 55.6[3]	48.8[1] 51.6[2]	50.4[1] 52.7[2] 52.2[3]	44.4[1] 46.5[2] 48.9[3]
Na (mol_c kg^{-1})	0.71	0.48	0.5[1] 0.6[2]	0.4[1] 0.6[2] 1.2[3]	0.4[1] 0.5[2]	0.5[1] 0.9[2] 1.4[3]	0.4[1] 0.5[2] 0.8[3]
CEC (mol_c kg^{-1})	30.8	26.52	27.4[1] 28.9[2]	28.9[1] 29.6[2] 28.3[3]	23.7[1] 27.0[2]	24.1[1] 23.9[2] 22.0[3]	22.4[1] 24.3[2] 25.2[3]
Carbonates (%)	18.34	24.66	30.7[1] 27.0[2]	23.6[1] 22.8[2] 25.6[3]	24.7[1] 24.5[2]	25.8[1] 25.5[2] 27.7[3]	26.2[1] 27.2[2] 28.7[3]
OM (%)	1.22	1.09	1.3[1]	1.2[1]	1.0[1]	0.8[1]	1.2[1]

			1.1[2]	1.1[2] 0.6[3]	0.7[2]	0.6[2] 0.4[3]	0.9[2] 0.7[3]
B Horizon							
Layer extent (m)	0.39-0.69[1] 0.69–1.09[2]	0.30–0.77	0.65–0.88	1.15–1.50[1] >1.50[2]	0.87–1.47	---	0.60–0.91
Clay (%)	53.0[1] 53.4[2]	52.5	43.9	55.6[1] 53.5[2]	53.0	---	48.1
Na (mol_c kg^{-1})	3.1[1] 3.7[2]	0.8	0.5	1.2[1] 1.2[2]	0.5	---	1.0
CEC (mol_c kg^{-1})	33.2[1] 31.1[2]	26.3	20.9	29.8[1] 26.3[2]	28.5	---	25.9
Carbonates (%)	16.3[1] 18.3[2]	26.1	49.8	23.9[1] 29.7[2]	25.6	---	29.2
OM (%)	0.8[1] 0.8[2]	0.7	0.6	0.7[1] 0.5[2]	0.6	---	0.7
BC Horizon							
Layer extent (m)	1.09–1.52	0.77–1.10	0.88–1.24	---	1.47–1.90	---	0.91–1.37
Clay (%)	52.4	52.9	45.1	---	35.6	---	47
Na (mol_c kg^{-1})	3.0	1.5	0.7	---	0.4	---	1.1
CEC(mol_c kg^{-1})	30.3	24.8	22.2	---	15.9	---	26.1
Carbonates (%)	20.1	26.9	41.1	---	44.8	---	31.1
OM (%)	0.7	0.4	0.4	---	0.2	---	0.5
C Horizon							
Layer extent (m)	>1.52	>1.10	>1.24	---	>1.90	>0.80	1.37–1.90[1] >1.90[2]
Clay (%)	43.7	52.0	47.7	---	32.8	50.1	46.5[1] 23.4[2]
Na (mol_c kg^{-1})	5.0	2.4	0.6	---	0.4	2.6	1.1[1] 0.6[2]
CEC (mol_c kg^{-1})	20.2	21.1	21.3	---	13.7	19.1	25.0[1] 13.7[2]
Carbonates (%)	35.9	26.4	35.6	---	46.4	27.7	32.1[1] 23.8[2]
OM (%)	0.2	0.3	0.2	---	0.3	0.2	0.3[1] 0.1[2]

Profile samples

The profile-averaged clay, sand and silt contents calculated for samples from 45 locations throughout the catchment were 48, 6 and 46 %, respectively (Table 3a). The coefficient of variation (CV) also increased with depth, being largest for the sand content (0-0.9 m) as compared to silt and clay content (50, 9, 12 %, respectively). Sand content showed positively skewed distributions, especially for the deeper layers, while clay content was negatively skewed. The kurtosis coefficient (KC) was found to be greater than 3 for sand content in the deeper layers. This indicates the presence of areas with intrusions of coarser sandy material in the dominantly fine textured clay soil.

The mean OM content found for the topsoil (0-0.3 m) was 1.0% (Table 3b), roughly 1.5 and 2 times larger than the mean OM content found for the 0.3-0.6 and 0.6-0.9 m layers. The corresponding CV increased with depth, from 27% in the topsoil to 53% in the deepest layer. Electrical conductivity was similar in the upper 0.6 m of soil profile, with an average of 0.18 dS m^{-1} for the two upper horizons, maximum values of 0.38 and 0.31 dS m^{-1}, and a CV of 25 and 28%, respectively (Table 3b). In the 0.6-0.9 m layer the mean EC value and corresponding CV roughly doubled those found in the upper layers.

In general, similar pH values were observed throughout the soil profiles, while stone content decreased and bulk density increased with depth (Table 3c). Profile-averaged pH was 8.7 indicating alkaline soil conditions. Mean stone content ranged from 3.8% in the deepest layer to 5.9% in the top layer. Bulk density ranged from 1.4 to 1.5 Mg cm^{-3}, which are common values for non- compacted clay soils.

Significant ($p < 0.05$) positive Pearson correlation coefficients were found between clay and OM content (0.30), and stone and OM content (0.57), while significant negative correlation coefficients were found between sand and clay content (-0.68), elevation and OM content (-0.54), and elevation and stone content (-0.56).

Table 3. 3 Descriptive statistics of a) soil texture (%), b) organic matter content (OM, %) and electrical conductivity (EC, dS m^{-1}), and c) pH, stone content (%) and bulk density (ρ_b, Mg cm^{-3}), for different depth intervals.

a)	**0-0.3 m**			**0.3-0.6 m**			**0.6-0.9 m**			**0-0.9 m**		
	sand	**silt**	**clay**	**sand**	**silt**	**clay**	**sand**	**silt**	**clay**	**sand**	**silt**	**clay**
N*	45	45	45	45	45	45	44	44	44	44	44	44
m	5.8	46.0	48.2	5.8	45.6	48.6	6.0	46.2	47.8	5.9	45.9	48.1
med	6.1	45.8	48.7	5.7	44.9	50.3	5.9	44.8	50.0	6.4	45.3	49.6
min	1.5	38.7	34.6	1.1	36.3	31.3	1	35.9	25.3	1.6	37.3	33.2
max	14.5	55.2	54.2	22.9	58.1	57.2	21.8	62.2	57.8	14.6	58.0	56.4
s	2.7	3.1	4.1	3.6	4.9	6.2	3.8	5.6	7.6	3.0	4.2	5.6
CV	46.9	6.7	8.5	61.5	10.7	12.6	63.3	12.1	15.9	49.8	9.1	11.6
skew	0.8	0.3	-0.7	2.3	0.6	-1.3	1.7	0.9	-1.3	0.8	0.8	-1.2
kurt	1.3	1.1	0.9	9.5	0.7	1.1	4.9	0.8	1.1	0.8	1.0	0.8

b)	**0-0.3 m**		**0.3-0.6 m**		**0.6-0.9 m**		**0-0.9 m**	
	OM	**EC**	**OM**	**EC**	**OM**	**EC**	**OM**	**EC**
N*	44	45	45	45	45	45	44	45
m	0.97	0.18	0.65	0.18	0.50	0.34	0.71	0.23
med	0.99	0.16	0.64	0.16	0.42	0.19	0.70	0.17
min	0.47	0.13	0.19	0.12	0.05	0.12	0.24	0.13
max	1.48	0.38	1.4	0.31	1.07	2.82	1.15	1.09
s	0.26	0.04	0.29	0.05	0.27	0.54	0.26	0.19
CV	27.2	25.35	44.79	28.26	53.21	155.96	36.87	80.94
skew	-0.07	2.82	0.43	1.22	0.30	4.00	0.10	3.80
kurt	-1.05	8.69	-0.63	0.31	-1.09	15.06	-1.28	13.99

c)	0-0.3 m			0.3-0.6 m			0.6-0.9 m			0-0.9 m		
	pH	**stone**	ρ_b	**pH**	**stone**	ρ_b	**pH**	**stone**	ρ_b	**pH**	**stone**	ρ_b
N*	45	14	45	45	15	45	45	14	45	45	23	45
m	8.6	5.9	1.39	8.7	5.5	1.46	8.7	3.8	1.51	8.7	3.1	1.45
med	8.6	4.1	1.42	8.8	3.7	1.49	8.8	3.3	1.52	8.7	2.2	1.48
min	8.0	2.5	0.45	8.2	2.7	1.06	7.9	2.6	1.25	8.3	0.9	1.02
max	8.6	19.3	1.75	9.1	13.3	1.67	9.2	6.5	1.77	9.1	8.6	1.66
s	0.19	4.7	0.21	0.2	3.6	0.11	0.3	1.1	0.08	0.2	2.5	0.11
CV	2.2	79.7	15.5	2.3	65.0	7.45	3.2	29.5	5.51	1.9	81.3	7.83
skew	-0.7	2.0	-2.1	-1.0	1.4	-1.3	-1.4	1.3	-0.2	-0.4	1.2	-1.44
kurt	2.0	3.0	6.8	0.6	0.2	2.5	1.7	0.5	2.5	-0.1	0.4	3.42

*N: number of measurements, m: mean, med: median, min: minimum, max: maximum, *s*: standard deviation, CV: coefficient of variation (%), skew: skewness, kurt: kurtosis.

Soil water content

Average SWCs for the dry 2011 survey were 0.05, 0.07 and 0.09 kg kg^{-1} for the 0-0.1, 0.1-0.2 and 0.2-0.3 m layers. Differences were significant at $p < 0.05$. Profile mean SWC and standard deviation were 0.06 and 0.02 kg kg^{-1}, while maximum and minimum values were 0.04 and 0.12 kg kg^{-1}, respectively. Overall, distributions were positively skewed.

Data from the wetter 2012 survey showed uniform SWC distributions across the soil profile. Also standard deviation and CV were similar for the top 0.4-m layer, but were half the value found for the 0.4-0.6-m interval. Profile-averaged mean and standard deviation were 0.22 and 0.03 kg kg^{-1}, while maximum and minimum values were 0.14 kg kg^{-1} and 37 kg kg^{-1}, respectively. Only the top 0-0.2 m layer was significantly wetter ($p < 0.05$) in 2012 than in 2011.

3.3.2 Terrain attributes

Slope map.-

Figure 3.2 shows the slope map of the entire catchment, with values ranging from 0 to 22%. The steepest slopes are located near the north-western edge of the catchment, and in the western and eastern part of the catchment. Flatter high elevation zones are found near the southern edge, while flatter low elevation zones appear in the central part of the catchment.

Aspect map.-

The eastern part of the catchment is predominantly north-facing (Fig. 3.2), resulting in higher SWC and subsequently higher ECa values, while the north-western and western part of the catchment, with the steepest slopes, is south-facing. East-facing areas are found in the central part of the catchment, while west-facing slopes are only found in two small areas near the north-western and south-eastern edges of the catchment.

Wetness index (WI) map.-

The topographic wetness index, $WI = \ln(a/\tan\beta)$, where a is the upslope contributing area and β the local slope angle in radians, was calculated using the D-8 procedure to identify areas with potential concentration of runoff water, possibly resulting in higher soil water contents (Fig. 3.2). The parallel lines in the derived wetness index were an artefact of the method used to calculate the upslope contributing area. The highest values, 7.5<WI<15, correspond to flatter low elevation areas of high flow accumulation, mainly in the central part of the catchment, while the lowest values, WI<7.5, are found in areas with a small flow accumulation on steep slopes.

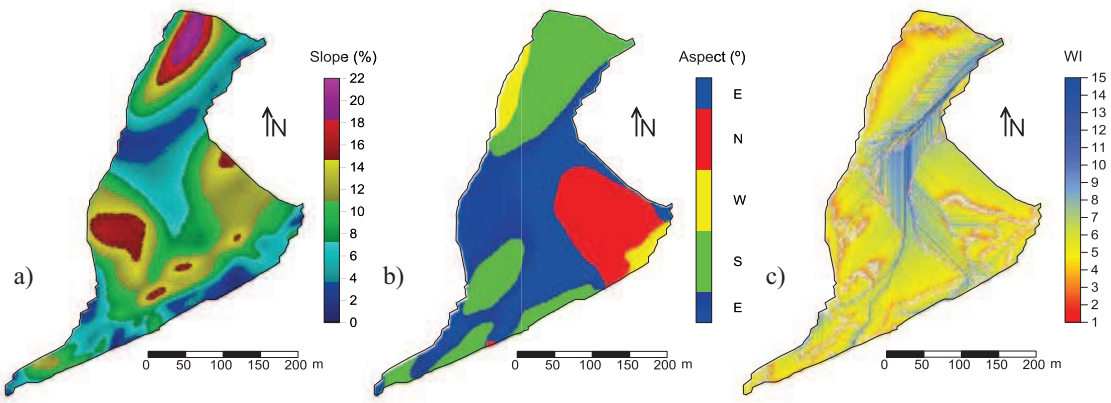

Figure 3. 2 Maps of a) slope, b) aspect and c) wetness index (WI) for the experimental catchment.

3.3.3 ECa measurements and patterns

Point ECa increased from 2011 to 2012 as a result of the larger soil water co[illegible]. Overall the different signals provided ECa values that increased with increasing DOE, yielding the smallest and highest values for the P1.1 and H2 signals, respectively, indicating the presence of more conductive material at deeper horizons. Average values ranged from 18.7 mS m^{-1} for P1.1 (2011) to 74.9 mS m^{-1} for H1 (2012). The values in 2012 roughly doubled those observed in 2011 for the P1.1, P2.1, and H1 coil configurations, while for H2 only a 10% increment was observed. The CV was similar across the four signals for 2011 and about 20 (H2) to 50% (P1.1) smaller in 2012 as compared to 2011, which is generally an effect of the higher mean ECa in 2012 and the increased soil water content in the topsoil. Skewness coefficients ranged from 0.3 (H2) to 1.1 (P1.1) in 2011, and close to 0.45 for all signals in 2012, except for H2 (.52). This shows the tendency to reduce skewness and overall variability as a result of increased soil water content, especially in the top layers where soil moisture increments were largest.

Spatially measured ECa in 2011 (Table 4 b) showed average values ranging from 19.7 (P1.1) to 60.6 (H2), similar to those observed for the point ECa measurements, and indicating the representativeness of the 45 samples locations in terms of ECa. The CV ranged from 43 (H2) to 61 (P1.1) and was slightly higher for the P1.1 signal as compared to the point measurements, while the skewness increment, with respect to the point measurements, decreased with smaller DOEs.

Table 3. 4 a) Descriptive statistics of point apparent electrical conductivity (ECa, mS m^{-1}), for the 2011 and 2012 surveys, and b) descriptive statistics of spatially measured ECa (mS m^{-1}), for the 2011survey See Table 1 for explanation of the four signals.

a)	2011				2012			
	P1.1	**P2.1**	**H1**	**H2**	**P1.1**	**P2.1**	**H1**	**H2**
N*	45	45	45	45	45	45	45	45
m	18.7	36.1	42.3	59.9	53.4	62.4	74.9	63.9
med	15.2	31.1	36.9	55.2	52.6	60.7	73.4	61.8
min	5.7	13.0	14.7	9.0	27.0	27.6	39.8	27.9
max	46.4	76.6	94.2	117.5	95.5	122.7	140.8	127.9
s	9.5	18.1	21.5	29.5	13.9	19.9	21.8	25.1
CV	50.8	50.0	50.8	49.3	26.0	31.8	29.0	39.2
skew	1.08	0.56	0.60	0.31	0.45	0.44	0.43	0.52
kurt	0.90	-0.83	-0.56	-1.01	1.33	0.51	0.34	-0.19

b)	2011			
	P1.1	**P2.1**	**H1**	**H2**
N*	11102	10736	11040	10707
m	19.7	35.9	43.1	60.6
med	17.2	34.9	41.8	62.7
min	2.6	2.4	7.1	0.7
max	113.5	89.6	134.2	132.5
s	12.1	17.2	21.7	26.2
CV	61.5	47.9	50.4	43.3
skew	2.6	0.7	0.9	0.3
kurt	10.4	0.1	0.9	-0.6

*N: number of measurements, m: mean, med: median, min:minimum, max: maximum, *s*: standard deviation, CV: coefficient of variation (%), skew: skewness, kurt: kurtosis.

The largest area of low ECa values was observed near the western edge of the catchment (Figure 3.3), while a smaller area could be identified in the eastern part. Both areas corresponded roughly to zones with steep slopes. The highest ECa values were generally observed in areas with high elevation, in the south and southeastern part of the catchment, characterized by a flatter topography. An area of intermediate ECa values extended from north to south across the catchment, roughly following the course of the main gully.

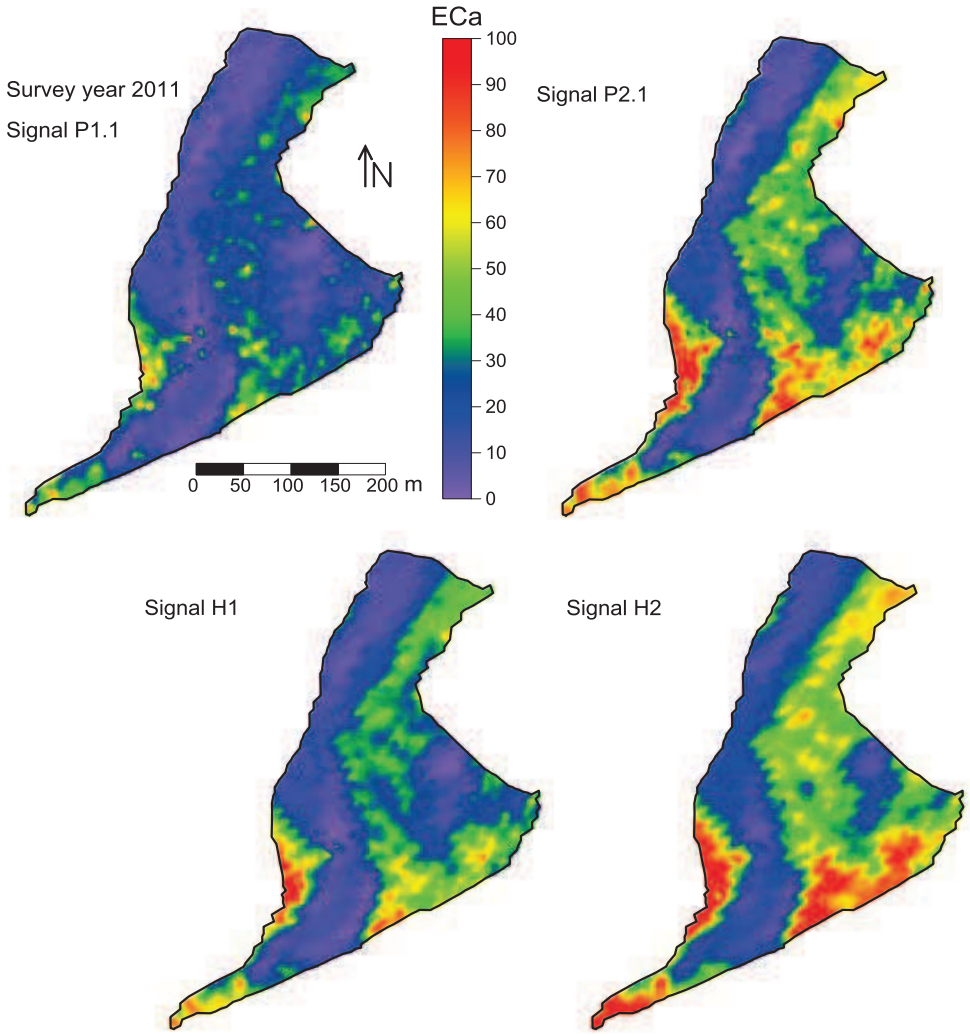

Figure 3. 3 Apparent electrical conductivity (ECa, mS m^{-1}) maps, corresponding to the four measured signals in 2011. See Table 1 for details on each signal.

Correlations between point ECa measured in 2011 and 2012 were significant at $p<0.01$ (Table 5) and increased with increasing DOE, ranging from 0.78 (P1.1) to 0.94 (H2). This shows that the increased topsoil water content caused the smallest correlation between both surveys for the signal with the smallest DOE. This smaller correlation, as compared to signals with higher DOE, indicate the potential usefulness of the P1.1 signal to evaluate spatially the topsoil moisture increment across the catchment. Patterns were also similar among the different signals (Table 5) for the same survey. Correlations between ECa signals for the wetter survey (2012) ranged from 0.79 (P1.1 × H2) to 0.98 (P2.1 ×H1) and were generally somewhat smaller than for the dry survey (2011), ranging from 0.92 (P2.1 × H2) to 0.99 (P1.1 × P2.1 and P2.1 × H1). For the P1.1 × H2 combination the largest difference in correlation between 2011 (0.95) and 2012 (0.79) was observed, as a result of topsoil wetting in 2012.

Table 3. 5 Correlation coefficients between point measurements of apparent electrical conductivity (ECa), for different coil configurations and for the 2011 and 2012 surveys. All coefficients are significant at $p < 0.01$. See Table 1 for explanation of the four signals.

		2011				2012		
		P1.1	**P2.1**	**H1**	**H2**	**P1.1**	**P2.1**	**H1**
2011	**P2.1**	0.99						
	H1	0.97	0.99					
	H2	0.95	0.92	0.93				
2012	**P1.1**	0.78	0.77	0.77	0.76			
	P2.1	0.85	0.85	0.86	0.88	0.96		
	H1	0.90	0.89	0.90	0.93	0.92	0.98	
	H2	0.85	0.86	0.88	0.94	0.79	0.91	0.96

3.3.4 Spatial classification of ECa

Given the strong correlation between different ECa signals and surveys the spatial classification was based on a single signal. The ECa maps for 2011 showed the best correspondence with the canopy coverage pattern of the orthophotograph. The P2.1 signal was chosen since its DOE (1 m) corresponds roughly to the analyzed soil profile depth (0.9 m) in this study. The probability density function of the interpolated 2011 P2.1 ECa measurements exhibited a bimodal distribution (Figure 3.4a). A sum of two Gaussian pdfs was fitted to the histogram and the parameters of both pdfs were estimated. For the first component, corresponding to the local maximum at the left-hand side of the pdf (Figure 3.4a), a mean value of 17.5 mS m^{-1} and a standard deviation of 4 mS m^{-1} was obtained. The second component, corresponding to the local maximum in the center of pdf, a mean value of 42.5 mS m^{-1} and a standard deviation of 15 mS m^{-1} was found. The mean ± the standard deviation of the second component was used to classify the ECa data. The highest ECa values, representing about 25% of the total population, were classified as a third group. As a result, the ECa data were classified according to ECa ≤. 27.5 mS m^{-1} (zone A), 27.5 < ECa < 57.5 mS m^{-1} (zone B), and ECa > 57.5 mS m^{-1} (zone C). This classification resulted in the map shown in Figure 3.4b. Small intrusions of higher or lower ECa values inside the three delimited areas were disregarded. Descriptive statistics for ECa (P2.1), corresponding to the three zones are shown in Table 3.6. Mean ECa values and corresponding standard deviations were 20.7, 44.2, 55.3 mS m^{-1}, and 5.6, 8.2 and 13.9 mS m^{-1}, for zones A, B, and C, respectively. From the comparison of the means and medians it can be deduced that near-normal ECa distributions were obtained for the three classes.

Table 3. 6 Descriptive statistics for the three delimited zones of interpolated apparent electrical conductivity (ECa, mS m^{-1}) corresponding to signal P2.1 for the 2011 survey.

	2011		
	Zone A	**Zone B**	**Zone C**
N*	37526	20372	18874
m	20.7	44.2	55.3
med	20.0	42.9	55.4
min	9.2	13.6	20.7
max	60.3	80.6	87.9
s	5.6	8.2	13.9
CV	26.9	18.5	25.1
skew	0.6	0.6	0.1
kurt	0.1	0.3	-1.0

*N: number of measurements, m: mean, med: median, min: minimum, max: maximum, *s*: standard deviation, CV: coefficient of variation (%), skew: skewness, kurt: kurtosis.

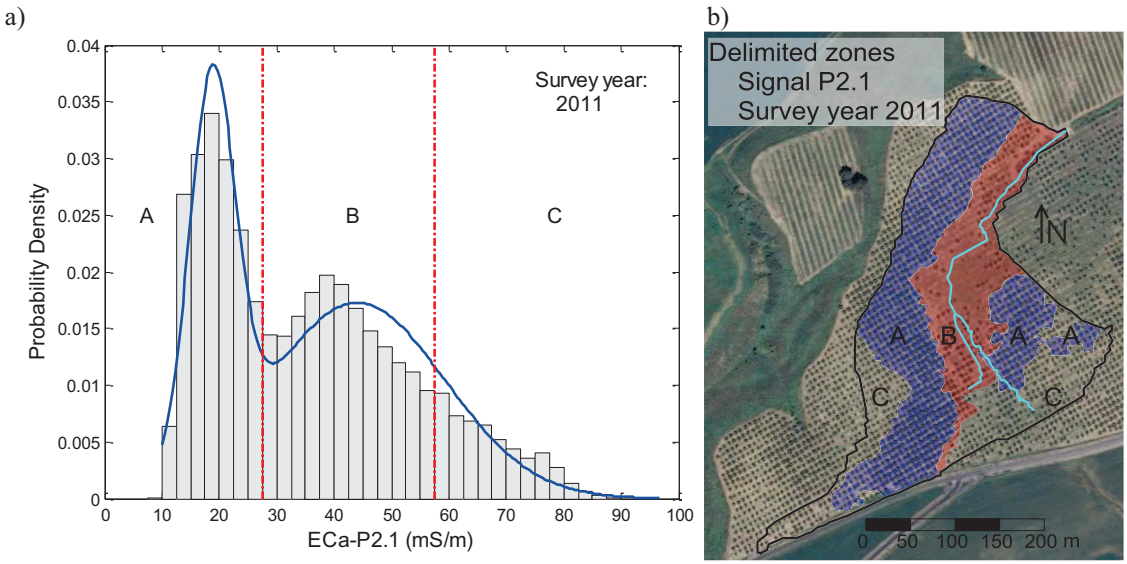

Figure 3. 4 a) Histogram and fitted probability density function of interpolated apparent electrical conductivity (ECa) corresponding to signal P2.1(survey 2011). The dashed lines represent the limits between the three ECa classes (ECa≤27.5; 27.5≤ECa≤57.5; ECa>57.5 mS m^{-1}) used to delimit the three zones. b) Orthophotograph with the three delimited zones (A, B and C) superposed.

3.3.5 Correspondence between ECa and canopy coverage

A strong correspondence existed between the spatial ECa patterns (Figures 3.3 and 3.4) and canopy coverage as observed from the orthophotograph (Figure 3.1). Canopy coverage was 45, 12 and 23% in areas A, B, and C, respectively (Figure 3.5). Zone A, with an area of 3.8 ha and 903 trees, showed the best developed canopies. Only 5% of the trees were missing within this area. Therefore, a canopy coverage of 45% was considered as optimal for this catchment.

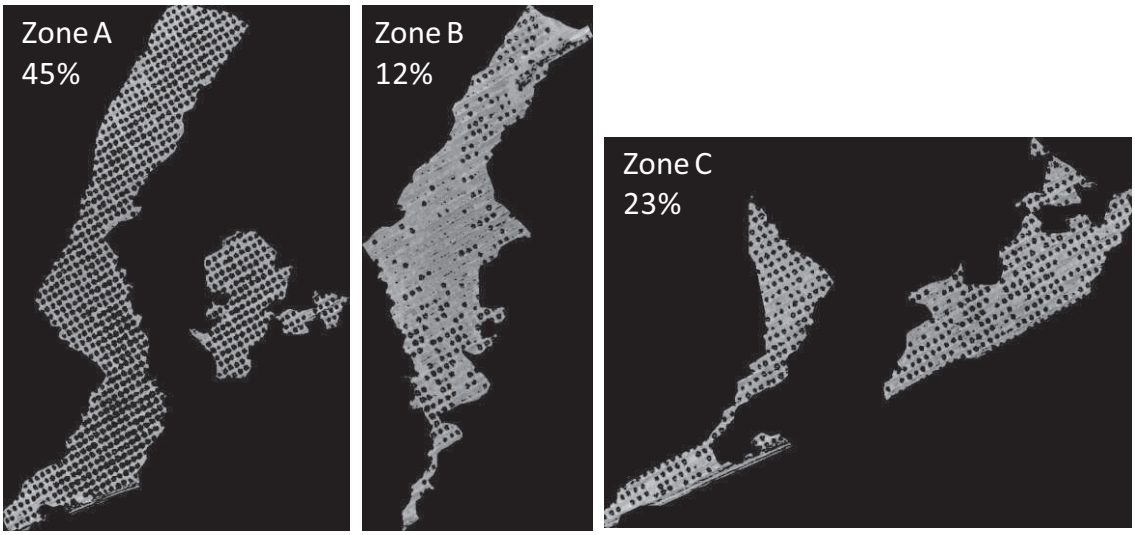

Figure 3. 5 Classified images used for calculating the total tree canopy coverage in the three delimited areas.

Table 3.7 shows the descriptive statistics of projected canopy area of individual trees for the three zones. The number of trees in zone A doubled those found in zone C and quadrupled the number of trees found in zone B. The percentage of missing trees in zones A, B and C was 5, 63 and 23%, respectively. Mean CA in zones A, B and C was 19, 12 and 10 m^2, respectively. Maximum values ranged from 21 m^2, in zones B and C, to 33 m^2 in zone A. Standard deviation ranged from 3 m^2, in zones B and C, to 5 m^2 in zone A. The small skewness and kurtosis values indicated near-normal distributions for CA in the three zones. A one-way ANOVA showed that the means of the three zones were significantly different ($p<0.05$).

Table 3. 7 Number of missing trees and descriptive statistics of projected canopy area (CA) for the three delimited zones.

	CA (m^2)		
	Zone A	**Zone B**	**Zone C**
Missing trees (%)	1.6	73.3	13
N*	858	181	349
m	19	12	10
med	19	11	10
min	5	5	4
max	33	21	21
s	5	3	3
CV	27	28	31
skew	0.1	0.4	0.4
kurt	-0.1	-0.1	0.2

*N: number of trees, m: mean, med: median, min: minimum, max: maximum, *s*: standard deviation, CV: coefficient of variation (%), skew: skewness, kurt: kurtosis.

For each tree, mean ECa was calculated from the interpolated ECa data within the CA. Figure 3.6 shows the relationship between CA and the corresponding mean ECa for the three different zones. Although small CAs were found over the entire ECa range, CAs larger than 20 m^2 only occurred below a threshold ECa of 30 ms m^{-1}. The smallest CAs occurred mostly at ECa values ranging from 60 to 80 mS m^{-1},

corresponding to zone C. Slightly larger CAs were found for ECa values ranging roughly from 30 to 60 mS m^{-1}, corresponding to zone B.

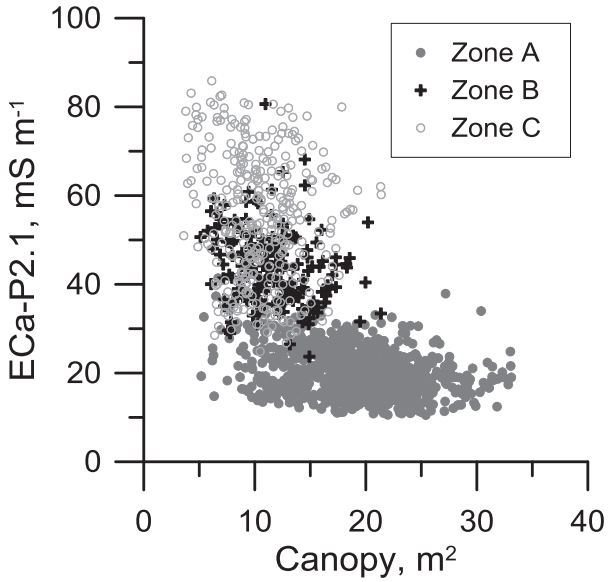

Figure 3. 6 Relationship between projected canopy area (m^2) and apparent electrical conductivity (ECa) for signal P2.1, distinguishing data from the three delimited zones.

3.3.6 Spatial ECa and tree development patterns

Transect data

Data from the nine soil profiles along the transect (see Figure 3.1) indicated high ECa, Z, clay and SWC values at the SW end of the transect (point 18), while at the central, low elevation section of the transect intermediate to high ECa values were observed, and the highest clay and SWC (Figure 3.7). Lower ECa values and high Z, clay and stone content were found at the NE end (point 26). Soil and terrain conditions in the surroundings of the gully (near point 23) result in wetter soil conditions and might lead to saturation and water logging under persisting extremely wet weather conditions. As a result of the shallow C horizon (Table 3.2), similar conditions were found at the SW end of the transect, although the higher elevation of this location would prevent water logging.

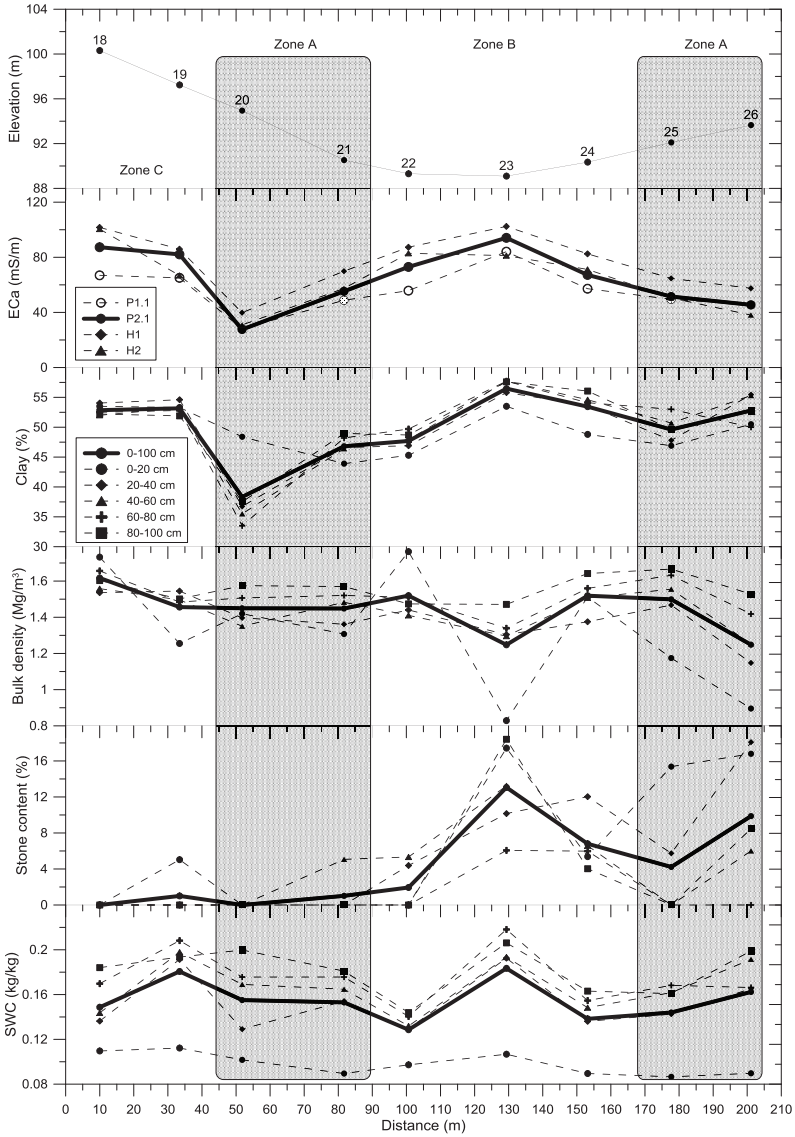

Figure 3. 7 Elevation, apparent electrical conductivity (ECa), clay content, bulk density, stone content and soil water content (SWC) for different horizons at nine locations along the transect shown in Fig. 1.

Spatial soil profile data set

Findings from the transect (Figure 3.7) were then evaluated for the entire field by comparing soil profile properties in the three zones (Table 3.8). A one-way ANOVA showed that clay content in zone A was significantly ($p<0.05$) lower than in zones B and C, with an increasing significance for deeper soil layers (results not shown). Zone B presented a significantly higher soil OM content at all depths as compared to the other two zones, and the highest profile-averaged soil water and stone content, while all soil horizons in zone C contained significantly less sand than the other zones. Silt, EC, pH and bulk density did not show significant differences between the three delimited areas. This means that the observed variations in ECa along the transect are not caused by EC, but are rather a result of soil water content variations and changes in the amount of adsorbed cations of the solid phase (Rhoades et al. 1976; Mualem and Friedman 1991). As a result of the significant differences in clay and sand content, significant differences in bulk density would be expected. Figure 3.7 shows that the variations in bulk density along the profile and the

transect do not reflect clearly the variations in clay content. The bulk density of these expansive clay soils depends also on soil water content, which might obscure the expected relationships with texture.

Table 3. 8 Mean of soil profile-averaged (0-0.9 m) soil water content (SWC, %), measured during the 2012 survey, stone content (%), clay and sand contents (%) and organic matter content (OM, %) for the different zones. Different letters indicate significant differences ($p<0.05$).

Zone	SWC	Stone content	Clay content	Sand content	OM
A	21.6 (b)	2.0 (b)	46 (b)	6.7 (a)	0.7 (b)
B	23.4 (a)	5.7 (a)	50 (a)	6.8 (a)	0.97 (a)
C	22.7 (ab)	1.7 (b)	47.5 (a)	3 (b)	0.53 (b)

The correlations of SWC and soil texture with ECa were higher for the wetter than for the dry survey, as expected (Table 3.9). Under dry soil conditions a significant relationship between OM content and ECa-P1.1 was found, probably as a result of the accumulation of organic residues in downslope areas, leading to higher soil water retention, and as a result of the indirect relationship with clay content. A strong positive correlation between ECa and stone content was found for the 2011 survey. This could be an indirect effect of the downslope accumulation of stones (zone B), where also water accumulates and where clay content is highest. In dry environments, Nobel et al. (1992) and Sauer and Logsdon (2002) found that rock fragments protected the soil underneath from evaporation, leading to wetter soil conditions as compared to bare soil.

Table 3. 9 Correlation coefficients between point-measured apparent electrical conductivity (ECa) corresponding to signals P1.1 and P2.1, and profile averaged (0-0.9 m) clay, organic matter (OM), and stone content for the dry 2011 survey, and soil water content (SWC), sand and clay content for the wetter 2012 survey.

	2011			2012		
ECa	Clay content	OM	Stone content	SWC	Sand content	Clay content
P1.1	0.50*	0.54*	0.61*	0.65*	-0.46*	0.60*
P2.1	0.51*	0.38	0.75*	0.51*	-0.47*	0.58*

The point ECa and topsoil (0-0.2-m) SWC data showed positive increments from 2011 to 2012, except for the H2 signal (Figure 3.8), with decreasing ECa increments for increasing DOEs. No general relationships were found between the ECa and the SWC increments. However, when considering separately the three zones, relationships between ECa and SWC increments appeared for zone A, especially for the signals with the shallowest DOE (P1.1 and P2.1), although with considerable dispersion ($R^2 < 0.26$),. In contrast to zones B and C, positive ECa increments were obtained for the H2 signal in zone A. This indicates that, as a result of better infiltration and water transmission conditions in this zone, SWC also increased in deeper layers, resulting in a positive ECa H2 increment. For the same signal negative ECa increments were found in zone C. Topsoil SWC increments were highest in this zone since water did not move towards deeper layers, as a result of the rather shallow C horizon in this area. Zone B showed an intermediate behavior with a general lack of relationship between ECa and SWC increments for all signals.

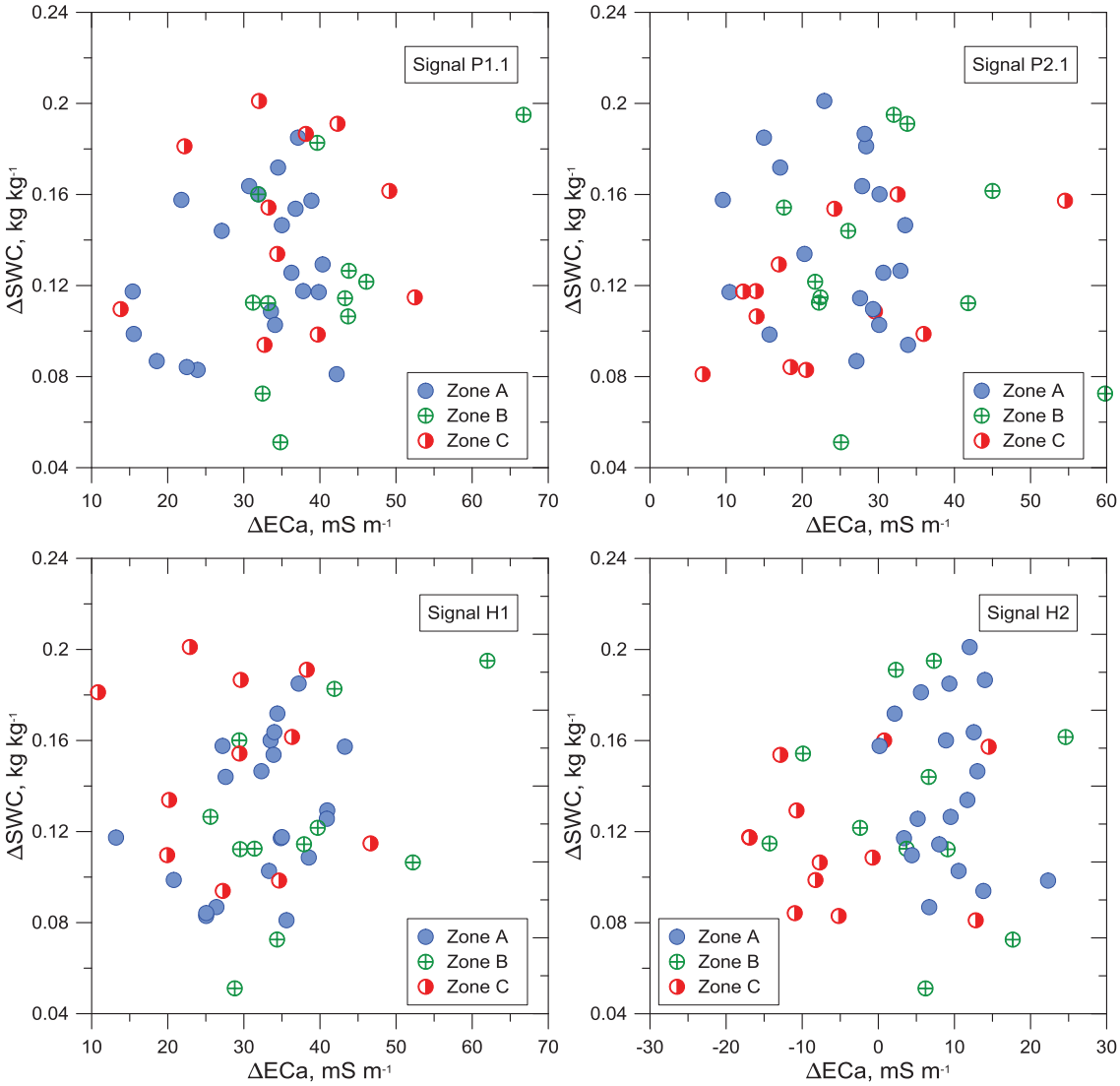

Figure 3. 8 Relationship between soil water content increments (ΔSWC) and apparent electrical conductivity increments (ΔECa) for the four different signals, from the dry to wetter survey of 2011 and 2012, respectively.

3.4 Discussion

Under non-saline conditions, ECa is mainly influenced by the time-variable water content, and subsequently, by soil texture. According to Friedman (2005) the EMI signals in non-saline soils are related to soil moisture, soil texture and soil depth. McCutcheon et al. (2006) found that volumetric soil water content was the dominant factor affecting the spatial and temporal ECa variability, while Harvey and Morgan (2008) found the clay content as the dominant factor. Abdu (2008) made a calibration between ECa and clay content to estimate the soil water holding capacity.

The approach presented here is based on the hypothesis that in this olive-planted catchment with a Vertisol, ECa measurements can be used to assess tree growth problems or die-off, even in advance of plantation establishment, taking also into account SWC, soil properties and topographic attributes. Deficient tree growth and die-off were obvious from field observations and from the orthophotography.

Soil profile samples were taken to understand the orchard-growth variability and EMI surveys were conducted in order to delimit areas with unsatisfactory tee development.

Summary statistics and Pearson's correlation coefficients were calculated from all measured soil properties. Positive correlations between clay and OM content were expected, as both were higher in downslope areas. The negative correlation between Z and stone content was possibly a result of relative stone enrichment in the central part of the transect, near the gully (point 23 in Fig.3.7), as a consequence of the loss of the smaller soil particles. The negative correlation between Z and OM can be explained by the downslope movement of OM and soil particles, and the poor drainage conditions along the downslope area of the field, resulting in limited carbon mineralization.

Soil water content for the 2012 survey was significantly larger than in 2011. Soil water content increased with depth in the 2011 survey, while it decreased with depth in 2012 as a result of the immediacy of the measurements to the last rainfall event.

Measured ECa values were higher in 2012 than in 2011 as a result of the larger SWC in 2012. Also ECa increased with increasing depth of exploration, indicating the presence of more conductive material in deeper soil layers. The spatial ECa pattern was similar for the four measured signal. Maps of topographic attributes such as slope, aspect and wetness index reflected partially the ECa patterns and confirmed the underlying relationships between soil properties and ECa. A spatial classification based on the bimodal P2.1 ECa (DOE = 1 m) distribution was performed to delimit areas with impaired tree development conditions. The ECa data were grouped into three classes, based on the decomposition of the bimodal pdf and resulting in the delimitation of three different areas (A, B, and C). Estimated canopy coverage, projected canopy area and percentage of missing trees supported the validity of this classification.

To identify the underlying relationships between ECa and soil properties causing the spatial patterns in the tree development, a preliminary analysis of point ECa, Z, clay, ρ_b,and stone and soil water content on a transect was made before exploring the entire catchment. Detailed data from the transect (Fig.3.7) provided insight into the relationships between ECa, soil properties, and olive development. Elevation ranged from101 m a.m.s.l. at the SW end of the transect (point 18) to 89 m a.m.s.l. near the gully (point 23). Apparent electrical conductivity for the four signals was highest at the SW end of the transect, as a result of the high and homogeneously distributed clay content across the soil profile in this area. This homogeneous soil profile reveals the Vertic character of this soil. Moving down the slope intrusions of coarser material are found in deeper layers (*e.g.* location 20), as a result of Quaternary and possibly Holocene reworking of the fluvial terrace deposits inside the valley. The presence of stones and coarse fragments was even more prominent along the eastern slope of the transect (Fig. 3.7, points 24-26), resulting in overall lower ECa values despite the high clay contents observed throughout the soil profile. The highest profile-averaged clay content was observed at location 23, in the lowest part of the transect, corresponding to the area where tree development was deficient. At this location clay content was especially high in the deeper layers, resulting in poor drainage conditions which possibly led to root

asphyxia and to diseases such as Verticilium wilt. Figure 3.7 shows also the high profile-averaged gravimetric water content observed at this location at the moment of the sampling. High clay contents and a shallow C horizon were found at the SW end of the transect and can also cause tree development-limiting conditions (see Figure 3.1). Overall, ECa at the NE end of the transect was smaller than the values observed at the SW end, despite the high clay contents found in both areas. The lower ECa values are a result of the higher stone contents observed at locations 23-26, modulated at least partially by higher soil water contents. Bulk density was found not to affect ECa significantly in this study.

The entire catchment was then explored, in accordance to the three delimited zones (Figure 3.4). Pearson's correlation coefficients were calculated between ECa for the P2.1 signal and measured soil properties. Significant correlations were found for clay, sand, OM, stone and SWC. Each of these soil properties were then classified according the zone to which they belonged. Zone A, with the low ECa values, covered an area of high elevation and steep slopes, and showed a significantly lower water and clay content, as compared to zones B and C, while it doubled sand content of zone C, and showed significantly lower stone contents than in zone B. These results suggested that optimal tree development in zone A, with a canopy coverage of 45% (Figure 3.5), might be a result of satisfactory drainage conditions. Zone B, with intermediate ECa values, a flatter downslope area and showed significantly higher water and clay content than in zone A, with significantly higher stone contents than in zones A and C. Unsatisfactory tree development from zone B, with a canopy coverage of 12%, might be a consequence of poor drainage conditions, leading to wetter soil conditions and possibly temporal waterlogging during extremely wet spells, possibly resulting in root asphyxia and infestation by soil-borne pathogens with the consequent wilting effects, especially on young trees. Zone C, with high ECa values, corresponded to a rather flat upslope area, showing intermediate canopy coverage and intermediate water content with respect to zones A and B, and with a significantly higher clay content than in zone A and half of the sand content than in zones A and B. This zone also showed significantly lower stone content than zone B. This zone showed a canopy coverage of 23%, corresponding to intermediate growing conditions.

Results from the entire catchment support those found along the transect. Relationships between soil properties and ECa found along the transect can be used to interpret the observed ECa variations across the entire catchment, and to delimit the most suitable zones for successful development of the olive trees.

Overall, the proposed methodology enabled us to identify the causative variables for deficient tree development or die-off found in this field by using EMI surveys and soil properties measured at eight points along a transect. The zone where the problem was manifested could be accurately delimited using ECa data. Based on this information management practices, such as removing infested trees or not replanting dead trees, can be proposed within the delimited area to reduce inputs and to prevent further spreading of the disease by installing soil management practices (e.g. no-till and cover crops) that limit the transport of soil particles and vegetative material by tillage or runoff water. Moreover, the proposed method can be implemented before the establishment of plantations, to identify and delimit areas with

potential unsatisfactory olive tree development and/or areas with appropriate conditions for infestation by soil-borne pathogens.

3.5 Conclusions

Tree growth problems and die-off are important constraints for profitable olive growing in soils with deficient drainage conditions. In this work zones with impaired olive tree development were detected and delimited, based on ECa measurements. Topographic attributes and soil properties (elevation, soil texture, SWC, OM and stone content) were related with tree development. Also relationships between soil properties and ECa under dry and wetter soil conditions were evaluated to identify the key drivers behind the constrained tree development. The results showed that variations in ECa were mainly related with variations in water, clay, sand, and stone content. The area with the lowest average ECa (zone A) showed optimal tree growth and the highest elevation range, while in the downslope area with intermediate ECa values (zone B) tree-growth and die-off problems ocurred. Also the area with the highest ECa values (zone C) showed acceptable tree development. The downslope position of zone B, in combination with its high clay, OM, stone and water contents possibly cause deficient drainage conditions and can lead to saturation and water logging during extremely wet spells. Such conditions promote root asphyxia and the spread of soil-borne diseases. The relationships between SWC and ECa increments for different signals after rainfall confirmed the better drainage conditions in zone A. Correlations between ECa and soil properties were significant but small, possibly as a result of the large differences in explored soil volumes by both measurements and the non-uniform contribution of the different soil layers to the ECa signal. However the relationships found between ECa and soil properties under different SWCs were useful for assessing soil–olive tree development interactions in this heavy clay soil. In addition, the potential of time-lapse ECa maps, corresponding to the different signals, was explored by analyzing the relationship between ECa and SWC increments across the catchment. Time-lapse ECa mapping constitutes a promising avenue for further analysis of the soil water dynamics across this olive-cultivated catchment, and assessment of its relationship with olive tree development, using measurements corresponding to different SWC situations.

REFERENCES

Abdu H, Robinson DA, Seyfried M, Jones SB (2008) Geophysical imaging of watershed subsurface patterns and prediction of soil texture and water holding capacity. WaterResour Res 44: W00D18, doi:10.1029/2008WR007043

Atwell MM, Wuddivira M, Gobin J, Robinson DA (2013) Edaphic controls on Sedge invasion in a tropical wetland assessed with electromagnetic induction. Soil SciSoc Am J. 77:1865-1874

Calderón R, Navas-Cortés JA, Lucena C, Zarco-Tejada PJ (2013) High-resolution airborne hyperspectral and thermal imagery for early detection of Verticillium wilt of olive using fluorescence, temperature and narrow-band spectral indices. Remote Sens Environ 139:231–245

Callegary J, Ferré TPA, Groom R (2007) Vertical spatial sensitivity and exploration depth of low-induction-number electromagnetic-induction instruments. Vadose Zone J 6:158–167

Callegary J, Ferré TPA, Groom R (2012) Three-dimensional sensitivity distribution and sample volume of low-induction-number electromagnetic-induction instruments. Soil Sci Soc Am J 76:85–91

CAP (2012) Estudios y estadísticas de superficies y producciones agrarias. Available at: http://www.juntadeandalucia.es/agriculturaypesca/portal/servicios/estadisticas/estadisticas/agrarias/superficies-y-producciones.html . Accessed 12February 2014

Clodoveo, ML, Camposeo, S, De Gennaro, B, Pascuzzi, S, Roselli, L (2014) In the ancient world virgin olive oil has been called “liquid gold” by Homer and the “great healer” by Hippocrates. Why is this mythic image forgotten? Food Res Int (Accepted manuscript)

Corwin DL, Lesch SM (2003) Application of soil electrical conductivity to precision agriculture: Theory, principle and guidelines. Agron J 95:455-471

Corwin DL, Lesch SM (2005) Apparent soil electrical conductivity measurements in agriculture. Comput Electron Agric 46:11-43

Corwin DL, Plant RE (2005) Applications of apparent soil electrical conductivity in precision agriculture. Comput Electron Agric 46:1-10

Davis JC (2002) Statistics and data analysis in Geology.3rd ed. John Wiley Chichester, UK

de Backer, G, Bagnara, S, Crepaldi, G, Fernandez-Cruz, A, Godtfredsen, J, Jacotot, B, Paoletti, R, Renaud, S, Ricci, G, Rocha, E, Trautwein, E, Urbinati, GC, Varela, G, Williams, C (1997). International consensus statement on olive oil and the Mediterranean diet: implications for health in Europe. Eur J Cancer Prev 6:418–421

Domsch H, Giebel A,(2004) Estimation of soil textural features from soil electrical conductivity recorded using the EM38. PrecAgric 5:389-409

Doolittle JA, Brevik EC (2014) The use of electromagnetic induction techniques in soil studies. Geoderma 223-225:33–45

Dualem Inc. (2007) DUALEM-21S user’s manual. Dualem Inc., Milton. Canada

European Commision. (2012) EU agriculture - Statistical and economic information – 2012. Available at: http://ec.europa.eu/agriculture/statistics/agricultural/2012/index_en.htm, Accessed 12 February 2014

ESRI 2008. ArcGIS Desktop: Release 9.3. Redlands, CA: Environmental Systems Research Institute.

FAOSTAT (2012) Agricultural statistics.http://faostat.fao.org, Accessed 3 November 2014

Friedman SP (2005) Soil properties influencing apparent electrical conductivity: a review. Comput Electron Agric 46:45–70

Gómez JA, Sobrinho TA, Giráldez JV, Fereres E (2009) Soil management effects on runoff, erosion and soil properties in an olive grove of southern Spain. Soil Tillage Res 102:5-13

Johnson CK, Mortensen DA, Wienhold BJ, Shanahan JF, Doran JW (2003)Site-specific management zones based on soil electrical conductivity in a semiarid cropping system. Agron J 95:303-315

Jung WK, Kitchen NR, Sudduth KA, Kremer RJ, Motavalli PP (2005) Relationship of apparent soil electrical conductivity to claypan soil properties. Soil Sci. Soc. Am. J.69:883–892

Keller GV, Frischknecht FC (1966) Electrical methods in geophysical prospecting. Pergamon Press, New York

Kitchen NR, Sudduth KA, Myers DB, Drummond ST, Hong SY (2005) Delineating productivity zones on claypan soil fields using apparent soil electrical conductivity. Comput Electron Agric 46:285–308

López-Escudero FJ, Mercado-Blanco J (2011) Verticillium wilt of olive: a case study to implement an integrated strategy to control a soil-borne pathogen. Plant Soil 344:1-50

Loumou, A, Giourga, C (2003). Olive groves: 'The life and identity of the Mediterranean'. Agric Human Values, 20:87–95

MAGRAMA(2012) Encuesta sobre superficies y rendimientos de cultivos. 2012. Available at: http://www.magrama.gob.es/es/estadistica/temas/novedades/Olivar2012_tcm7-262578.pdf, Accessed 12February 2014

Martínez G, Vanderlinden K, Espejo AJ, Giráldez JV, Muriel JL (2010) Field-scale soil moisture pattern mapping using electromagnetic induction. Vadose Zone J 9:871-881

Martínez G, Vanderlinden K, Pachepsky Y, Espejo AJ, Giráldez JV (2012) Estimating topsoil water content of clay soils with data from time-lapse electrical conductivity surveys. Soil Sci 177:369-376

McCutccheon MC, Farahani HJ, Stednick JD, Buchleiter GW, Green TR (2006) Effect of soil water on apparent soil electrical conductivity and texture relationships in a dryland field. Biosyst Eng doi:10.1016/j.biosystemseng.2006.01.002

McNeill JD (1980). Electromagnetic terrain conductivity measurement at low induction numbers. Technical Note TN-6.Geonics Limited, Missisauga, Ontario, Canada

Minasny B, Whelan BM, Triantafilis J, McBratney AB (2013) Pedometrics research in the vadose zone – Review and perspectives. Vadose Zone J, doi:10.2136/vzj2012.0141

Mualem Y, Friedman SP (1991) Theoretical prediction of electrical conductivity in saturated and unsaturated soil. Water Resour Res 27:2771–2777

Navas-Cortés JA, Landa BB, Mercado-Blanco J, Trapero-Casas JL, Rodríguez-Jurado D, Jiménez-Díaz RM (2008) Spatiotemporal analysis of spread of infections by Verticillium dahliae pathotypes within a high tree density olive orchard in southern Spain. Phytopathology 98:167–180

Nobel PS, Miller PM, Graham EA(2012) Influence of rocks on soil temperature, soil water potential, and rooting patterns for desert succulents. Oecologia 92:90-96

Palomo MJ, Moreno F, Fernández JE, Dıaz-Espejo A, Girón IF (2002) Determining water consumption in olive orchards using the water balance approach. Agr Water Manage 55:15-35

Rhoades JD, Corwin DL (1981) Determining soil electrical conductivity-depth relations using an inductive electromagnetic soil conductivity meter. Soil Sci Soc Am J 45:255-260

Rhoades JD, Raats PAC, Prather RJ (1976) Effects of liquid-phase electrical conductivity, water content, and surface conductivity on bulk soil electrical conductivity. Soil Sci Soc Am J 40:651–655

Robinson DA, Abdu H, Lebron I, Scott J (2012) Imaging of hill-slope soil moisture wetting patterns in a semi-arid oak savanna catchment using time-lapse electromagnetic induction. J Hydrol 416-417:39-49

Robinson DA, Lebron I, Quejereta JI (2010) Determining soil-tree-grass relationships in a California oak savanna using eco-geophysics. Vadose Zone J 9:528–536

Robinson DA, Abdu H, Jones SB, Seyfried M, Lebron I, Knight R (2008) Ecogeophysical imaging of watershed-scale soil patterns links with plant community spatial patterns. Vadose Zone J 7:1132–1138

Rodriguez-Perez JR, Plant RE, Lambert JJ, Smart DR (2011) Using apparent soil electrical conductivity (ECa) to characterize vineyard soils of high clay content. Precis Agric 12:775–794

Sauer TJ, Logsdon SD (2002) Hydraulic and physical properties of stony soils in a small watershed. Soil Sci Soc Am J 66:1947–1956

Saey T, Simpson D, Vitharana UW, Vermeersch H, Vermang J, Van Meirvenne M (2008). Reconstructing the paleotopography beneath the loess cover with the aid of an electromagnetic induction sensor. Catena, 74:58–64

Saey T, Simpson D, Vermeersch H, Cockx L, Van Meirvenne M (2009) Comparing the EM38DD and DUALEM-21S Sensors for Depth-to-Clay Mapping. Soil Sci Soc Am J 73:7–12

Sánchez-Hernández ME, Ruiz-Dávila A, Pérez de Algaba A, Blanco-López MA, Trapero-Casas A (1998) Occurrence and etiology of death of young olive trees in southern Spain. Eur J Plant Pathol 104:347–357

Semple EC (1931) The geography of the Mediterranean region: Its relation to ancient history. AMS Press, New York

Sherlock M, McDonnell JJ (2003) A new tool for hillslope hydrologists: Spatially distributed measurements of groundwater and soil water using electromagnetic induction. Hydrol Proc 17:1965-1978

Soil Survey Staff (1999) Soil taxonomy: A basic system of soil classification for making and interpreting soil surveys. 2nd ed. NRCS USDA Hbk 436

Testi L., Villalobos FJ, Orgaz F, Fereres E. (2006) Water requirements of olive orchards: I simulation of daily evapotranspiration for scenario analysis. Irrigation Sci 24:69-76

Triantafilis J, Lesch SM (2005) Mapping clay content variation using electromagnetic induction techniques. Comput Electron Agric 46:203–237

Vitharana U, Van Meirvenne M, Simpson D, Cockx L, De Baerdemaeker J (2008) Key soil and topographic properties to delineate potential management classes for precision agriculture in the European loess area. Geoderma 143:206–215

Vitharana UWA, Van Meirvenne M, Cockx L, Bourgeois J (2006) Identifying potential management zones in a layered soil using several sources of ancillary information. Soil Use Manage 22:405-413

Whelan BM, McBratney AB, Minasny B (2002) Vesper 1.5 – spatial prediction software for precision agriculture. In: Robert PC, Rust RH, Larson WE. (eds.) Precision Agriculture, Proceedings of the 6th International Conference on Precision Agriculture, ASA/CSSA/SSSA, Madison, Wisconsin

Chapter 4. Apparent electrical conductivity measurements in an olive orchard under wet and dry soil conditions: significance for clay and soil water content mapping

4.1 Introduction

Olive trees are one of the most common crops in Spain, and especially in Andalusia, where it represents about 26% of the region's agricultural production value (CAPDR, 2011). Already in the classical Greek agricultural literature (Semple, 1931, chapter XIV) recommendations are found for cultivating olive trees on steep slopes, avoiding lowland soils which are prone to waterlogging during wet periods and fungal diseases (Pedrera-Parrilla et al. 2014). More recently, the evolution of the olive oil market and the introduction of better agricultural practices extended olive cultivation to all kinds of soils, including the adoption of drip irrigation to improve yield and fruit quality. In spite of the progress in the cultivation techniques, most of the olive cropping-related environmental issues such as soil erosion and non-point source water pollution still remain. Traditional olive cropping systems rely heavily on soil tillage, leaving an appreciable bare soil fraction prone to erosion losses, especially on the steep slopes under the characteristic high-intensity winter rainfall regime of the region (Gómez et al. 1999). Alternative conservation practices such as the implantation of vegetative soil cover strips are increasingly implemented. Such management practices are highly effective in reducing soil losses, but can pose a burden on water conservation in the long term (Maetens et al. 2012), which is a priority for most rainfed olive farmers. Therefore mixed, farm-specific and spatially-explicit soil management strategies have to be developed in which different soil management strategies are combined across the orchards. Accurate high-resolution soil information, as provided by electromagnetic induction sensors (EMI) is essential for the successful design of such management strategies (Pedrera-Parrilla et al. 2014).

Proximal soil sensing (PSS) was described by Viscarra-Rossel et al. (2011) as "the use of field-based sensors to obtain signals from the soil when the sensor's detector is in contact with or close to (within 2 m) the soil". Electromagnetic induction (EMI) is classified as a noninvasive,

active, mobile and indirect PSS technique. Within this group, electrical conductivity-based sensors have become useful to investigate the magnitude and spatial heterogeneity of soils. These sensors use electrical circuits to determine the ability of soil to conduct electrical charge. Since the electrical properties of the soil are determined by its physical and chemical properties, their variation across a field can serve as a proxy for the spatial variability of the latter properties (Saey et al. 2009). Nowadays, the use of PSS methods allows a more efficient exploration of cropped areas as a result of the non-invasive and non-contact nature of the methods, and the high data density that can be obtained in a small time window, as compared to traditional soil sampling strategies.

In an agricultural context, the variations in apparent electrical conductivity (ECa) within a field are generally dominated by one or two soil properties such as salinity, water content, texture… (Corwin and Lesch, 2003), and ECa can be used as a proxy for the dominant property. Under non-saline conditions ECa depends, in theory, on soil water content and temperature (Keller and Frischknecht, 1966). According to Friedman (2005) the EMI signals in non-saline soils are related to soil moisture, soil texture and soil depth. However, ECa is indirectly also affected by other factors. Several studies (Corwin and Lesch, 2003; Sudduth et al. 2005; Johnson et al. 2003; Amezketa, 2007; Sheets and Hendrick, 1995; Domsch and Giebel, 2004; Doolittle and Brevik, 2014) have demonstrated the adequacy of ECa data as secondary information to estimate other soil properties (e.g. clay, water, and organic matter contents). A large number of empirical relationships have been established relating ECa with properties. Consequently, ECa has emerged as an effective indicator of soil productivity (Kitchen et al. 1999) and has been studied in support of decisions on soil management (Johnson et al. 2003; Corwin and Lesch, 2003; Vitharana et al. 2006).

Several studies (e.g. Rhoades et al. 1976; Nadler and Frenkel, 1980; Kachanoski et al. 1988; Martínez et al. 2012) have described the effect of soil water content (SWC) on soil ECa and the corresponding contribution of SWC variations to variations of ECa. Variations in SWC may therefore complicate the interpretation of ECa measurements in relation to time-stable soil properties such as clay content. A few studies (Brevik et al. 2006; Islam et al. 2012) have suggested that this problem can be overcome by performing EMI surveys when SWC is close to field capacity. However, these conditions are hard to fulfill in the Mediterranean regions as a result of the persistence of long dry spells throughout the year. Field capacity levels are only achieved after a long period of intense rainfall during fall or winter. Drying is very fast during spring and summer inducing extremely low values of SWC. Whereas the use of EMI sensors for mapping the soil ECa has been discussed for various agricultural applications (e.g. Adamchuk et al. 2004; Viscarra-Rossel et al. 2011; Doolittle and Brevik, 2014), their value for agricultural

practices in water-limited agro-ecosystems such as olive orchards remains poorly understood. The practical challenges involved in surveying olive orchards include (1) steep slopes on which olive trees are planted, (2) appearance of gullies, rills and bedrock outcropping as a result of soil erosion, and (3) scarceness of soil moisture conditions near field capacity as a result of the local the climatology. In this study, we address the latter challenge by surveying the ECa of a rainfed olive orchard under both dry and wet soil conditions using EMI. Our aims were to (1) to characterize and compare the spatial variability of soil ECa under wet and dry soil conditions, and (2) to interpret the ECa variability in terms of SWC and clay content.

4.2 Materials and methods

4.2.1 Study site

The experimental catchment "La Manga" (36° 52' 21" N, 5° 7' 44"W), located in Setenil de las Bodegas in the SW of Spain covered 6.7 ha of a rainfed olive orchard (Fig. 1). The trees were planted in 1995 on a 7 × 7-m grid, with an average tree density of about 200 trees ha^{-1}.The mean elevation is 740 m (Fig. 2) and the mean slope is 10 %. The orchard is under minimum tillage and weeds are controlled with herbicides. The soil subgroup is an intergrade between Lithic and Typic Rhodoxeralf (Soil Survey Staff, 1999, pp. 269-270; García del Barrio et al. 1971) with a loamy sandy texture and a maximum depth of 1.2 m to the calcarenite bedrock. The climate is Mediterranean, with a mean annual precipitation of 1100 mm. On average, 75% of the rainfall occurs from October to May, while 25% occurs between June and September as intense and brief rain showers. An area of 1.2 ha in the SE of the catchment was transformed from cereal to olives in 2006. Different management practices are required for the recently established olive trees in this upslope area, which therefore was disregarded in the remainder of this study. A gully intersects the catchment from the SE towards the catchment outlet in the NW and separates the two main subareas and slopes of the catchment.

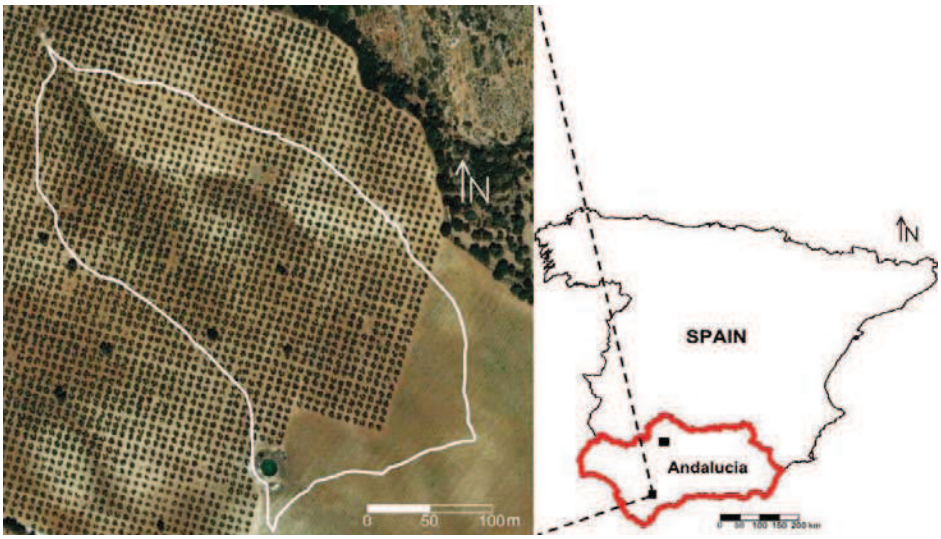

Figure 4. 1 Aerial photograph of the study field, overlying the catchment boundaries and the gully.

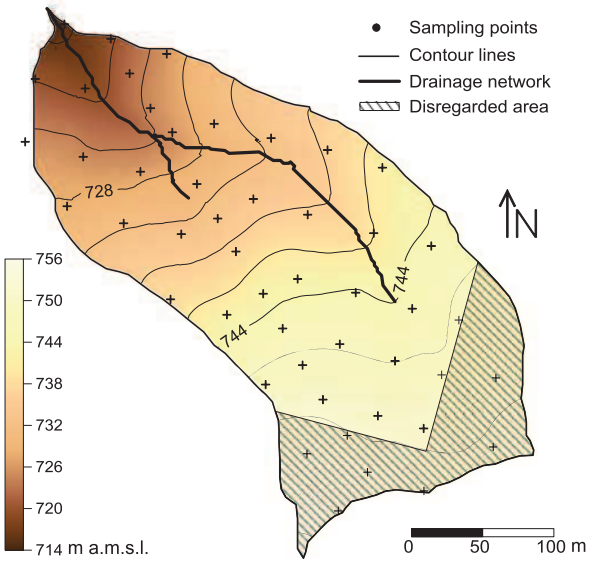

Figure 4. 2 Topography of the studied catchment area in meters above mean sea level (m.a.m.s.l.), drainage network, disregarded area at the southern part of the field with a different management system and location of soil sampling crosses.

4.2.2 EMI sensor set-up

In this study, the ECa survey was performed using a Dualem-21S sensor (DUALEM, Milton, Canada). This EMI sensor is composed of four receiver coils at distances of 1, 1.1, 2, and 2.1 m from the transmitter coil, with a horizontal-coplanar (H) or perpendicular (P) coil pair orientation. This allows the sensor to register four ECa signals simultaneously, representative of four different soil volumes. The depth of exploration (DOE) can be arbitrarily defined as the

depth at which 70% of the response is obtained from the soil volume above that depth (McNeill, 1985; Saey et al. 2009).

We developed a customized mobile measurement configuration for the Dualem-21S sensor, similar to the one presented by Saey et al. (2008), with some modifications for operation in rugged landscapes. A rigid articulated arm was added to provide more stability to the polyvinyl chloride sled and prevent overturning. In addition the GPS antenna was mounted on the sled (Fig. 3) since on sloping and rough terrain the sled does not necessarily follow the path of the towing vehicle on which the GPS antenna is usually mounted. The Dualem-21S was positioned inside the sled at a total height of 0.075 m above the soil surface, as a result of a polyvinyl chloride wear-and-tear plate which is mounted underneath the sled to protect it from corrosion by dry soil and stones. The all-terrain vehicle was equipped with a real time kinematics-differential GPS receiver (Trimble, Sunnyvale, CA) and a rugged Allegro-TK6000 computer (Juniper Systems, Logan, UT) to simultaneously log ECa measurements, coordinates and terrain elevation.

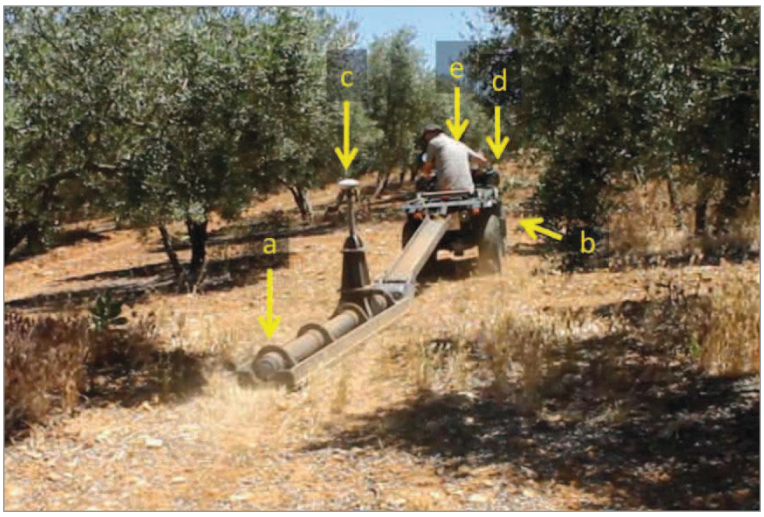

Figure 4. 3 Mobile EMI survey configuration with: (a) sensor sled with a Dualem-21S inside, (b) all-terrain vehicle, (c) GPS-antenna, (d) GPS and (e) field computer.

4.2.3 ECa surveying

Two ECa surveys were performed under dry (ECa-d) and wet soil conditions (ECa-w), in August 2012 and November 2012, respectively. In the days preceding the surveys the more recently planted area was tilled with a disc harrow. Both ECa surveys were conducted at a speed range of 5-10 km/h, along parallel measurement lines along the alleys in-between the tree rows with an approximate separation of 7 m. Inline measurements were recorded every second. A soil moisture/temperature sensor network, equipped with 5TE sensors (Decagon Devices, Pullman, WA), was deployed at eleven locations across the catchment (Espejo et al. 2014). The average

soil temperature measured by the network was used to standardize the ECa values to a reference temperature of 25ºC (Sheets and Hendrickx, 1995).

4.2.4 ECa data processing

After each field survey, ECa measurements were collected at 48 fixed locations on a pseudo-regular grid. Since these ECa measurements were made over a much shorter time interval than the catchment-wide ECa survey, they were used as calibration measurements to evaluate possible drift in the ECa data. We first linked each ECa calibration location to the nearest measurement location from the ECa survey. Subsequently the existing ECa drift was modeled using linear regression. The relationships between measured ECa data and calibration ECa data, from the ECa-w and ECa-d surveys, and then we calculated the difference between their measurements values. These differences were plotted in function of the spent survey time (Delefortrie et al. 2014) and the time drift was modeled through linear regression. The obtained relationship was then used to subtract a time-dependent ECa drift from the original ECa survey measurements.

The field GPS coordinates were recorded in the WGS84 coordinate system and were transformed to the Universal Transverse Mercator projection ETRS89 datum 30N, using the Utm9e-200803 software (Núñez-Maderal, 2008).

To investigate the spatial variability structure of the ECa data, we used Surfer (Golden Software Inc., Golden, Colorado, USA). The non-standardized ECa data were interpolated on a 1 × 1-m grid using ordinary point kriging (Goovaerts, 1997). Finally, to remove the effect of different measurement values between the wet and dry survey, variogram analysis was performed using standardized ECa data (Davis, 2002).

4.2.5 Soil sampling and analysis

An exhaustive soil survey was performed in 2012. Soil profile samples were collected at 48 locations using a 0.093-m diameter cylinder auger (Eijkelkamp Agrisearch Equipment, Giesbeek, The Netherlands) and a percussion drill. Soil samples were taken at 0.1-m depth intervals, from the soil surface down to the bedrock. The samples were analyzed in the laboratory for soil texture according to the hydrometer method (Grossman and Reinsch, 2002). Assuming that processes that can change soil texture (e.g. soil erosion, bedrock weathering) occur over larger time scales than those considered in this study, soil texture analyses was only performed for one survey date. At the same 48 locations, the field was sampled for gravimetric SWC, under dry (August 2012) and wet (November 2012) soil conditions, using a 0.05-m

diameter Edelman hand auger to a depth of 0.2 m; the destructive nature of this measurement technique does not enable repeated SWC observation in the same soil volume. Therefore gravimetric sampling was performed within a 1-m radius from the exact location of the measurement point. Previous study based on soil water retention curves indicated 0.24 kg kg^{-1} as average field capacity in this field and 0.11 kg kg^{-1} as the average wilting point. Henceforth, SWC near field capacity are considered wet soil conditions and SWC far below the wilting point are considered dry soil conditions.

4.3 Results and discussion

4.3.1 ECa drift correction

The linear regression in figure 4a indicates absence of ECa drift in the ECa-w measurements, with a coefficient of determination of 0.98. The linear regression between measurements from the calibration location and the nearest survey measurement location indicated that measured ECa-d data were on average 1.3 times greater than the calibration ECa data (Figure 4b), with a coefficient of determination of 0.89. To correct the time-dependent ECa-d measurements (Delefortrie et al. 2014), the drift was modeled as a function of the spent survey time using linear regression ($r = 0.7$ ($p < 0.05$); $r^2 = 0.5$). After the drift correction some negative values appeared and, in order to keep all the ECa-d measurements, they were all referenced to zero. Henceforth, ECa-d refers to drift-corrected ECa-d.

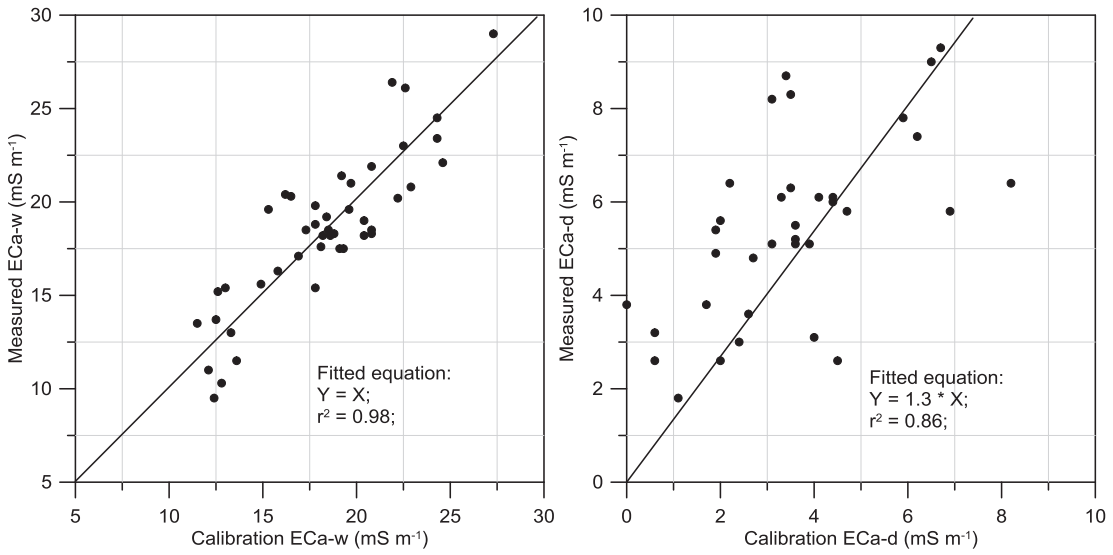

Figure 4. 4 Relationship between each ECa calibration location and the nearest measurement location from the (a) ECa-w and (b) ECa-d surveys. Fitted equation and determination coefficient (r^2) are enclosed into the corresponding plot.

4.3.2 ECa data

Table 1 shows the correlation coefficients among different ECa coil configurations for each survey. Correlation coefficients with P1.1 decreases as the DOE increases for both surveys; (P1.1 x P2.1) > (P1.1 x H1) > (P1.1 x xH1). Greater correlations are found between (P1.1 x P2.1), (P2.1 x H1) and (H1 x H2) for both surveys; signals that explore a more similar soil volume are better correlated. Since all the ECa signals are significantly correlated and the maximum soil depth is 1.2 m, in the remainder of this paper, we will focus on the ECa signal from the 1 m H coil configuration; with a DOE of approximately 1.5 m. Some summary statistics of the ECa-d and ECa-w data sets are given in Table 2. The mean ECa was 4.4 mS m^{-1} and 26.8 mS m^{-1} under dry and wet soil conditions, respectively, which is consistent with a general increasing trend in ECa with SWC. Both the range of the data sets (0.0–11.5 mS m^{-1} for ECa-d versus 14.5–42.0 mS m^{-1} for ECa-w) and the standard deviation (1.7 mS m^{-1} for ECa-d versus 4.7 mS $m^{-1}$for ECa-w) indicate a larger dispersion of ECa under wet soil conditions. However, the coefficient of variation (CV) suggests that the relative variability is larger in dry than in wet conditions (40% versus 20%). Both, ECa-d and ECa-w could be fitted by a normal probability distribution function, evaluated using the Shapiro-Wilk test.

Table 4. 1 Correlation coefficients among different ECa coil configurations for each survey. All correlations are significant correlated ($p<0.05$)

ECa-d				
	P1.1 m	P2.1 m	H1 m	H2 m
P1.1	1			
P2.1	0.92	1		
H1	0.83	0.91	1	
H2	0.70	0.86	0.90	1
ECa-w				
	P1.1 m	P2.1 m	H1 m	H2 m
P1.1	1			
P2.1	0.96	1		
H1	0.86	0.92	1	
H2	0.70	0.82	0.88	1

Table 4. 2 Some summary statistics of apparent electrical conductivity, under dry (ECa-d, mS m^{-1}) and wet (ECa-w, mS m^{-1}) soil conditions.

	min	max	mean	median	s	CV	kurtosis	skewness
ECa -d	0.0	11.5	4.4	4.4	1.7	38	0.3	-0.5
ECa -w	14.5	42.0	26.8	26.8	4.7	17	0.0	-0.6

*min: minimum, max: maximum, s: standard deviation, and CV: coefficient of variation (%).

4.3.3 Clay content and SWC analysis

Summary statistics of clay content and the SWC for dry (SWC-d) and wet (SWC-d) soil conditions, are shown in Table 3. Clay content ranged from 12 to 24 %, with a mean value of 18 % and a standard deviation of 2.7 %. The large range of clay content is a consequence of a clay fringe at the central part of the catchment. The SWC ranged from 0.01 to 0.02 kg kg^{-1} under dry conditions and from 0.11 to 0.17 kg kg^{-1} under wet soil conditions. The mean SWC-d was 0.02 kg kg^{-1}) while the mean SWC-w was 0.13 kg kg^{-1}. These values are representative of extreme soil moisture states that characterize the study region. Note the small range of SWC under dry soil conditions. The large difference between these mean values illustrates the strong seasonal variations in SWC in the Mediterranean regions. In addition, the CV of the SWC within the catchment is twice as large under dry (20 %) as compared to wet conditions (12 %), indicating the heterogeneous spatial distribution of soil properties in this field. Clay content and SWC can be fitted by a normal probability distribution function, evaluated by the Shapiro-Wilk test.

Table 4. 3 Summary statistics of SWC, under dry (SWC-d, kg kg^{-1}) and wet (SWC-w, kg kg^{-1}) soil conditions, and clay content (%). Soil samples for SWC determination were taken to a depth of 0.2 m, while soil samples for clay content determination were taken from the soil surface down to the bedrock.

	min	max	mean	median	*s*	CV	kurtosis	skewness
SWC-d	0.01	0.02	0.02	0.02	0.00	21	0.17	0.01
SWC-w	0.11	0.17	0.13	0.13	0.02	12	-0.34	0.47
Clay content	12.0	23.0	18.2	18.9	2.7	15	-0.5	0.1

*min: minimum, max: maximum, *s*: standard deviation, and CV: coefficient of variation (%).

Relationships between the spatial patterns of these properties under dry and wet soil conditions (Figure 5) showed higher SWC with higher clay contents. The relationship was significant ($r = 0.66$; $p < 0.05$) and similar for both surveys.

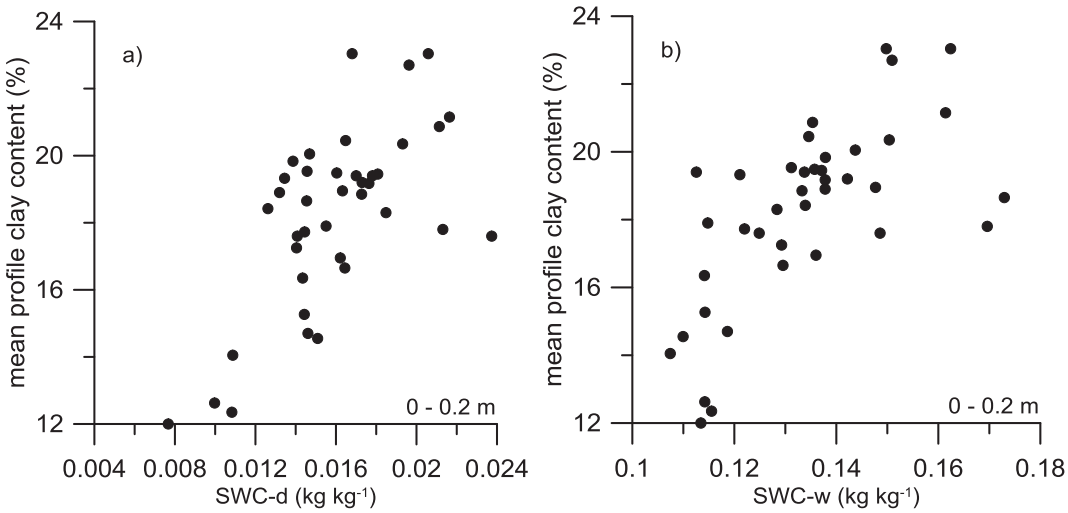

Figure 4. 5 Relationships between SWC and clay content under (a) dry and (b) wet soil conditions.

Spatial patterns of these soil properties are shown in figure 6. Clay content greater than 20 % is located at the central part and at the NW of the catchment, which correspond to the NE facing slope (figure 6a). Above-average SWC-d (figure 6b) and SWC-w (figure 6c) values are found in the same zones. The lowest clay content and SWC are both located at the N of the catchment, which correspond to the SW facing slope (figure 6). Because ECa responds not only to variations in SWC, but also to other controlling factors which affect the conductivity of the solid and liquid soil phases (Zhu et al. 2010; Friedman et al. 2005), we observed that clay content influences the spatial pattern of ECa in this field.

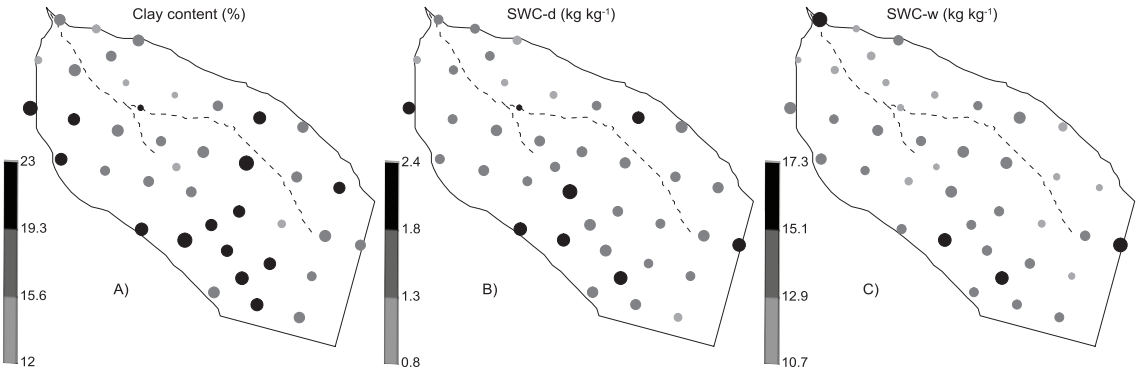

Figure 4. 6 Location map for clay content (a), SWC-d (b) and SWC-w (c), with superposition of the drainage network. The diameter of the circles is proportional to values of the variables.

4.3.4 Variogram analysis and kriging

Figure 7 shows the experimental variogram and the corresponding fitted spherical variogram model for the ECa-w and ECa-d, before and after standardization.

$$\gamma(h) = c_0 + c_1 \cdot \left(\frac{3h}{2a} - \frac{1}{2}\left(\frac{h}{a}\right)^3 \right) \qquad if \qquad 0 < h \leq a \tag{4.1}$$

$$\gamma(h) = c_0 + c_1 \qquad if \qquad h < a$$

$$\gamma(0) = 0$$

The parameters of the fitted variogram models are given in Table 4. The generally higher variogram values for the ECa-w data as compared to the ECa-d data (Figure 7, left) are consistent with the higher standard deviation. The relative nugget effect (RNE) is identical for both surveys, indicating that the unstructured proportion of the total spatial variability is independent of the general soil moisture conditions. This is confirmed by the resemblance of the variograms for wet and dry conditions after standardization (Figure 7, right), indicating that the spatial structure of standardized ECa remains constant in time. Different results are found for different soils, *e.g.* on an agricultural alluvial plain with a buried riverbed crossing the plain, where Nagy et al. (2013) concluded that volumetric moisture content could be mapped by applying ECa measurements.

Table 4. 4 Parameters of the spherical variogram and standardized spherical variogram models for apparent electrical conductivity under dry (ECa-d, mS m^{-1}) and wet (ECa-w, mS m^{-1}) soil conditions.

	C_0	C_1	a (m)	RNE
ECa-d non-standardized	0.57	2.95	145	16.19
ECa-w non-standardized	4.10	25.00	130	14.09
ECa-d standardized	0.20	1.18	140	14.50
ECa-w standardized	0.18	1.14	130	13.64

*C_0 the nugget variance, C_1 the structured variance, a the range, and RNE the relative nugget effect (%).

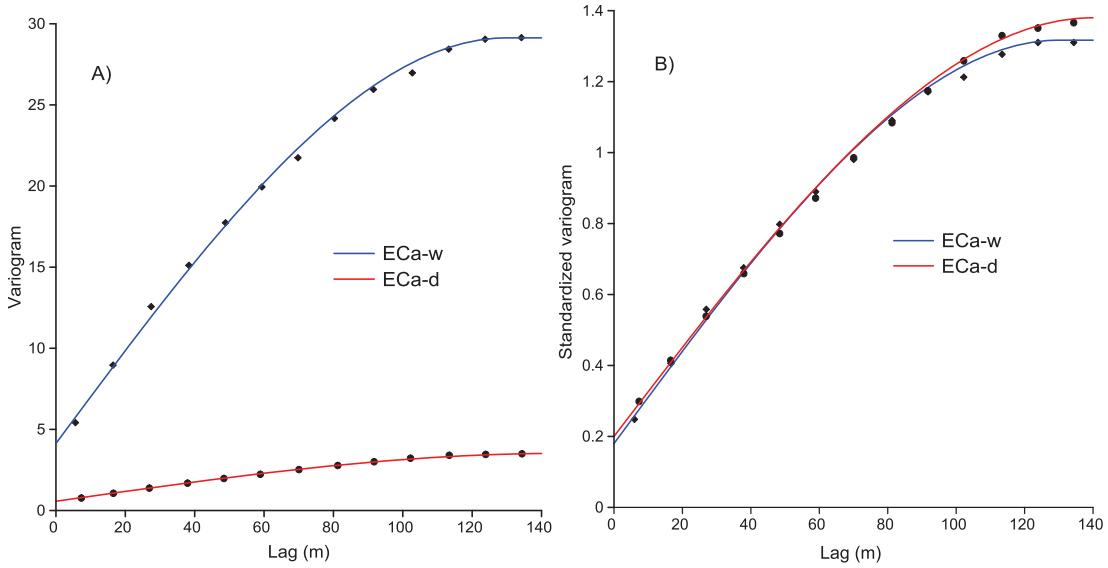

Figure 4. 7 a) Experimental variograms and the corresponding fitted models for the ECa-w and ECa-d, and b) standardized experimental variograms and the corresponding fitted models for the ECa-w and ECa-d.

The maps of the interpolated ECa-w and ECa-d data are shown in Figure 8a and 8b, as well as the map of ΔECa (Figure 8c). Both ECa maps show similar patterns. The highest ECa values are observed in a SW-NE oriented zone at the center of the field and in a narrow zone around the northern part of the gully. The lowest ECa values occur in the NE of the catchment area, on the SW-facing slope. The ΔECa map shows higher ECa differences mainly near the gully. Similitudes between the ΔECa map and the aerial photograph (Fig. 1) are observed. Lighter shades of grey on the photograph and the blue areas on the map, as well as the darker shades of grey and the red areas, are similarly spatial distributed. Indicating what has been found in other studies, ECa can be used as a proxy to determine soil properties.

The ECa-w and ΔECa map (Fig. 8b and 8c) showed, additionally, two small and elongated areas along the gully, with high ECa values. These two areas could not be identified on the ECa-d map probably due to the small range of SWC under this soil conditions (Fig. 8a). Because the ECa-w survey was performed a few days after an intense rainfall event, the high ECa values in these two areas can be explained by soil water accumulation, in the downslope area near the edge of the gully. This fact recommends that measuring the ECa under different moisture conditions can provide additional information about the relationships between soil moisture dynamics and soil texture.

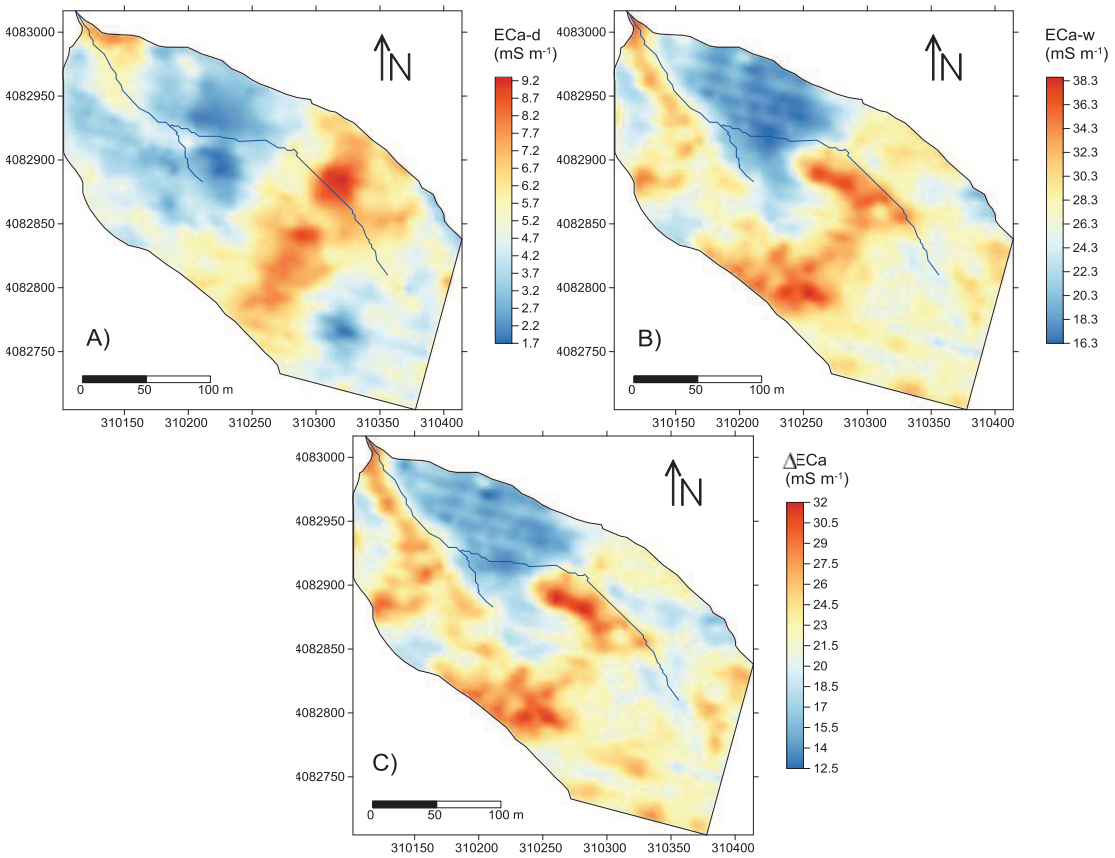

Figure 4. 8 Interpolated ECa-d (a) and ECa-w (b) measurements, and ΔECa map of the difference (c) between interpolated ECa-w and ECa-d, with superposition of the main drainage network.

4.3.5 Relation between ECa and soil properties

The computed Pearson correlation coefficients (*r*) between ECa-d, ECa-w, SWC-d, SWC-w and clay content are included in Table 5. The ECa data from the different surveys are strongly correlated ($r = 0.68$) suggesting that the spatial ECa pattern is stable in time, which agrees with our inferences from comparing the standardized variogram mentioned above. Similar results were obtained by Serrano et al. (2013). For both surveys, a significant correlation between ECa and clay content was observed, which is consistent with the dominant influence of soil texture on soil ECa as reported in several previous studies (e.g. Corwin and Lesch, 2005). However, the correlation was almost twice as high under wet as compared to dry conditions (0.64 versus 0.35), suggesting that ECa is a more valuable proxy for clay content if the ECa survey is performed under wet soil conditions. The correlation between ECa and SWC under wet soil conditions doubled the correlation found under dry soil conditions (0.6 versus 0.3), suggesting that ECa is more valuable to estimate soil water content under wet than dry soil conditions. Note the similarity between the figures for the ECa-clay and ECa-SWC relationships. Clay content and SWC show a strong positive correlation that is stable in time as evidenced by an identical correlation ($r = 0.66$) for both surveys. This result indicates that soil texture, and clay content in

particular, is a key factor determining the soil water dynamics in this water-limited environment. The SWC data sets of the two survey dates are also strongly correlated (r = 0.63). This is a remarkable result given the extremely small SWC-d data range found across the field (0.016 kg kg^{-1}) and provides evidence of the accuracy and precision of the used gravimetric sampling strategy.

Hence, the relative spatial variations of SWC seem to remain constant over time, which could be attributed to their strong relation with the spatial variations in clay content, presumed to be stable over the time window considered. This effect is confirmed by the location maps of clay content and SWC shown in figure 6 and by the relationships shown in figure 5: the areas with highest clay content correspond with areas with the highest SWC, for both survey dates.

Table 4. 5 Correlation coefficients among ECa (mS m^{-1}), clay content (%), and SWC (kg kg^{-1}), under wet (-w) and dry (-d) soil conditions.

	ECa-d	ECa-w	Clay content	SWC-d	SWC-w	ΔECa	ΔSWC
ECa-d	1						
ECa-w	0.68*	1					
Clay content	0.35*	0.64*	1				
SWC-d	0.27	0.46*	0.66*	1			
SWC-w	0.15	0.54*	0.66*	0.63*	1		
ΔECa	0.31	0.91*	0.63*	0.45*	0.61*	1	
ΔSWC	0.11	0.51*	0.60*	0.49*	0.98*	0.59*	1

*Significant correlations ($p<0.05$)

To investigate the effect of varying SWC over time on ECa, the difference between the co-located SWC measurements from the two survey dates (ΔSWC) and the corresponding differences between the ECa measurements (ΔECa) were also calculated (Table 5). The high correlation (r = 0.60) between these differences shows that the higher mean SWC in November as compared to August contributed to the corresponding higher mean ECa. In addition, it indicates that locations with larger differences in SWC also show larger differences in ECa (Fig. 8c). In addition, the high correlations between clay content and ΔECa (r = 0.63) and between clay content and ΔSWC (r = 0.60) suggest that the locations with the highest ΔSWC correspond to locations with the highest clay content. Thus, while seasonal variations of ECa can be related to variations in SWC, spatial variations of ECa can, similarly, be traced to variations in clay content, both directly and indirectly through their effect on the spatial distribution of soil water.

4.4 Conclusions

Although the use of EMI sensors is recommended under wet soil conditions (near field capacity; 0.24 kg kg^{-1} in this study catchment), our study showed that this is not an absolute prerequisite. Similar to previous studies, we found the soil ECa to be strongly positively correlated with clay content. Surveying of ECa during wet periods of the Mediterranean climate will result in overall higher ECa measurement values and in higher correlations between ECa and clay content. Hence, to establish quantitative relationships between soil ECa and clay content, seasons favoring wet soil conditions might provide a more appropriate ECa survey timing. However, relative spatial variations in ECa showed to be stable in time and, hence, are independent of the general soil water statues, as was explained by their dominant relation with the soil clay content. Soil texture, in particular clay content– a soil property that is relatively stable in time, at least on a seasonal time scale- was dominantly related to ECa, and also to ΔSWC, thus, dry soil conditions do not necessarily undo the advantages of EMI-based ECa surveying for the spatial investigation of soil properties such as soil texture. Nonetheless, repeated surveying over time can provide additional information about highly-time variable soil properties such as SWC. We concluded that ECa surveys are a useful source of soil information, independently of the soil moisture content. Wet soil conditions, however, were more appropriate to estimate clay content from soil ECa. Since the spatial ECa-SWC relationship is also affected by other ECa controlling factors such as clay content it is challenging to infer the spatial SWC distribution from ECa surveys, especially for small SWC data ranges. ECa surveys are however more useful for estimating the temporal evolution of SWC. Despite the extreme climatological conditions in which olives are cultivated, EMI-based soil surveying can be considered a key tool for precision soil management in such cropping systems.

REFERENCES

Adamchuk V.I., Hummel J.W., Morgan M.T. Upadhyaya S.K. 2004. On-the-go soil sensors for precision agriculture. Comput. Electron. Agr., 44, 71-91.

Amezketa E. 2007. Use of an electromagnetic technique to determine sodicity in saline-sodic soils. Soil Use Manage., 23(3):278-285.

Brevik E.C., Fenton T.E., Lazari A. 2006. Soil electrical conductivity as a function of soil water content and implications for soil mapping. Precis. Agric., 7:393-404.

CAPDR (2011). Ley del olivar. Available at: http://www.juntadeandalucia.es/agriculturaypesca/portal/contenidos-destacados/anteproyecto-de-ley-del-olivar.html. Accessed 8 July 2014.

Corwin D.L., Lesch S.M. 2003. Application of soil electrical conductivity to precision agriculture: Theory, principle and guidelines. Agron. J., 95:455-471.

Corwin D.L., Lesch S.M. 2005.Characterizing soil spatial variability with apparent soil electrical conductivity: I. Survey protocols. Comput. Electron. Agr., 46:103-133.

Davis J.C. 2002. Statistics and data analysis in geology, third ed. Wiley, New York.

Delefortrie S., De Smedt P., Saey T., Van De Vijver E., van Meirvenne M. 2014. An effcicient calibration procedure for correction of drift in EMI survey data. L. Appl. Geophys., DOI:10.1016/jappgeo.2014.09.004.

Domsch H, Giebel A. 2004. Estimation of soil textural features from soil electrical conductivity recorded using the EM38. Precis. Agric., 5:389-409.

Doolittle J.A., Brevik C. 2014. The use of electromagnetic induction techniques in soils studies. Geoderma, 223-225:33-45.

Dualem Inc. 2007. DUALEM-21S user's manual. Dualem Inc., Milton. Canada.

Espejo A., Giráldez J.V., Vanderlinden K., Taguas E.V., Pedrera A. 2014. A method for estimating soil water diffusivity from moisture profiles and its applications across an experimental catchment. J. Hydrol., 516:161-168.

Friedman S.P. 2005. Soil properties influencing apparent electrical conductivity: a review. Comput. Electron. Agric., 46:45–70.

García del Barrio I., Malvárez L., González J.I. 1971. Mapas provinciales de suelos. Cádiz. Ministerio de Agricultura. Madrid.

Gómez J.A, Giráldez J.V., Pastor M., Fereres E. 1999. Effects of tillage method on soil physical properties, infiltration and yield in an olive orchard. Soil Till. Res., 52(3-3):167-175.

Goovaerts P. 1997. Geostatistics for natural resources evaluation. Oxford UniversityPress, Oxford, UK.

Grossman R.B., Reinsch T.G. 2002. The solid phase, in: Dane, J. H., Topp, G. C. (Eds.), SSSA Book Series: 5. Methods of Soil Analysis. Part 4 – Physical Methods. Soil Science Society of America, Inc. Madison, Wisconsin, USA, pp. 201-415.

Islam M.M., Meerschman E., Saey T., De Smedt P., Van De Vijver E., van Meirvenne, M. 2012. Comparing apparent electrical conductivity measurements on a paddy field under flooded and drained conditions. Precis. Agric., 13:384-392.

Johnson C.K., Mortensen D.A., Wienhold B.J., Shanahan J.F., Doran J.W. 2003. Site-specific management zones based on soil electrical conductivity in a semiarid cropping system. Agron. J., 95:303-315

Kachanoski R.G., Wesenbeeck I.V., Gregorich E., 1988. Estimating spatial variations of soil water content using noncontacting electromagnetic inductive methods. Can. J. Soil Sci., 68:715-722.

Keller G.V., Frischknecht F.C. 1966 Electrical methods in geophysical prospecting. Pergamon Press, New York.

Kitchen N.R., Sudduth K.A., Drummond S.T. 1999 Soil electrical conductivity as a crop productivity measure for claypan soils. J. Prod. Agric., 12:607-617.

Maetens W., Poesen J., Vanmaercke M. 2012. How effective are soil conservation techniques in reducing plot runoff and soil loss in Europe and the Mediterranean? Earth-Sci. Reviews, 115:21-36.

Martínez G., Vanderlinden K., Pachepsky Y., Espejo A., Giráldez J.V. 2012. Estimating topsoil water content of clay soils with data from time-lapse electrical conductivity surveys. Soil Sci., 177:369-376.

McNeill J.D. 1980. Electromagnetic terrain conductivity measurement at low induction numbers. Technical Note TN-6.Geonics Limited, Missisauga, Ontario, Canada.

Nadler A., Frenkel H. 1980. Determination of soil solution electrical conductivity from bulk soil electrical conductivity measurements by the four electrode method. Soil Sci. Soc. Am. J., 44:1216-1221.

Nagy V., Milics G., Smuk N., Kovács A.J., Balla I., Jolánkai M., Deákvari J., Szalay K.D., Fenyvesi L., Štekauerová V., Wilhem Z., Rajkai K., Németh T., Neményi M. 2013. Continuous field soil moisture content mapping by means of apparent electrical conductivity (ECa) measurement. J. Hydrol. Hydromech., DOI: 10.2478/johh-2013-0039.

Núñez-Maderal E. 2008. Calculadora Geodésica edición especial para la Península Ibérica, Cartesia.org, Spain.http://www.cartesia.org/download.php?op=viewdownloaddetails&lid=172&ttitle=Calculadora_UTM-Geogr%E1ficas_Espa%F1a. Accessed 11 July 2014.

Pedrera-Parrilla A., Martínez G., Espejo-Pérez A.J., Gómez J.A., Giráldez J.V.,Vanderlinden K. 2014. Mapping impaired olive tree development using electromagnetic induction surveys. Plant Soil, DOI: 10.1007/s11104-014-2207-5.

Rhoades J.D., Raats P.C.A., Prather R.J. 1976. Effects of liquid-phase electrical conductivity, water content, and surface conductivity on bulk soil electrical conductivity. Soil Sci. Soc. Am. J., 40:652-655.

Saey T., Simpson D., Vitharana U.W.A., Vermeersch H., Vermang J., van Meirvenne, M. 2008. Reconstructing the paleo-topography beneath the loess cover with the aid of an electromagnetic sensor. Catena, 74(1):58-64.

Saey T., Simpson Vermeersch H., Cockx L., Van Meirvenne M. 2009. Comparing the EM38DD and DUALEM-21S sensors for depth-to-clay mapping. Soil Sci. Soc. Am. J., 73, 7-12.

Semple E.C. 1931. The geography of the Mediterranean region: Its relation to ancient history. AMS Press, New York

Serrano J.M., Shahidian S., Marques da Silva J.R. 2013. Apparent electrical conductivity in dry versus wet soil conditions in a shallow soil. Precis. Agric., 14:99-114.

Sheets K.R., Hendrickx J.M.H. 1995. Noninvasive soil water content measurement using electromagnetic induction. Water Resour. Res., 31(10), 2401-2409.

Soil Survey Staff. 1999. Soil taxonomy: A basic system of soil classification for making and interpreting soil surveys. 2nd ed. NRCS USDA Hbk 436.

Sudduth K.A., Kitchen N. R., Wiebold W.J., Batchelor W.D., Bollero G.A., Bullock D.G., Clay D.E., Palm H.L., Pierce F.J., Schuler R.T., Thelen K.D. 2005. Relating apparent electrical conductivity to soil properties across the north-central USA. Comput. Electron. Agr., 46:263-283.

Viscarra-Rossel R.A., Adamchuk V.I., Sudduth K.A., McKenzie N.J., Lobsey C. 2011. Proximal soil sensing: an effective approach for soil measurements in space and time. Adv. Agron., 113, 243-291.

Vitharana U.W.A., van Meirvenne M., Cockx L., Bourgeois J. 2006 Identifying potential management zones in a layered soil using several sources of ancillary information. Soil Use Manage., 22:405-413.

Zhu Q., Lin H., Doolittle J. 2010. Repeated electromagnetic induction surveys for determining subsurface hydrologic dynamics in an agricultural landscape. Soil Sci. Soc. Am. J., 74:1750Y1762.

Chapter 5. Assessing the contribution of the clay content to apparent electrical conductivity measurements under varying soil water contents.

5.1. Introduction

Soil is spatially heterogeneous due to differences in origin or parent material, climate, topography, time and management practices (Sommer, 2006). In an agricultural context the spatial variability of subsoil horizons is governed by pedogenic process, while the topsoil variability is predominantly influenced by farming practices (Sinegani et al. 2005). This often causes the topsoil to be more homogeneous than the subsoil due to tillage homogenization.

Nowadays, the use of non-invasive and non-contact geophysical methods makes it easier to explore cropped areas. Electromagnetic induction (EMI) sensors that measure the soil apparent electrical conductivity (ECa) use electrical circuits to determine the ability of a soil to conduct electrical charge. Soil spatial variability is then expressed in terms of spatial soil ECa variability. The magnitude and spatial heterogeneity of ECa in a field is often dominated by one or two soil properties (Corwin and Lesch, 2003), and ECa can be used as a proxy for the dominant property. Several studies (Corwin and Lesch, 2003; Sudduth et al. 2005; Johnson et al. 2003: Amezketa, 2007: Sheets and Hendrickx, 1995; Domsch and Giebel, 2004) have demonstrated the usefulness of ECa measurements as secondary information to map other soil properties. Several studies have tried to establish relationships between ECa and soil properties such as water content, salinity, clay content, organic matter content (OM), depth to contrasting soil layers, soil compaction, and organic carbon content (Kachanoski et al. 1988; Brevik et al. 2006; Slavich and Petterson, 1990; Corwin and Lesh, 2005; McCutcheon et al. 2006; Saey, 2008; Brevik and Fenton, 2004; Martinez et al. 2009). Although ECa was historically used to evaluate soil salinity (Rhoades et al. 1976), nowadays it has emerged as an effective and rapid indicator of soil variability and soil productivity (Kitchen et al. 1999), to support decisions on

soil management, and to evaluate spatio-temporal variability of soil properties (clay content, soil water content, salinity...)

Soil water content can hamper the straightforward interpretation of ECa. Rhoades et al. (1976) and Nadler and Frenkel (1980) found that soils with higher water contents showed greater ECa. Even under homogeneous soil conditions, moisture variability can account for an important fraction of the total ECa variability. In low conductive environments with a small ECa range, a general understanding of the soil water content in the surveyed areas is highly recommended to assess its potential effect on ECa (Brevik et al. 2006).

As a result, the relationship between ECa and a time-stable property (*e.g.* clay content) depends also on the status of the transient properties such as soil water content. In an attempt to reduce these effects, Brevik et al. (2006) recommends to perform EMI surveys only under wet soil conditions, preferably close to field capacity. In dry environments, where such soil moisture conditions are seldom met, it will be necessary to determine which properties dominate the sensor's response in order interpret correctly the information from the ECa data.

Numerous methods have been proposed to disentangle the contribution of soil properties to geophysical signals (ECa): principal component analysis, time-lapse imaging, inversion, correlation and regression analysis… A literature review shows that there is not a uniquely valid method for that purpose. Peralta et al. (2013) calculated a principal component-stepwise regression and showed that clay, OM, soil water content (SWC), and cation exchange capacity were the key loading factors for explaining ECa, and based on these results three homogeneous zones were delimited on the basis of an analysis of variance (ANOVA). Robinson et al. (2012) estimated soil moisture content from the ECa difference values obtained by time-lapse imaging. Martinez et al. (2009) improved the spatial distribution of soil organic carbon taking into account normalized ECa differences and fuzzy k-means classification. In a later study, Martinez et al. (2012) combined multiple EMI surveys to include more information coming from the ECa variability, and results from a multiple regression analysis between ECa and SWC increased. Based on the hypothesis of a two layered soil, Saey et al. (2008) implemented an inversion model to estimate the depth to the clay layer, and Triantafilis and Santos (2013) used the inversion algorithm EM4Soil.

But from all proposed methods, correlation analysis and multiple regression analysis are the most extended approximation for determining relationships between ECa and soil properties. Kachanoski et al. (1988) based their study on a correlation analysis between soil ECa, SWC and soil properties, and on a lineal regression analysis from which a second-order equation was used

to estimate SWC from ECa. Harvey et al. (2009) estimated clay content from ECa based on a linear regression analysis, after results obtained from a correlation analysis between ECa and soil properties. Siri-Prieto et al. (2006) calculated a correlation analysis between ECa and measured soil properties, followed by a regression analysis; a second-order polynomial equation was used to estimate clay and phosphorous from ECa data. McCutcheon et al. (2006) adopted a correlation analysis and a regression analysis between soil properties, SWC and ECa, deducing from the latter an exponential equation to estimate SWC from ECa data. Abdu et al. (2008) combined an ECa map with flow paths derived from a digital elevation model, proposing two models for predicting spatial texture and water holding capacity using multiple regression.

Apparent electrical conductivity is influenced by soil water content and temperature. Such a relationship has been widely used in literature to infer soil water and clay content under wet conditions, but in the seasonally dry Mediterranean regions the spatio-temporal variability of soil moisture content is too high to safely use it. The general objective of this work is to obtain a better understanding of the sensor response and the relative contribution of different soil properties (clay content, stone content, SWC, bulk density and soil depth) to the geophysical signals at different water contents, which are commonly found in water-limited environments, where soil is only moist during short periods of the year. Hence, a specific objective of this study is to evaluate the spatial relationship between EMI measured ECa and soil properties as a function of SWC.

5.2. Material and methods

5.2.1 Site description

The experimental catchment, "La Manga" (36° 52' 21" N, 5° 7' 44"W), located in Setenil de las Bodegas, SW Spain covers 6.7 ha of a rainfed olive orchard (Figure 5.1). The trees were planted in 1995 on a 7 ×7-m grid, with an average tree density of about 200 trees ha^{-1}.The mean elevation is 740 m a.m.s.l. (Figure 5.2) and the mean slope is 10%. The orchard is under minimum tillage and weeds are controlled with herbicides. The soil subgroup is an intergrade between Lithic and Typic Rhodoxeralf (Soil Survey Staff, 1999, pp. 269-270; García del Barrio et al. 1971) with a loamy sandy texture and a maximum depth of 1.2 m to the calcarenite bedrock. The climate is Mediterranean, with a mean annual precipitation of 1100 mm. 75% of the rainfall occurs from October to May. An area of 1.2 ha in the SE of the catchment was transformed from cereal to olives in 2006. Different management practices are required for the recently established olive trees in this upslope area. A gully drains the catchment from the SE

towards the catchment outlet in the NW and separates the two main subareas with different slopes.

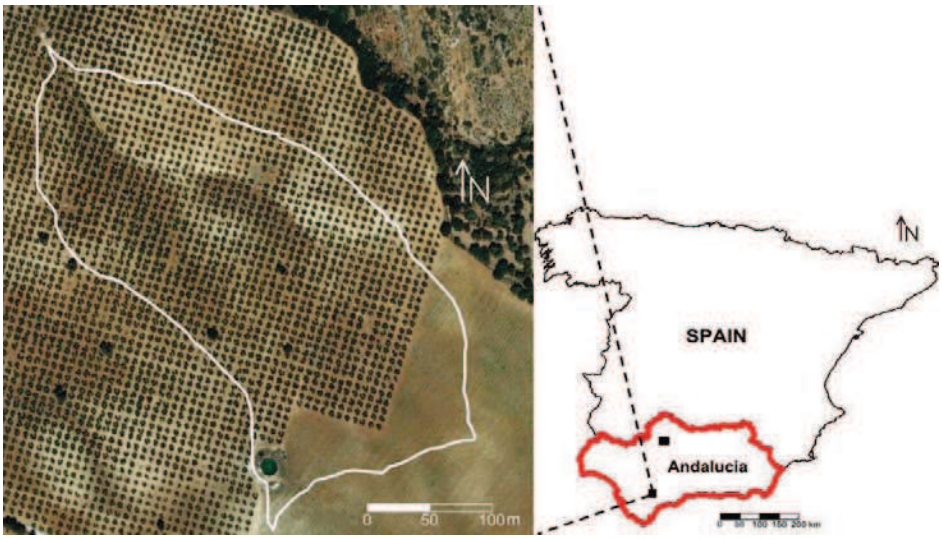

Figure 5. 1 Aerial photograph of the "La Manga"study field and catchment boundary.

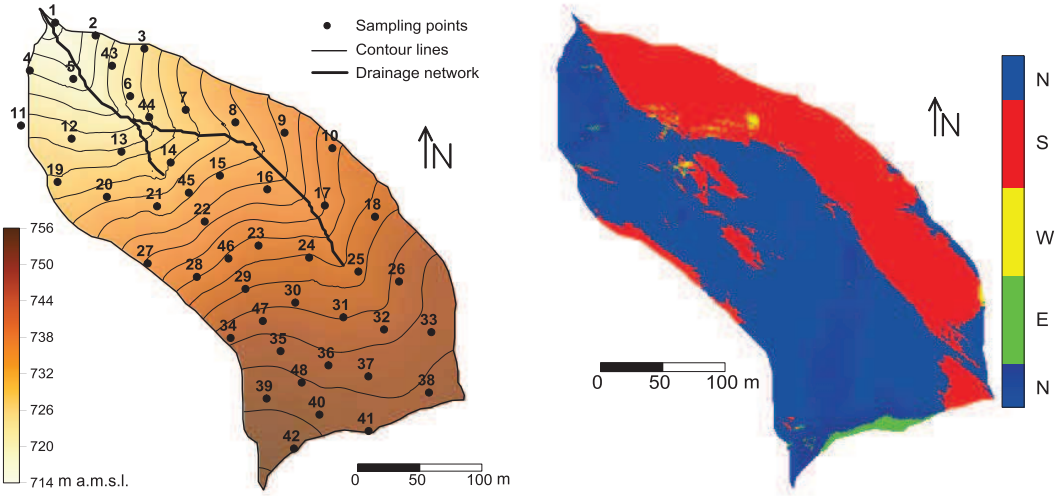

Figure 5. 2 Left: Topography, drainage network and location of soil sampling points; Right: Aspect map.

5.2.2 Soil sampling strategy

Soil profile samples were collected at 48 locations on a pseudo-regular grid using a 0.093-m diameter steel cylinder with a percussion drill. Soil samples were taken at intervals of 0.1 m from the surface down to 1.2 m, where possible. The samples were analyzed in the laboratory for stone content, soil texture, pH, electrical conductivity ($EC_{1:5}$), OM and bulk density (ρ_b).

The catchment was periodically sampled for gravimetric SWC (Figure 5.3), at 0-0.1 and 0.1-0.2 m depth intervals, at the same 48 locations and on 18 occasions, during two hydrological years, using a 0.05-m diameter Edelman auger.

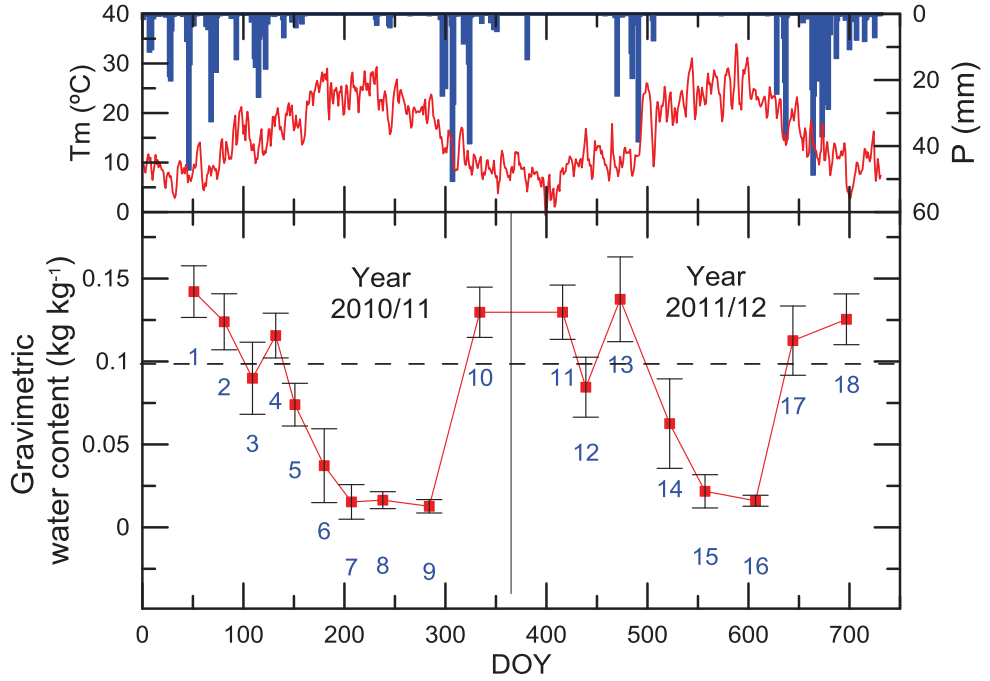

Figure 5. 3 Temporal evolution of dialy mean temperature (Tm, Cº), precipitation (P, mm) and spatially averaged gravimetric soil water content (0-0.2 m) for agronomical years 2011 and 2012. Error bars indicate standard deviations.

5.2.3 Apparent electrical conductivity surveying

At the same 48 locations also ECa was measured during 9 of the 18 SWC surveys (surveys 9, 10, 11, 12, 14, 15, 16, 17 and 18) using a DUALEM-21S EMI sensor (DUALEM, Milton, Canada). In addition 7 field-wide surveys were conducted (surveys 10, 12, 13, 15, 16, 17 and 18). The DUALEM-21S works at a frequency of 9 kHz and is composed of four receiver coils located at distances of 1, 1.1, 2 and 2.1 meters from the transmitter coil and arranged in horizontal-coplanar (H) and perpendicular (P) configurations, allowing simultaneous ECa measurements of four different soil volumes with different depths of exploration (DOE). DOE (Table 5.1) is defined as the depth at which 70% of the response is obtained from the soil volume above that depth (McNeill, 1980; Saey et al. 2008). The EMI soil sensor is hosted in a non-metallic sled and pulled by an all-terrain vehicle (ATV), at a speed of 5-10 km/h. The DUALEM-21S was positioned inside the sled at a total height of 0.075 m above the soil surface, as a result of a wear-and-tear plate which is mounted underneath the sled to protect it from corrosion by dry soil and stones. The ATV was equipped with a real time kinematic-differential GPS receiver (Trimble, Sunnyvale, CA) and a ruggedAllegro-TK6000 field computer (Juniper Systems, Logan, UT) to simultaneously log ECa measurements, coordinates and terrain elevation. The average soil temperature measured by a sensor network (Espejo et al. 2014), consisting of 5TE devices (Decagon Devices, Pullman, WA), was used to standardize the ECa

values to a reference temperature of 25ºC (Sheets and Hendrickx, 1995).Then the ECa data were filtered and interpolated (Whelan et al. 2002) to create maps for the four ECa signals. GPS coordinates were registered in WGS84 and transformed to the Universal Transverse Mercator projection ETRS89 datum 30N, with the software Utm9e-200803 (Núñez-Maderal, 2008).

Table 5. 1 Intercoil distance (*ID*, m), coil configuration and depth of exploration (*DOE*, m) for each signal measured by the DUALEM-21S.

Signal	ID	Coil configuration	DOE
P1.1	1.1	Perpendicular	0.5
P2.1	2.1	Perpendicular	1
H1	1	Horizontal co-planar	1.5
H2	2	Horizontal co-planar	3

5.2.4 Data analysis

Principal component analysis

The interpolated maps (1 × 1m) for the 7 ECa-H1 field-wide surveys were computed using Vesper (Whelan et al. 2002). After that, a principal component analysis (PCA) was performed in Matlab (version R2009b, The Mathworks Inc., USA) for the 7 ECa-H1 maps to obtain the dominant spatial pattern of ECa-H1. Based on the spatial distribution of this principal component the 48 sampling locations were then grouped into three classes (C1-C3).The area with the recently established olive trees was considered as a separate category(C4).

Correlation analysis

The Pearson's correlation coefficient (R) was calculated to evaluate the effect of different SWC conditions on the linear relationships between 1) the four ECa signals, and 2) ECa data and soil profile data, for each survey date and therefore for different soil moisture conditions.

Relationship between clay content and ECa-H1

The relationship between clay content and ECa-H1 was further evaluated, for each sampling date, using a linear regression (Equation 5.1).

$$ECa_j = c + m \cdot Clay_j \quad (5.1)$$

Where *c* and *m* are the corresponding parameters, *Clay* is the clay content, %, and the subindex *j* stands for the survey date.

To quantify the quality of the fit, the coefficient of determination (R^2) was used.

Relationship between SWC and ECa-H1

An exponential model was fitted to the relationship between ECa-H1 and SWC for each sampling location *i*,

$$ECa_i = a \cdot \exp\left(b \cdot \theta_i\right) \tag{5.2}$$

where *a* and *b* are fitted parameters, and the subindex *i. (i=1, 2,3…48)* represents the sampling location for the moisture, θ, and the apparent electrical conductivity (mS m^{-1})

To quantify the precision of the calibration, the root mean squared error (RMSE) between measured (ECa_m) and estimated (ECa_e) values was used,

$$RMSE = \sqrt{\sum_{i=1}^{N}\left(ECa_{e,i} - ECa_{m,i}\right)^2 \Big/ N}\,, \tag{5.3}$$

where *N*=48.

Analysis of variance

An analysis of variance (ANOVA) was performed to check whether differences in measured soil data (SWC, ECa-H1 and soil profile data) between the different classified areas of the catchment were significant.

5.3. Results and Discussion

5.3.1 Soil profile samples

Descriptive statistics of soil profile data (Table 5.2) indicated that the stone content ranged from 0 (at six sampling locations) to 21%. Mean stone content was 7% and the coefficient of variation (CV) was 88%, indicating the great spatial variability of this soil property. The OM content ranged from 0.43% to 2.10% with average values of 0.98%. This large range could be associated with the different soil management practices in the catchment. Mean pH was 8.3, with a standard deviation of 0.2. The pH distribution was negatively skewed and leptokurtic. Soil texture as described in paragraph 5.2.1 is represented in this table by the clay and sand contents. Average values were18.2 and 70.3 %, and CV values were14 and 5 %, respectively. This indicated a high and spatially rather uniform sand content. The $EC_{1:5}$ showed mean values of 0.11 dS m^{-1} and a standard deviation of 0.02 dS m^{-1}. Bulk density showed values ranging

from 1.33 to 1.97 Mg m^{-3}, a CV of 7.4 with a rather low variability. The different management practices could also influence these ρ_b values.

Table 5. 2 Descriptive statistics of stone content (%), organic matter (OM, %), pH, clay and sand contents (%), electrical conductivity (EC1:5, dS m-1) and bulk density (ρb , Mg m-3) for 0 – 0.2 m depth interval.

	Stone	OM	pH	Clay	Sand	$EC_{1:5}$	ρ_b
N	48	48	48	48	48	48	24
Mean	7.2	0.98	8.3	18.2	70.3	0.11	1.73
SD	6.4	0.31	0.2	2.5	3.4	0.02	0.13
C.V.	88.2	32.0	2.8	13.7	4.8	16.3	7.4
Minimum	0.0	0.43	7.4	12.0	61.8	0.06	1.37
Median	6.0	0.93	8.4	18.5	70.3	0.11	1.77
Maximum	20.7	2.10	8.8	24.0	77.3	0.14	1.97
Skewness	0.5	0.85	-1.5	-0.2	0.1	-0.40	-1.01
Kurtosis	-1.2	1.69	4.0	0.3	0.0	-0.02	1.55

*N number of measurements, SD standard deviation and C.V. coefficient of variation (%).

Spatial distributions of stone and clay content (Figure 5.4) were interpolated from the stone and clay contents at the 48 sampling locations. Maps showed that higher stone contents mainly occurred on the south facing slope, the lowest values of clay contents were located at the N part, while the highest clay contents appeared in a fringe at the central part and at the S part of the catchment. At the N part, the combined presence of the highest stone contents and the lowest clay contents, induce a greater intensity of soil erosive processes.

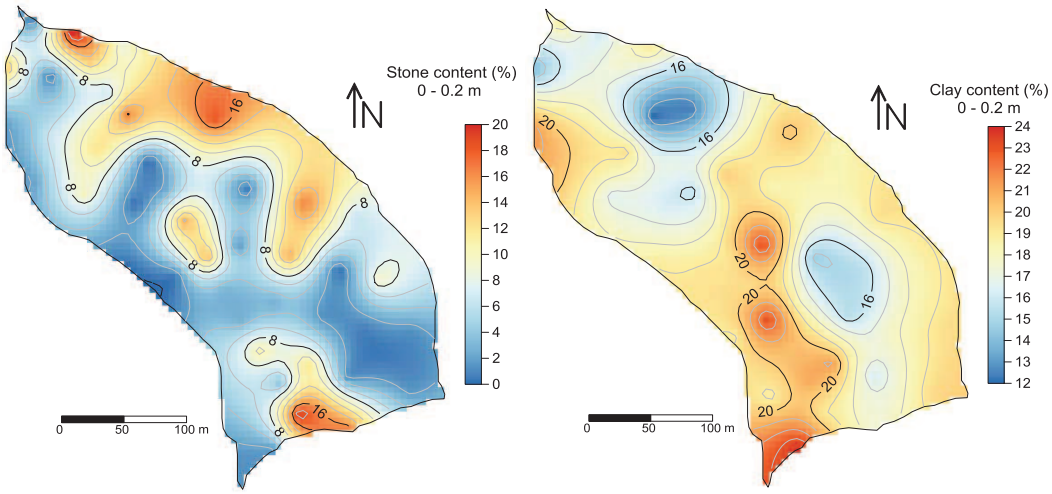

Figure 5. 4 Left: Stone content map and, Right: clay content (%) maps.

5.3.2 Soil water content

Descriptive statistics of soil water content (Table 5.3) indicated that mean SWC below 0.02 kg kg^{-1} were commonly found during summer and were associated with higher CV, while values over 0.11 kg kg^{-1} were easily achieved during wet periods. Surveys 12 and 14 showed intermediate mean SWC values. Survey 17 showed a kurtosis coefficient higher than three and a positive skewness coefficient. The SWC state on this survey date is the result from a drying period interrupted by intense and brief rainfall events, resulting in a non-uniform wetting of the soil profile and the catchment.

Table 5. 3 Descriptive statistics of soil water content (SWC, kg kg^{-1}) for each survey number.

Survey	9	10	11	12	14	15	16	17	18
N	45	47	47	48	47	46	48	48	48
Mean	0.01	0.13	0.13	0.09	0.07	0.02	0.02	0.11	0.13
SD	0.00	0.02	0.02	0.02	0.03	0.01	0.01	0.02	0.02
C.V.	35.8	12.9	13. 9	21.1	39.3	51.7	34.1	18.2	14.5
Minimum	0.01	0.10	0.10	0.03	0.02	0.01	0.01	0.07	0.10
Median	0.01	0.13	0.13	0.09	0.07	0.02	0.02	0.11	0.13
Maximum	0.02	0.19	0.19	0.14	0.12	0.05	0.03	0.20	0.19
Skewness	0.71	0.74	0.92	0.01	-0.01	1.15	0.12	1.61	0.81
Kurtosis	-1.50	1.74	1.30	1.80	-0.54	0.52	-0.57	5.00	1.04

*N number of measurements, SD standard deviation and C.V. coefficient of variation (%).

The spatial SWC distribution (Figure 5.5) under dry and wet soil conditions (surveys 16 and 18) was interpolated from the SWC values at the 48 sampling locations. High SWCs were found in a fringe in the central part of the catchment and in the SE, corresponding to the area with young olive trees subjected to different soil management practices. The highest SWC values near the S limit of the catchment were caused by seepage losses from a neighbor irrigation water deposit.

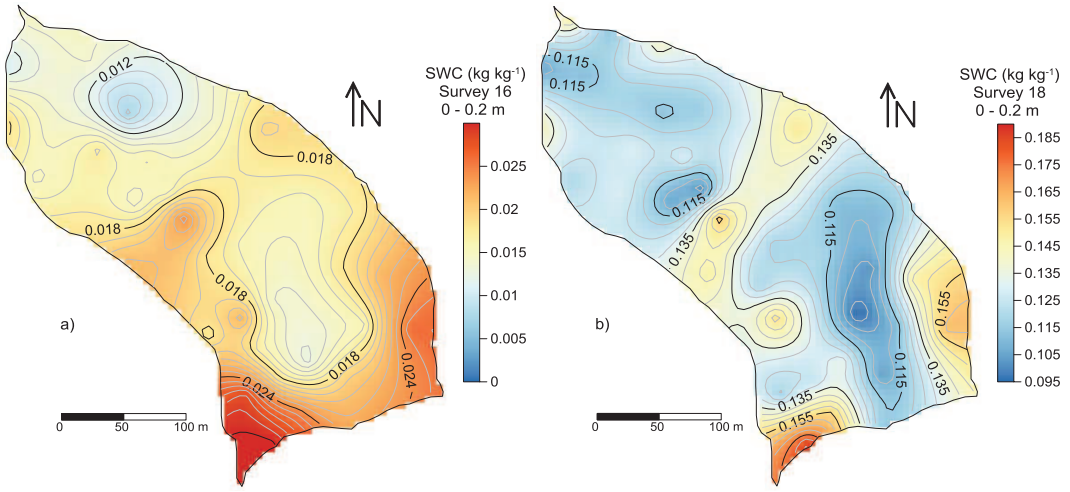

Figure 5. 5 Map of soil water content (SWC) for surveys (a) 16 and (b) 18.

5.3.3 ECa measurements and surveys

ECa measurements

Descriptive statistics of ECa-H1 measurements (Table 5.4) revealed that surveys 17 and 18 had the highest mean ECa and the lowest CV. Surveys 10, 11 and 12 showed intermediate mean ECa and CV, while surveys 9, 14, 15 and 16 presented the lowest mean ECa and the highest CV, corresponding to dry soil conditions. These surveys had a minimum value of 0 mS m^{-1}, which is a result from the zeroing transformation. Survey 11 had only 31 data because of problems associated with the measurement equipment.

Table 5. 4 Descriptive statistics of apparent electrical conductivity (ECa, mS m^{-1}) for each survey number.

Survey	9	10	11	12	14	15	16	17	18
N	46	48	31	48	48	46	48	48	48
Mean	4.7	14.7	16.1	10.2	6.6	4.1	3.5	25.9	26.5
SD	2.7	4.8	5.3	4.1	3.4	2.7	2.1	5.1	5.4
C.V.	58.0	32.9	32.8	40.1	52.0	66.5	60.0	19.8	20.6
Minimum	0.0	6.3	8.3	1.5	0.0	0.0	0.0	17.2	16.7
Median	4.8	13.8	17.5	10.3	6.4	3.8	3.4	26.0	26.8
Maximum	14.4	30.5	30.6	20.3	15.6	15.7	10.9	36.6	39.6
Skewness	0.7	0.9	0.4	0.1	0.3	1.7	1.1	0.3	0.0
Kurtosis	2.1	1.3	0.1	-0.1	0.2	5.2	1.8	-0.6	-0.5

*N number of measurements, SD standard deviation and C.V. coefficient of variation (%).

Correlation coefficients between the different ECa signals are plotted in figure 5.6 for each survey date and corresponding different SWCs. All correlations ranged from 0.75 to 0.97, indicating high and significant ($p<0.05$) relationships between the signals. Signal P2.1 had the highest correlation with signal H1for all survey dates except for survey 17, for which signal H2 showed the highest values (See Table 5.1 for details on each signal). The SWC state on survey 17 was the result of a drying period interrupted by intense and brief rainfall events, producing a non-uniform wetting of the soil profile and the catchment. Furthermore the porous characteristic of the calcarenite can increase, at some locations, the ECa values measured from signal H2. Overall correlations between signals slightly increased for increasing SWCs. The different explored soil volumes, the different profile clay contents, the depth to the bedrock, the topography and the profile SWC influenced the ECa measurements of each signal in a particular way. Under dry soil conditions correlations are expected to be lower as compared to wet soil conditions where SWC can have a potentially significant effect on ECa (Brevik et al. 2006).

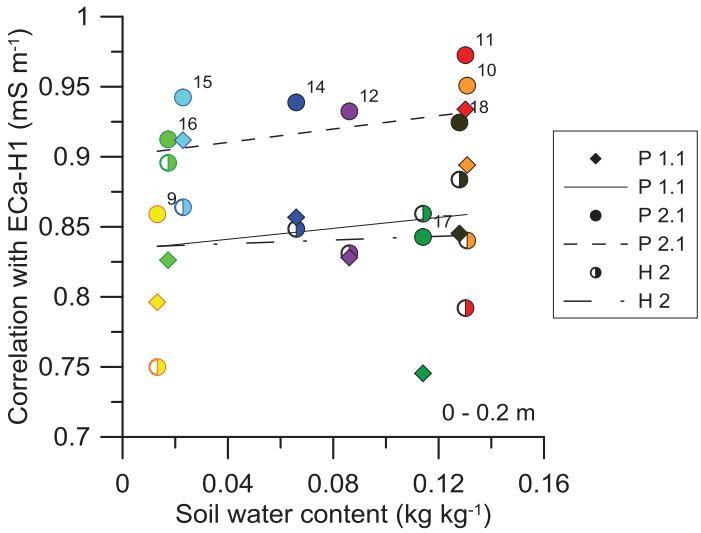

Figure 5. 6 Correlation coeffcients between signal H1 and signals P1.1, P2.1 and H2 for each survery. See Table 5.1 for details on each signal. All correlations are significant atp<0.05 Different colors are associated to different survey dates.

ECa surveys

Descriptive statistics of ECa-H1 maps (Table 5.5) showed that surveys 17 and 18 had the highest mean ECa and the lowest CV. Surveys 10, 12 and 13 showed intermediate mean ECa and CV, while surveys 15 and 16 presented the lowest mean ECa, corresponding to dry soil conditions. All surveys followed a Gaussian distribution (Shapiro–Wilk test).

Table 5. 5 Descriptive statistics of apparent electrical conductivity (ECa, mS m^{-1}) maps for each survey number.

Survey	10	12	13	15	16	17	18
N	54387	54387	54387	54387	54387	54387	54387
Mean	14.2	10.0	14.9	7.3	5.2	30.1	26.9
SD	4.1	3.6	3.4	2.6	1.7	3.4	4.1
C.V.	0.3	0.4	0.2	0.4	0.3	0.1	0.2
Minimum	4.5	1.5	6.9	1.3	1.3	21.8	17.7
Median	14.9	10.5	15.2	7.2	5.4	30.2	27.1
Maximum	26.5	19.7	26.4	14.6	9.3	41.4	37.4
Skewness	-0.3	-0.4	-0.2	0.1	-0.2	0.1	-0.2
Kurtosis	2.7	2.7	2.9	2.5	2.5	2.8	2.7

*N number of measurements, SD standard deviation and C.V. coefficient of variation (%).

PCA computed for all ECa-H1 maps showed that the first principal component (PC1) accounted for 86% of the total variance. The PC1 was considered as the dominant spatial pattern of ECa-H1 (Figure 5.7) and descriptive statistics (Table 5.6) indicated a non-skewed normal distribution. Values lower than the first quartile (x < -5.2) and greater than the third quartile (x > 4.5) were used to delimit three different areas in the catchment. Based on this classification, the 48 sampling locations were classified: C1, sampling locations inside the first quartile area, C3,

sampling locations inside the third quartile area, C2, sampling locations which does not belong to classes C1 nor C2, and C4, sampling locations in the area with young olive trees.

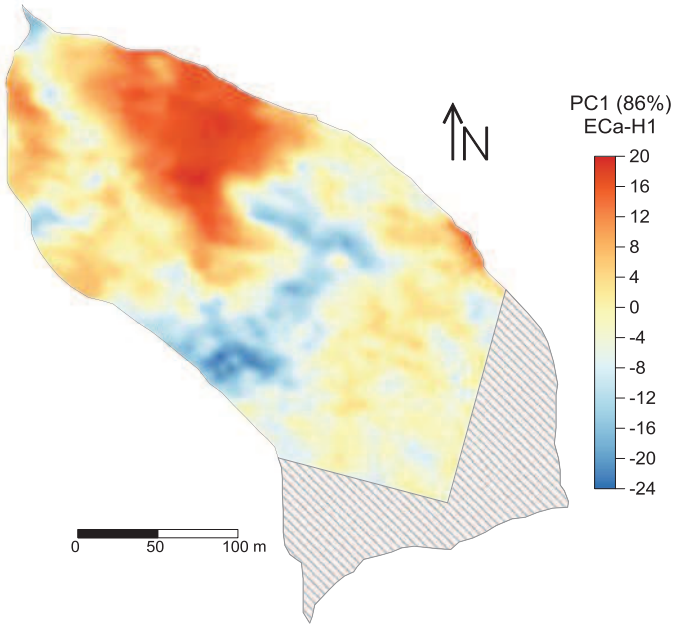

Figure 5. 7 Map of the first principal component (PC1) for apparent electrical conductivity (ECa-H1).

Table 5. 6 Descriptive statistics of the first principal component of apparent electrical conductivity (ECa, mS m^{-1}) maps.

	PC1
N	54387
Mean	0.0
SD	8.2
C.V.	
Minimum	-23.4
1st Quartil	-5.2
Median	-1.0
3rd Quartil	4.5
Maximum	19.6
Skewness	0.3
Kurtosis	-0.2

*N number of measurements, SD standard deviation and C.V. coefficient of variation (%).

5.3.4 Relationship between ECa and soil properties

Spatial relationships between profile soil properties and ECa-H1 were explored to determine the influence of the measured soil properties on the SWC-ECa relationships. Correlation coefficients were calculated, for each survey date, between profile soil properties and ECa (Table 5.7). Significant correlations were mostly found from intermediate (0.02 kg kg^{-1}< x

<0.11 kg kg^{-1}) to wet soil conditions (x> 0.11 kg kg^{-1}). Stone content, pH, $EC_{1:5}$ and soil depth showed significant correlations at these SWC values. Only clay content was significantly correlated to ECa for all survey dates. Clay content-ECa correlations under wet soil conditions doubled the correlations found under dry soil conditions. This fact, in addition to the positive R values, indicated positive increments in the clay content and ECa as soil water content increased. Therefore locations or areas with higher profile clay content will show higher ECa values. Negative R values for stone content indicated an increase in ECa as stone content decreased. Therefore locations or areas with higher profile stone content will have lower ECa values. Relationship between pH and ECa is not indicative of a physical phenomenon. Correlation between $EC_{1:5}$ and ECa suggested that soil solution is partially influencing soil ECa but the other two pathways described by Rhoades et al. (1989) and Rhoades and Corwin (1991) have also account to ECa, and negative values are probably due to the different measured soil volumes for SWC and ECa. Finally, the positive relationship between soil depth and ECa data pointed out the low influence of the calcarenite to the ECa.

Table 5. 7 Correlation coefficients between soil properties and ECa-H1 (mS m^{-1}) for each survey number.

Survey	Stone	OM	pH	Clay	Sand	$EC_{1:5}$	ρ_b	Soil depth
9	-0.28	0.01	-0.21	0.49*	0.23	-0.28	-0.22	0.18
10	-0.45*	-0.04	-0.23	0.52*	-0.06	-0.21	-0.06	0.23
11	-0.34	-0.23	-0.11	0.39*	0.13	-0.05	0.09	0.20
12	-0.44*	-0.33*	-0.38*	0.33*	0.28	-0.38*	-0.07	0.40*
14	-0.45*	-0.14	-0.39*	0.41*	0.30*	-0.44*	-0.23	0.37*
15	-0.27	-0.02	-0.16	0.36*	0.23	-0.31*	-0.30	0.18
16	-0.22	-0.01	-0.17	0.34*	0.21	-0.33*	-0.22	0.13
17	-0.45*	0.00	-0.37*	0.59*	0.08	-0.29*	-0.19	0.32*
18	-0.39*	-0.19	-0.41*	0.42*	0.16	-0.23	0.00	0.29*

* Significant correlations ($p<0.05$)

Although the explored soil volumes by the ECa and profile soil measurements differ in several orders of magnitude and no strong correlations were expected, the potentially significant clay vs. ECa relationship could be tested.

R and R^2 coefficients were calculated between clay content and ECa-H1 (Figure 5.8) and plotted for each survey date and, consequently, for different soil moisture conditions. Clay content-ECa correlations increased with increasing SWCs, on contrary, sand content-ECa correlation decreased. R^2 values lower than 0.35 were obtained, indicating that linear relationships were not adequate to determine the spatial dependence between clay content and ECa.

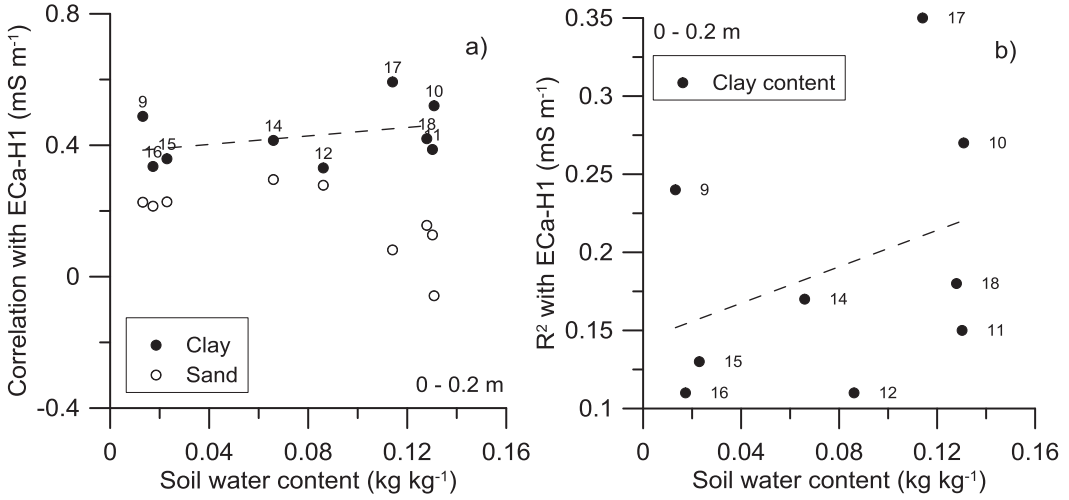

Figure 5. 8 a) Pearson coefficients for clay and sand content versus apparent electrical conductivity (ECa-H1) and b) Spearman coefficients for clay content versus ECa-H1, for each survey number.

5.3.5 Relationships between ECa and SWC

Spatial relationships

Spatial and temporal relationships between SWC and ECa-H1 for each survey number were explored. Correlations between ECa-H1 and SWC at each survey date ranged from 0.15 to 0.55 for surveys 17 and 14, respectively (Figure 5.9.a), indicating a weak spatial relationship, possibly as a result of the rather small range in SWC values on each survey date.

Figure 5.9 shows also SWC vs. ECa-H1 relationships for surveys 14, 10 and 18. Surveys 10 and 14 showed the highest R values for the spatial relationships between SWC and ECa-H1, and survey 18 had the highest mean ECa value and a mean SWC greater than 0.11 kg kg^{-1}. The rest of surveys, with R values lower than 0.4 showed a shape similar to the shape of survey 18, where the steep slope of the linear relationship results in a low R value. Point 42, marked on surveys 10 and 18 is located near the water deposit and shows the highest SWC values. Survey 14 showed intermediate to low mean SWC and intermediate to low mean ECa-H1 values which increased the range of SWC and ECa-H1 values and led to the highest R value, while the rest of surveys presented smaller SWC ranges, corresponding to dry or wet soil conditions

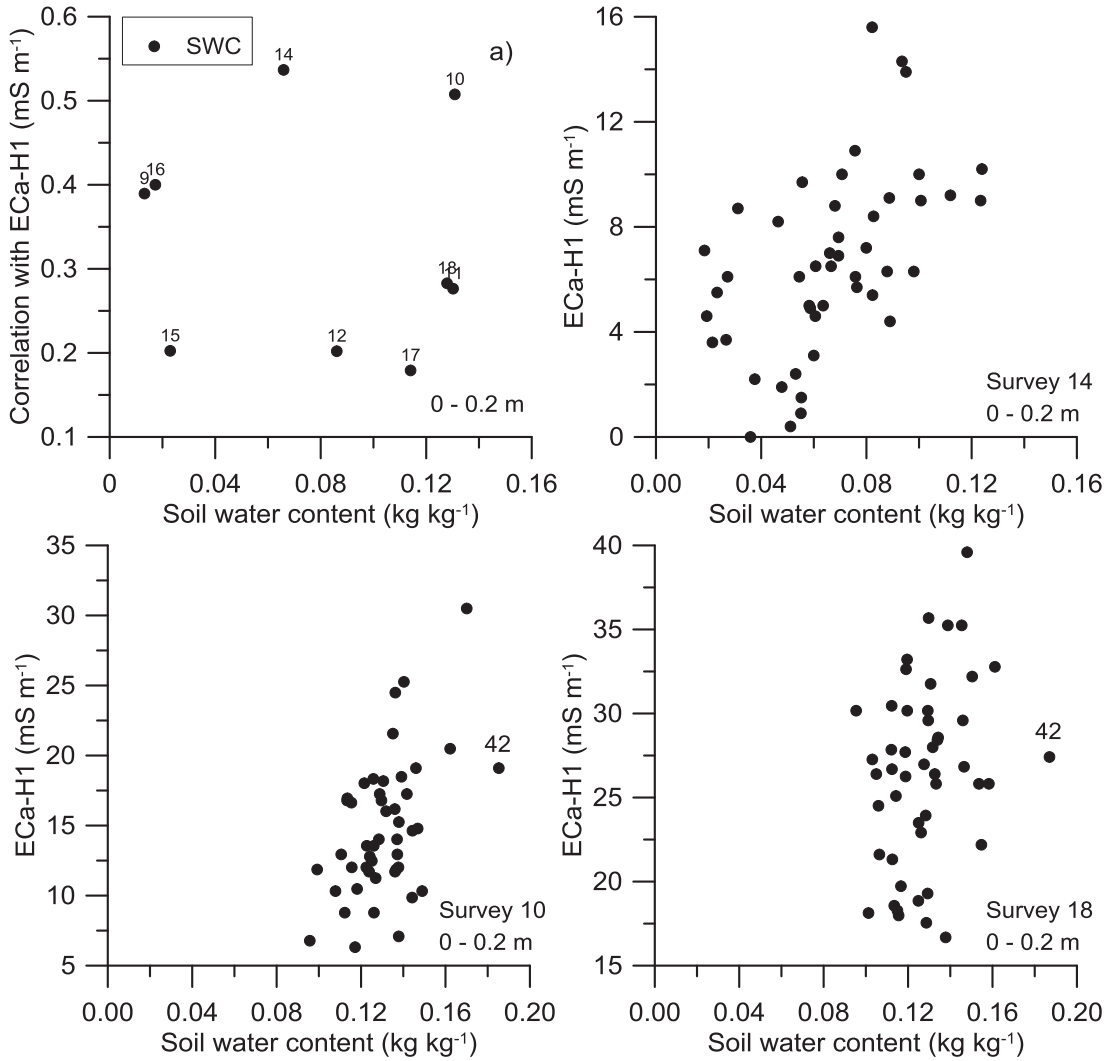

Figure 5. 9 Spatial relationship between soil water content and apparent electrical conductivity (ECa-H1) for (a) all survey dates, and surveys 14, 10 and 18. Point 42, located near to the water deposit, presents the highest SWC values.

Temporal relationships

The temporal relationship, (Figure 5.10), on the contrary, showed clearly increasing ECa-H1 with increasing SWC. The largest increments in ECa-H1 with increasing SWC were found for SWC greater than 0.11 kg kg^{-1}. The soil volume characterized by ECa-H1 is much larger than the volumen characterized by soil samples for gravimetric SWC determination (0.2-m), hence explored soil volumen below this depth contributes to the ECa-H1 response. Soil volumen below the explored topsoil can be moister than the soil samples as ocurred in surveys 17 and 18, or dryer as ocurred in surveys 10 and 11.

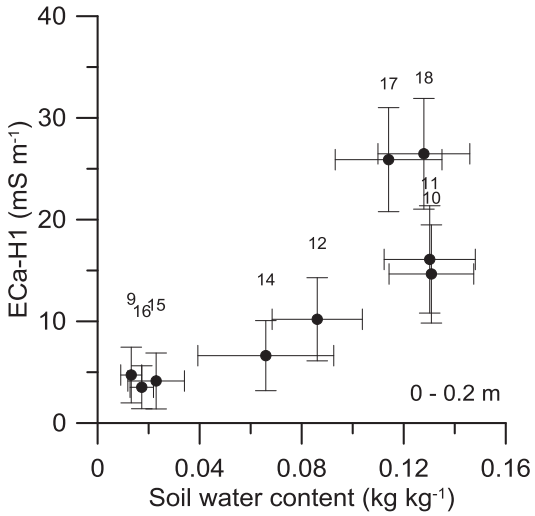

Figure 5. 10 Temporal relationships between soil water content and apparent electrical conductivity (ECa-H1) for each survey number. Error bars indicate the standard deviations.

5.3.6 Statistical tests (ANOVA)

SWC and ECa data

Based on the low spatial relationship between the SWC and ECa-H1 data, the existence of different areas in the field was estudied based on the PC1 classification. An ANOVA test was calculated for all SWC and ECa data, for each delimited class. The ANOVA results do not detected significant differences between classes for SWC except for surveys 12, 14 and 16. Figure 5.11.a shows the boxplots, for each delimited class, of SWC and ECa-H1 for survey 16. Survey 16 showed significanty higher SWC for C4, corresponding to the area with young olive trees. Note, however, the small magnitude of these SWC differences. Sgnificant differences between C1 and C4 for ECa data are apreciated.

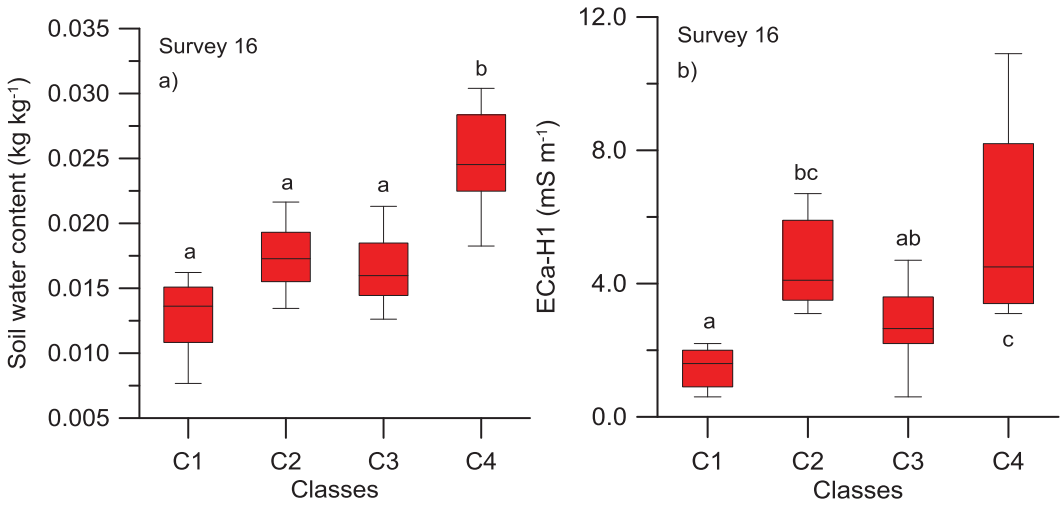

Figure 5. 11 Box and whisker plots, for each delimited class, of a) soil water content and b) apparent electrical conductivity (ECa-H1) for survey 16", lowercase letters indicate homogeneous groups.

Figure 5.12 presents the boxplots, for each delimited class, of SWC and ECa-H1 for survey 14. This survey showed intermediate SWC and ECa values. The ANOVA test appreciated significant differences between C1 and C4 for SWC, and significantly lower ECa values for C1. The same results were obtained for survey 12.

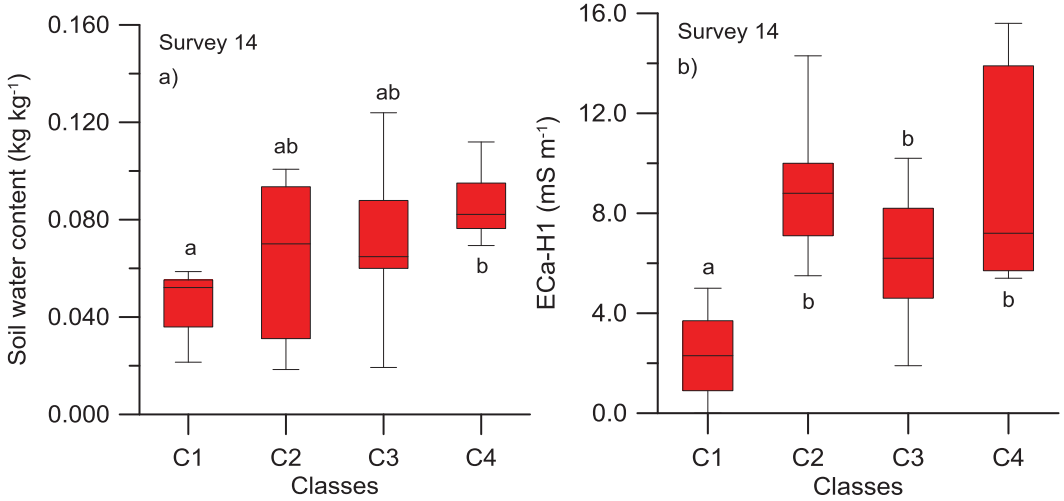

Figure 5. 12 Box and whisker plots, for each delimited class, of a) soil water content and b) apparent electrical conductivity (ECa-H1) for survey 14, lowercase letters indicate homogeneous groups.

The relationship between SWC and ECa-H1 for survey 14 was then plotted (Figure 5.13) distinguishing data from classes C1, C2, C3 and C4. Different relationships should be calculated for the heterogeneous classes, pointing out the difficulty to estimate spatial relationships between SWC and ECa in this spatially heterogeneous field.

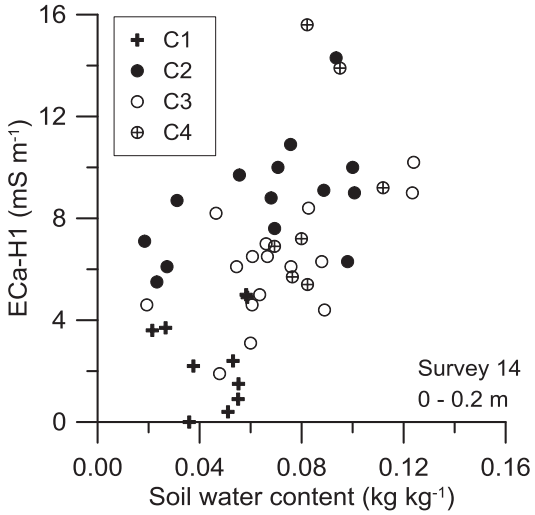

Figure 5. 13 Spatial relationship between soil water content and apparent electrical conductivity (ECa-H1) for survey 14,distinguishing data from classes C1, C2, C3 and C4.

Soil profile samples

An ANOVA test was performed for all profile soil data, for each delimited class. Results from the ANOVA indicated no significant differeces between classes for stone content, sand content, $EC_{1:5}$ nor soil depth, but significant differences (Figure 5.14) were found for OM, pH, clay content, and bullk density. Significant differences for OM and ρb in C4 are related to the specific mangement practices, which increased OM due to organic fertilization and decreased ρ_b as a result of tillage. Classes C2 and C4 showed significantly higher clay contents. These higher clay contents in areas C2 and C4 are probably related to the significantly higher ECa values on these two areas (Figures 5.11 and 5.12) as compared to C1 and C3. Also the significantly higher pH values in C1 indicated that rock fragments from the underlying bedrock are mixed, by cultural practices, with the soil.

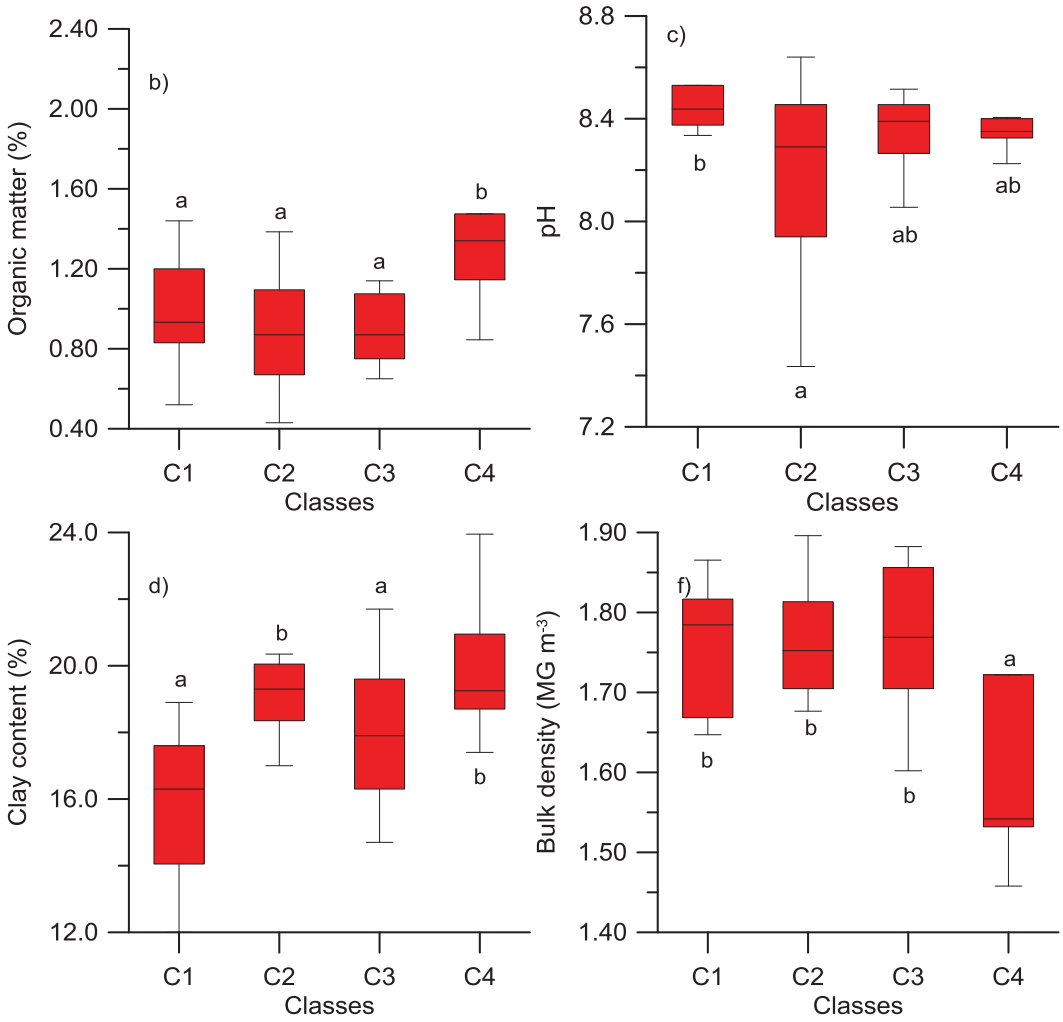

Figure 5. 14 Box and whisker plots for each delimited class, of organic matter, pH, clay content and bulk density, lowercase letters indicate homogeneous groups.

5.3.7 Exponential relationship (SWC-ECa)

Based on the results from the temporal relationships between SWC and ECa-H1 an exponential model [Equation 5.2] was adjusted for each sampling location. Descriptive statistics of the adjusted parameters "a" and "b" are described in table 5.8. Mean values were 3.9 and 14, respectively. Parameter "a" showed greater CV and half the range of parameter "b" (8.9 and 21.8, respectively)

Table 5. 8 Summary descriptive statistics of the adjusted parameters "a" and "b" between ECa and SWC at each sampling location.

	a	b
N	48	48
Mean	3.9	14.0
SD	2.0	4.4
C.V.	52.4	31.4
Minimum	0.6	6.6
1st quartile	2.4	11.5
Median	3.7	13.2
3rd quartile	5.0	15.9
Maximum	9.5	28.4
Skewness	0.8	1.4
Kurtosis	0.3	2.3

*N number of measurements, SD standard deviation and C.V. coefficient of variation (%).

An ANOVA test was calculated for both parameters in terms of the four classes described above (Figure 5.15). Parameter a" showed significant differecenes between C1 and C2 and C4. Parameter "b" showed no significant differeces between classes. The spatial distribution of parameter "a" (Figure 5.16) was interpolated from the "a" values at the 48 sampling locations. Higher values were found in the N part of the catchment, near to the flume, at the S part, near the area with young trees, and in the central part, along a fringe, where higher SWC values (Figure 5.5) and lower PC1 (Figure 5.7) values were found. Results revealed that profile soil properties must influence the SWC and ECa-H1 relationships.

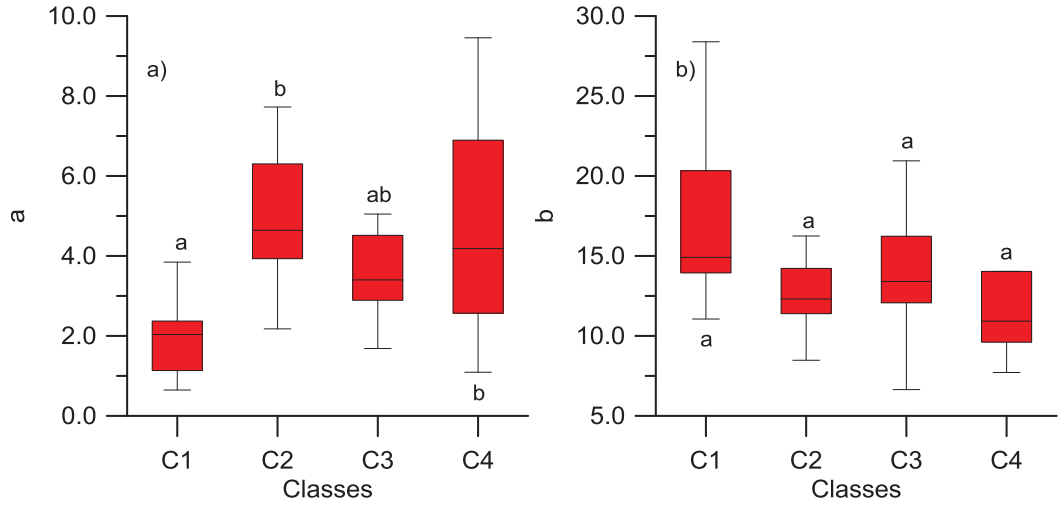

Figure 5. 15 Box and whisker plots for each delimited class, for parameters "a" and "b", lowercase letters indicate homogeneous groups.

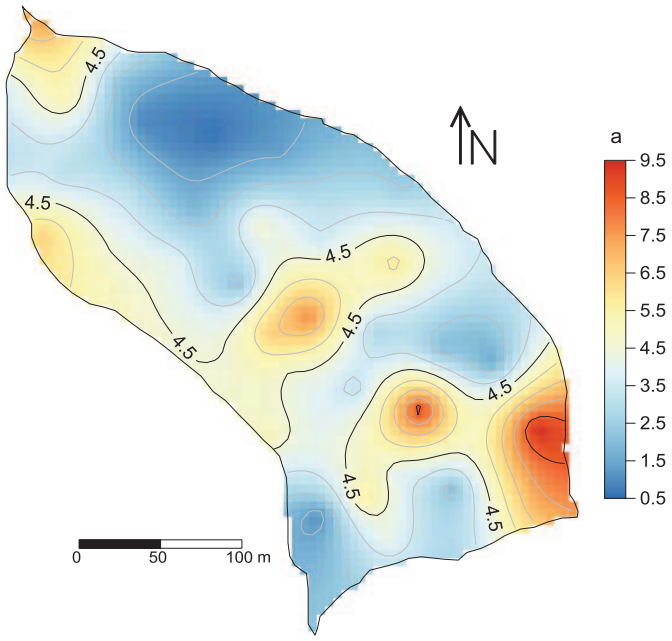

Figure 5. 16 Map of parameter "a" from equation [5.2].

From all studied soil profile properties, the time stable soil property: clay content, showed 1) the highest R values in time with ECa and 2) similar results in the ANOVA test as those obtained for the parameter "a". In figure 5.17 a relationship between (a) both adjusted parameters "a" and "b" and the relationship between (b) parameter "a" and clay content are appreciated, distinguishing data from classes C1, C2 and C3. Lower "a" values are related with C1, low to intermediate values with C3, and high values with C2. A negative relationship between both parameters was expected. Finally, the relationship between "a" and clay content showed that C1 shows clay contents approximately under 18%, C3 shows all range of clay contents and C2 shows clay contents approximately above 18%. Linear regressions through the origin showed an

R^2 of 0.8 and 0.9 for C1 and C2. The behavior of C3 is probably due to the spatial differences in topography; most of the selected points are located near the gully.

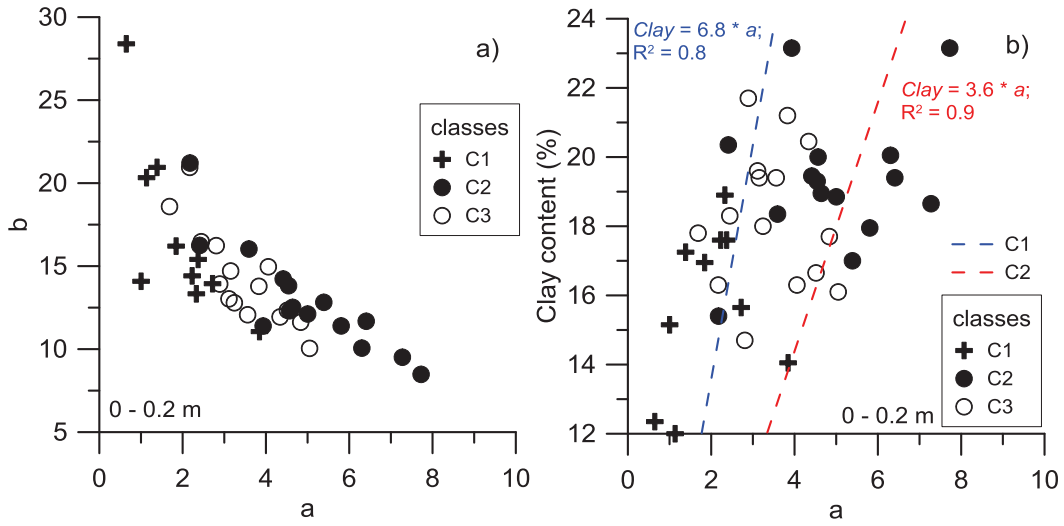

Figure 5. 17 a) Relationship between parameters "a" and "b", b) relationship between parameter "a" and clay content, distinguishing data from classes C1, C2 and C3. A linear regression through origin is shown for C1 and C2.

5.4 Conclusions

Soil ECa data were used to delimit potential areas in an olive orchard. From a PCA based on seven EMI surveys, the spatial pattern of ECa was obtained as the first principal component. Based on this classification on different areas, soil measurements (SWC, profile soil data and ECa measurements) were studied in the four classes. ANOVA tests detected significant differences between classes for OM, pH, clay content and bulk density. Also significant differences between classes were observed for SWC at intermediate soil moisture. Relationships between soil profile data and ECa were also studied; soil texture was the single soil property that showed positive and significant correlations for all survey dates. Spatial and temporal relationships between SWC and ECa were explored. Low R values between ECa and SWC relationships for each survey date were obtained as consequence of the different soil characteristics of each delimited area. Temporal relationships between ECa and SWC were modeled through an exponential relationship. Parameters from the model were evaluated for significant differences between classes and related to the time stable clay content. Results indicated a strong influence of clay contents on the relationship between SWC and ECa.

REFERENCES

Abdu H., Robinson D.A., Seyfried M., Jones S.B. 2008. Geophysical imaging of watershed subsurface patterns and prediction of soil texture and water holding capacity. Water Resour. Res., DOI: 10.1029/2008WR00743.

Amezketa E. 2007. Use of an electromagnetic technique to determine sodicity in saline-sodic soils. Soil Use Manage., DOI: 10.1111/j.1475-2743.2007.00094.x.

Brevik E., Fenton T. Lazari, A. 2006. Soil electrical conductivity as a function of soil water content and implications for soil mapping. Precis. Agric., 7, 393-404.

Brevik E.C., Fenton T.E. 2004. The effect of changes in bulk density on soil electrical conductivity as measured with the geonics EM-38. Soil survey horizons, 45(3):73-110.

Corwin D.L., Lesch S.M. 2005. Apparent soil electrical conductivity measurements in agriculture. Comput. Electron. Agric, 46:11-43.

Corwin D.L., Lesch S.M. 2003. Application of soil electrical conductivity to precision agriculture. Agron. J., 95:455-471.

Domsch H., Giebel A. 2004. Estimation of soil textural features from soil electrical conductivity recorded using the EM38. Precis. Agric., 5, 389-409, 2004.

Dualem Inc. 2007. DUALEM-21S user's manual. Dualem Inc., Milton. Canada.

Espejo A., Giráldez J.V., Vanderlinden K., Taguas E.V., Pedrera A. 2014. A method for estimating soil water diffusivity from moisture profiles and its applications across an experimental catchment. J. Hydrol., 516:161-168.

García del Barrio I., Malvárez L., González J.I. 1971. Mapas provinciales de suelos. Cádiz. Ministerio de Agricultura. Madrid.

Harvey O.R., Morgan C.L.S. 2009. Predicting regional-scale soil variability using a single calibrated apparent soil electrical conductivity model. Soil Sci. Soc. Am. J., DOI: 10.2136/sssaj2008.0074.

Johnson C.K., Eskride K.M., Corwin, D.L. 2003. Apparent soil electrical conductivity: applications for designing and evaluating field-scale experiments. Comput. Electron. Agr., 46: 181-202.

Kachanoski R.G., Gregorich E.G., Van Wesenbeeck I.J. 1988. Estimating spatial variations of soil water content using noncontacting electromagnetic inductive methods. Can. J. Soil Sci., 68:715-722.

Kitchen N.R., Sudduth K.A., Drummond S.T., 1999.Soil electrical conductivity as a crop productivity measure for claypan soils. J. Prod. Agric., 12:607-617.

Martinez G., Vanderlinden K., Ordoñez R., Muriel J. L. 2009. Can apparent electrical conductivity improve the spatial characterization of soil organic carbon?. Vadose Zone J., DOI: 10.2136/vzj2008.0123.

Martinez-García G., Vanderlinden K., Pachepsky Y., Giráldez-Cervera J.V., Espejo-Pérez A.J. 2012. Estimating topsoil water content of clay soils with data from time-lapse electrical conductivity surveys. Soil Sci., DOI:10.1097/SS.0b013e3182eda57.

McCutcheon M.C., Faharani H.J., Stednick J.D., Buchleiter G.W., Green T.R. 2006. Effect of soil water on apparent soil electrical conductivity and texture relationships in a dryland field. Biosyst. Eng., DOI: 10.1016/j.biosystemseng.2006.01.002.

McNeill J.D. 1980. Electromagnetic terrain conductivity measurement at low induction numbers.Technical Note TN-6.Geonics Limited, Missisauga, Ontario, Canada.

Nadler A., Frenkel H. 1980. Determination of soil solution electrical conductivity from bulk soil electrical conductivity measurements by the from electrode method. Soil Sci. Soc. Am. J., Madison, 44: (5) 1216-1221.

Núñez-Maderal E. 2008. Calculadora Geodésica edición especial para la Península Ibérica, Cartesia.org, Spain.http://www.cartesia.org/download.php?op=viewdownloaddetails&lid=172&ttitle=Calculadora_UTM-Geogr%E1ficas_Espa%F1a. Accessed 11 July 2014.

Peralta N.R., Costa J.L., Balzarini M., Angelini H. 2013. Delineation of management zones with measurements of soil apparent electrical conductivity in the southeastern pampas. Can. J. Soil Sci., DOI:10.4141/CJSS2012-022.

Rhoades J.D., Manteghi N.A., Shouse P.J., Alves W.J. 1989. Soil electrical-conductivity and soil-salinity – new formulations and calibrations. Soil Sci. Soc. Am. J., 53(2):433:439.

Rhoades J.D., Raats P.A.C., Prather R.J. 1976. Effects of liquid-phase electrical-conductivity, water-content, and surface conductivity on bulk soil electrical-conductivity. Soil Sci. Soc. Am. J., 40(5):651-655.

Rhoades J.D., Corwin D.L. 1991. Determining soil electrical conductivity-depth relations using an inductive electromagnetic soil conductivity meter. Soil Sci. Soc. Am. J., 45: 255-260.

Robinson D.A., Abdu H., Lebron I., Jones S. 2012. Imaging of hill-slope soil moisture wetting patterns in a semi-arid oak savanna catchment using time-lapse electromagnetic induction. J. Hydrol., DOI: 10.1016/j.jhydrol.2011.11.034.

Saey T., Simpson D., Vitharana U.W.A., Vermeersch H., Vermang J., van Meirvenne M. 2008. Reconstructing the paleotopography beneath the loess cover with the aid of an electromagnetic induction sensor. Catena 74 (2008) 58–64.

Sheets K.R., Hendrickx J.M.H., 1995. Noninvasive soil water content measurement using electromagnetic induction. Water Resour. Res., 31(10), 2401-2409.

Sinegani A.A.S., Mahboobi A.A., Nazarizadeh F. 2005. The effect of agricultural practices on the spatial variability of arbuscular mycorrhiza spores. Turk. J. Biol., 29:149-153.

Siri-Prieto G., Reeves D.W., Shaw J.N., Mitchell C.C. 2006. World's oldest cotton experiment: relationships between soil chemical and physical properties and apparent electrical conductivity. Commun. Soil Sci. Plan., DOI: 10.1080/00103620600564018.

Slavich P.G., Petterson, G.H. 1990. Determining ECa-depth profiles from electromagnetic induction. Aust. J. Soil Res., 28(3):443-452.

Soil Survey Staff. 1999. Soil taxonomy: A basic system of soil classification for making and interpreting soil surveys. 2nd ed. NRCS USDA Hbk 436

Sommer M. 2006. Influence of soil pattern on matter transportation in and from terrestrial biogeosystems – a new concept for landscape pedology. Geoderma, 133:(1-2):107-123.

Sudduth K.A., Kitchen N.R., Wiebold W.J., Batchelor W.D., Bollero G.A., Bullock D.G., Clay, D.E., Palm H.L., Pierce F.J., Schuler R.T., Thelen K.D. 2005. Relating apparent electrical conductivity to soil properties across the north-central USA. Comput. Electron. Agr., DOI:10.1016/j.compag.2004.11.010.

Triantafilis J., Santos F.A. 2013. Electromagnetic conductivity imaging (EMCI) of soil using a DUALEM-421 and inversion modeling software (EM4Soil). Geoderma, DOI: 10.1016/j.geoderma.2013.06.001.

Whelan B.M., McBratney A.B., Minasny B. 2002. Vesper 1.5 – spatial prediction software for precision agriculture. In: Robert PC, Rust RH, Larson WE. (eds.) Precision Agriculture, Proceedings of the 6th International Conference on Precision Agriculture, ASA/CSSA/SSSA, Madison, Wisconsin.

Chapter 6. Delimiting ECa-based representative zones for field-average soil moisture estimation.

6.1 Introduction

Although soil moisture represents only 0.05% of the Earth's fresh water (Calamita, 2012), it is considered a key control for vadose zone, atmospheric, and climatologic processes. Spatial and temporal estimation of soil moisture at field or catchment scales is therefore necessary. Historically, soil moisture has been observed using spatially distributed field surveys which are time consuming, labor intensive and provide generally only a limited coverage of the surveyed area. Nowadays, soil moisture can be monitored in-situ using sensor networks, or can be estimated from remotely sensed soil information, using water balance models, or using hydrogeophysical techniques (Vereecken et al. 2008).

Spatio-temporal variability of soil moisture has been studied at field, catchment, regional and continental scales. Understanding soil moisture spatial and temporal variability of large areas is fundamental to improve predictions in hydrogeological models (Seneviratne et al. 2010). In agricultural applications, knowledge of spatio-temporal soil moisture variability at the field scale is useful to assess yield and crop growth optimization, to improve water conservation, to efficiently manage and schedule irrigation and to reduce diffuse contamination by fertilizers and pesticides in surface and ground waters.

During the last decades EMI surveys have been widely used to estimate the spatial variability of soil moisture and to characterize soil moisture dynamics at the field scale (Martínez et al. 2009; Robinson et al. 2012). The soil apparent electrical conductivity (ECa) is influenced by multiple soil properties, including soil moisture (Rhoades, 1976; Mualem and Friedman, 1991; Brevik and Fenton, 2002; Corwin and Lesch, 2005; Friedman, 2005). Therefore ECa data have to be interpreted on a case-by-case basis. ECa is influenced by soil water content (SWC), solute concentration, temperature, clay content and mineralogy (Friedman 2005; McNeil 1980), organic matter content (Rhoades, 1976; Sheets and Hendrickx 1995), and in general by agricultural management (Martínez, 2010).

Relationships between ECa and time invariant soil properties (e.g. clay content) depend generally on the state of the transient properties, mainly water content and solute concentration, but also temperature at the time of mapping (McCutcheon et al. 2006). In an attempt to standardize the measurement conditions, ECa surveys are recommended at water contents near field capacity (Corwin and Lesch, 2005; Brevik et al. 2006; Chapter 4 of this thesis). The high spatial variability of independent soil properties is therefore a drawback for efficient moisture mapping and for the straightforward interpretation of ECa maps. However, the interest in ECa mapping has been growing steadily, since it can be considered as a surrogate spatial map for soil texture, while it is one of the most effective ways of delimiting management zones for precision agriculture applications (Corwin and Lesch, 2003; Vitharana et al. 2006). James et al. (2003) concluded that ECa measurements are the simplest and least expensive way to characterize soil variability.

In semi-arid environments, soil water conservation and management is of prime importance. Temporal stability analysis (TSA) identifies locations which conserve the property of representing the mean or extreme values of the field soil water content at any time throughout the measurement period (Vachaud et al. 1985). The results of TSA are useful for up-scaling observed soil water contents to obtain average values across the observation area, to improve soil water monitoring strategies and to estimate any lost data.
A recent study suggests that intertwined factors and effects (design measures, vegetation cover, topography, climate...) play together to determine the temporal stability of soil moisture (Vanderlinden et al. 2012). Martínez et al. (2010) observed that the topsoil had the largest number of locations representing the mean soil water content of the field. Grayson and Wester (1998) related these locations, representing the mean soil water content, to topographic attributes.

A step forward in the TSA might be to identify representative zones in the field, instead of specific representative locations for the mean soil water content. The objective of this work is to test this hypothesis and identify representative areas using ECa surveys and TSA.

6.2. Materials and methods

6.2.1 Site description

The experimental catchment "La Manga" (36º52’21’’ N, 5º7’44’’W) is located in Setenil de las Bodegas in the SW of Spain (Figure 6.1). It covers an area of 6.7 ha dedicated to rainfed olive cultivation under minimum tillage with chemical weed control. The soil subgroup is an

intergrade between Lithic and Typic Rhodoxeralf (Soil Survey Staff, 1999, pp. 269-270; García del Barrio et al. 1971).The soil texture is loamy-sand and the maximum depth to the underlying calcarenite bedrock is 1.2 m. The climate is Mediterranean, with a mean annual precipitation of 1100 mm. Rainfall occurs mainly from October to May (75%) as intense and short showers. The mean elevation and slope are 740 m a.m.s.l. and 10%, respectively. At the highest part of the catchment, an area of 1.2 ha was transformed from cereal to olives in 2006. Throughout the study period, this area was 2-3 times/year tilled using a disc harrow, in contrast to the area with mature trees which was only tilled once/year. A gully intersects the catchment from SE to NW towards the catchment outlet and separates the two main slopes (Figure 6.2).

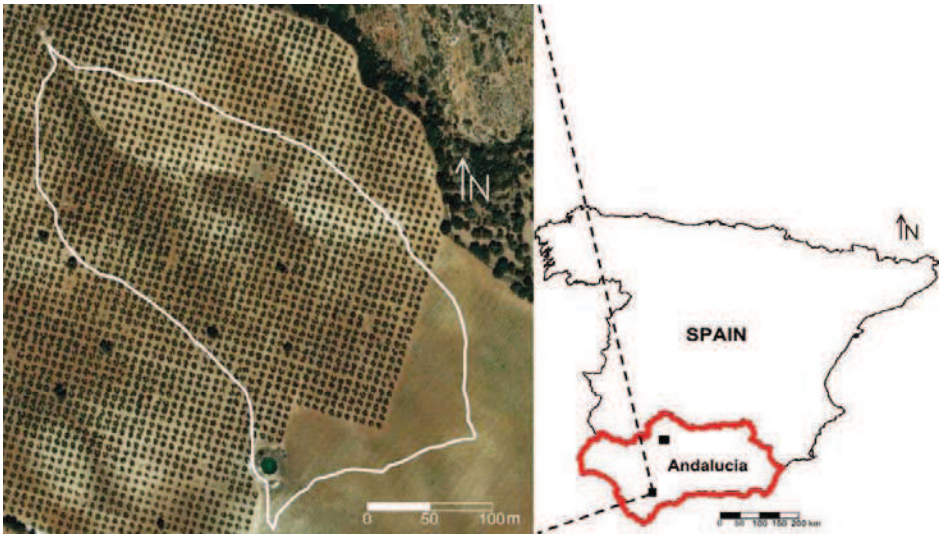

Figure 6. 1 Aerial photograph of the study field and the experimental catchment.

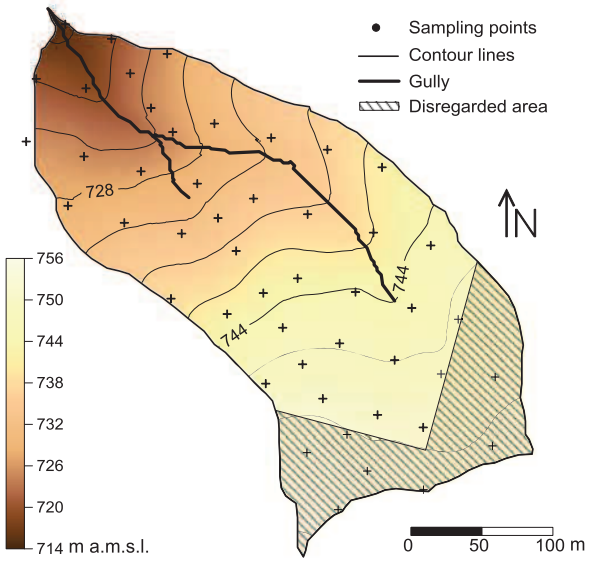

Figure 6. 2 Topography of the experimental catchment, gully, disregarded area for ECa maps and location of soil sampling crosses.

6.2.2 Soil water content

During two hydrological years (2010/11 and 2011/12) the field was sampled 18 times for gravimetric SWC, at 48 locations on a pseudo-regular grid (Fig. 6.2) using a 0.05-m diameter Edelman auger. Soil samples were taken at 0-0.1 and 0-0.2 m.

6.2.3 Apparent electrical conductivity surveys

ECa surveys were performed with the DUALEM-21S (D21S) sensor (DUALEM, Milton, Canada).This EMI sensor is composed of one transmitter coil and four receiver coils at distances of 1, 1.1, 2 and 2.1 meters from the transmitter coil. Coil pair orientations can be horizontal co-planar (H) and perpendicular (P). D21S's multi-coil configuration allows the sensor to measure simultaneously four different soil volumes. The depth of exploration (DOE), defined as the depth at which 70 % of the sensor response is achieved (McNeill, 1980; Saey et al. 2008), ranged from approximately 0.5 to 3 m.

The D21S (See chapters 2 and 4 of this thesis) was hosted inside a polyvinyl chloride (PVC) sled and pulled by an all-terrain vehicle. Auxiliary measurement equipment consisted of a real time kinematic-differential global positioning system (Trimble, Sunnyvale, CA) and a rugged Allegro-TK6000 field computer (Juniper Systems, Logan, UT).

Six field-wide ECa surveys were conducted during the drying-wetting period of the hydrological year 2011/12. Surveys were performed at a speed range of 5-10 km/h, with a distance of 7 m between parallel measurement lines, according to the olive inter-row spacing, and with an inline measurement frequency of 1 Hz. The average soil temperature measured by a sensor network (Espejo et al. 2014), consisting of 5TE devices (Decagon Devices, Pullman, WA), was used to standardize the ECa values to a reference temperature of 25ºC (Sheets and Hendrickx, 1995). Then the ECa data were filtered and interpolated (Whelan et al. 2002) to create maps for the four ECa signals. GPS coordinates were registered in WGS84 and transformed to the Universal Transverse Mercator projection ETRS89 datum 30N, with the software Utm9e-200803 (Núñez-Maderal, 2008). After the field-wide surveys, ECa was also measured at the 48 SWC sampling locations (Fig. 6.2).

6.2.4 Clay content

An exhaustive soil survey was performed in 2012. Soil profile samples were collected at the 48 SWC and ECa measurement locations (Fig. 6.2) using a 0.093-m diameter cylinder auger (Eijkelkamp Agrisearch Equipment, Giesbeek, The Netherlands) and a percussion drill. Soil samples were taken at 0.1-m depth intervals, from the soil surface down to the bedrock. The samples were analyzed in the laboratory for soil texture according to the hydrometer method (Grossman and Reinsch, 2002).

6.2.5 Data analysis

TSA was performed on the SWC and ECa data from the 48 locations and the available number of surveys in each case. The mean of the relative differences (MRD) and the standard deviation of the relative differences (SDRD) proposed by Vachaud et al. (1985) were calculated as follows:

$$RD_{ij} = \left(\theta_{ij} - \langle\theta\rangle_j\right)/\langle\theta\rangle_j \tag{6.1}$$

$$MRD_i = \frac{1}{\mathrm{N}}\sum_{j=1}^{j=N} RD_{ij} \tag{6.2}$$

$$SDRD_i = \sqrt{\frac{1}{N-1}\sum_{j=1}^{j=N}\left(RD_{ij} - MRD_i\right)^2} \tag{6.3}$$

Also the root mean squared error (RMSE) proposed by Jacobs et al. (2004) and the mean absolute bias error (MABE) proposed by Hu et al. (2010) were calculated according to:

$$RMSE_i = \sqrt{MRD_i^2 + SDRD_i^2} \tag{6.4}$$

$$MABE_i = \sum_{j=1}^{j=N}\left|\frac{RD_{ij} - MRD_i}{1 + MRD_i}\right|, \tag{6.5}$$

where *i* stands for location, *j* for the survey number, θ for the gravimetric SWC, *N* is the number of surveys, and *RD* is the relative difference (Vachaud et al. 1985). A third TSA was performed using interpolated ECa maps. MRD and SDRD were analyzed for each pixel.

In transforming the data to relative differences, the ECa data from each survey are standardized. Maps of the MRD are useful for identifying zones in the field with ECa values of similar magnitude, or lower or greater than the spatial mean.

At each location the relationship between the spatial mean (y) and the corresponding point value (x) at the different survey dates was also studied. Different relationships were fitted for both SWC and ECa, including linear relationships,

$$y = m \cdot x, \tag{6.6}$$

exponential relationships,

$$y = C \cdot (1 - \exp^{-A_0 \cdot x}), \tag{6.7}$$

and power law equations,

$$y = a \cdot x^b, \tag{6.8}$$

where m, C, A_0, a and b are parameters.

Correlation coefficients (R) and coefficients of determination (R^2) were calculated for each analyzed relationship to determine the type and degree of association between the spatial mean and point values, to compare these with the traditional measures of temporal stability (Eqs. 6.2-6.5). Finally, the soil profile mean clay content of the 48 soil profiles was calculated and relationships with parameters from equations 6.6, 6.7, and 6.8 were explored.

6.3 Results and discussion

6.3.1 Soil water content

The temporal evolution of mean temperature (Tm, ºC), precipitation (P, mm), mean gravimetric soil water content (SWC, kg kg^{-1}) and mean apparent electrical conductivity (ECa-H1, mS m^{-1}) are shown in figure 6.3. Since the maximum soil depth is 1.2 m, in the remainder of this paper, we examine the ECa signal from the 1-m H coil configuration; with a DOE of approximately 1.5 m.

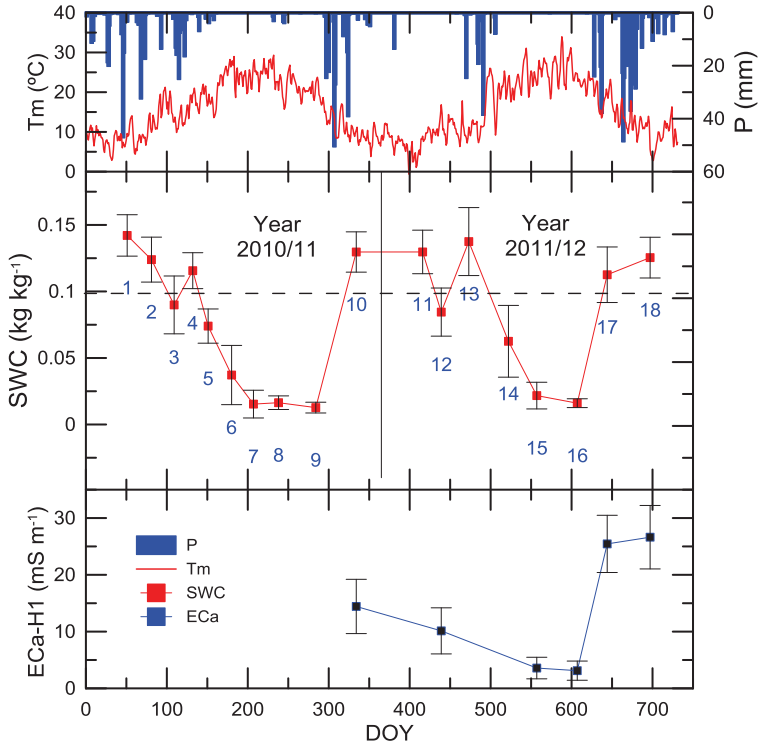

Figure 6. 3 Temporal evolution of mean temperature (Tm, ºC), precipitation (P, mm), gravimetric soil water content (SWC, kg kg^{-1}) and apparent electrical conductivity (ECa-H1, mS m^{-1}) for hydrologic years 2011 and 2012. Error bars indicate standard deviation.

Descriptive statistics of SWC (kg kg^{-1}) for each survey date (Table 6.1) indicated that mean SWC under 0.02 kg kg^{-1} occurred in summer while values over 0.11 kg kg^{-1} were common during autumn and winter. Surveys 13 and 17 showed a leptokurtic distribution and positive skewness coefficients. The SWC state on these survey dates is the result of a drying period interrupted by intense and brief rainfall events, resulting in a non-uniform wetting of the catchment.

Table 6. 1 Descriptive statistics of soil water content (SWC, kg kg^{-1}) data for each survey.

	Survey number								
	1 2/2011	2 3/2011	3 4/2011	4 5/2011	5 5/2011	6 6/2011	7 7/2011	8 8/2011	9 10/2011
N	47	48	42	48	48	44	35	48	45
Mean	0.14	0.13	0.09	0.12	0.08	0.04	0.02	0.02	0.01
SD	0.02	0.02	0.02	0.01	0.02	0.02	0.02	0.01	0.00
C.V.	13.2	14.0	24.8	12.9	19.4	57.4	91.4	49.5	35.8
Minimum	0.08	0.08	0.02	0.08	0.05	0.01	0.01	0.00	0.01
Median	0.14	0.13	0.09	0.11	0.08	0.03	0.01	0.02	0.01
Maximum	0.19	0.17	0.13	0.16	0.13	0.08	0.08	0.05	0.02
Skew	-0.31	-0.17	-1.43	0.31	0.74	1.11	1.78	1.20	0.71
Kurtosis	2.27	0.50	2.81	0.80	1.59	-0.01	1.83	2.43	-1.50

Survey number

	10 11/2012	11 2/2012	12 3/2012	13 4/2012	14 6/2012	15 7/2012	16 8/2012	17 10/2012	18 11/2012
N	47	47	48	46	47	46	48	48	48
Mean	0.13	0.13	0.09	0.14	0.07	0.02	0.02	0.11	0.13
SD	0.02	0.02	0.02	0.03	0.03	0.01	0.01	0.02	0.02
C.V.	12.9	13.9	21.1	19.2	39.3	51.7	34.1	18.2	14.5
Minimum	0.10	0.10	0.03	0.10	0.02	0.01	0.01	0.07	0.10
Median	0.13	0.13	0.09	0.13	0.07	0.02	0.02	0.11	0.13
Maximum	0.19	0.19	0.14	0.23	0.12	0.05	0.03	0.20	0.19
Skew	0.74	0.92	0.01	1.97	-0.01	1.15	0.12	1.61	0.81
Kurtosis	1.74	1.30	1.80	3.97	-0.54	0.52	-0.57	5.00	1.04

6.3.2 ECa measurements

Descriptive statistics of apparent electrical conductivity (ECa-H1, mS m^{-1}) for each survey date (Table 6.2) showed that surveys 17 and 18 had the highest mean ECa and a CV of 18 and 14%, respectively. Surveys 10 and 12 showed intermediate mean ECa and CV of 13 and 21%, while surveys 15 and 16 presented the lowest mean ECa and CV of 52 and 34%, corresponding to dry soil conditions. Surveys with the highest positive skewness coefficients were those with the lowest ECa values with minimum values of 0 mS m^{-1} (as a result of the zeroing transformation explained in section 6.2.3). The skewness is attributable to the high ECa values found in locations with differences in management practices especially during summer when they are more notable.

Table 6. 2 Descriptive statistics of apparent electrical conductivity (ECa-H1, mS m^{-1}) data for each survey.

	Survey number					
	10 11/2011	12 03/2012	15 07/2012	16 08/2012	17 10/2012	18 11/2012
N	48	48	46	48	48	48
Mean	14.7	10.2	4.14	3.52	25.9	26.5
SD	4.83	4.09	2.75	2.11	5.12	5.44
C.V.	32.9	40.1	66.5	60.0	19.8	20. 6
Minimum	6.31	1.45	0.00	0.00	17.20	16.68
Median	13.8	10.3	3.80	3.35	26.0	26.8
Maximum	30.5	20.3	15.7	10.9	36.6	39.6
Skew	0.88	0.09	1.70	1.07	0.30	0.05
Kurtosis	1.27	-0.11	5.25	1.82	-0.58	-0.51

6.3.3 Soil profile samples

Table 6.3 contains the descriptive statistics of mean profile clay content (%). The spatial distribution of clay content is given as a location map (Figure 6.4). In the N part of the catchment an area with the lowest clay content can be distinguished, while in the SE part an area with higher clay content can be appreciated, in addition to a N-S fringe at the central part of the catchment.

Table 6. 3 Descriptive statistics of mean profile clay content (%).

	N	Mean	SD	C.V.	Minimum	Median	Maximum	Skew	Kurtosis
Clay Content (%)	48	18.5	2.7	14.3	12.0	18.9	23.6	-0.55	0.29

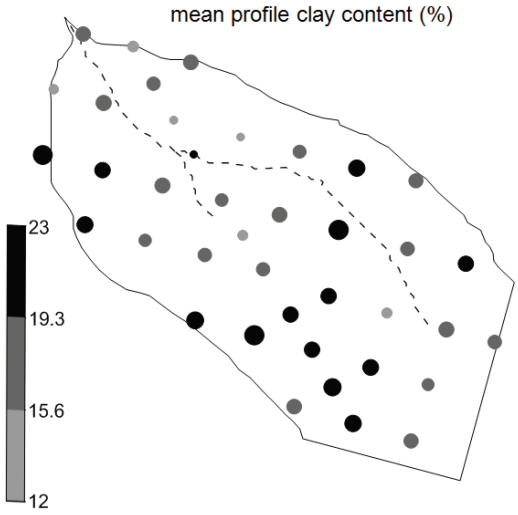

Figure 6. 4 Location map for clay content. The diameter of the circles is proportional to the values.

6.3.4 Temporal stability analysis of SWC and ECa measurements

A comparison of the different traditional measures of TSA for SWC and ECa is shown in Figs. 6.5 and 6.6. The RMSE, the MABE, and the SDRD with the ordered values of the absolute MRD for SWC and ECa are presented in these figures. SWC data indicated that for half of the 48 sampling points (Figure 6.5), with |MRD| values closest to zero, the associated RMSE, MABE and SDRD values were almost as high as the values associated with points showing the highest |MRD| values. This makes even more difficult the identification of locations with temporal stability of the SWC. Similar relationships were found for ECa data (Figure 6.6), especially for the MABE and the SDRD. For the RMSE, by taking the |MRD| values close to zero, the maximum RMSE is 0.4, and when establishing this value as a threshold, approximately the 70 % of the sampling points are retained.

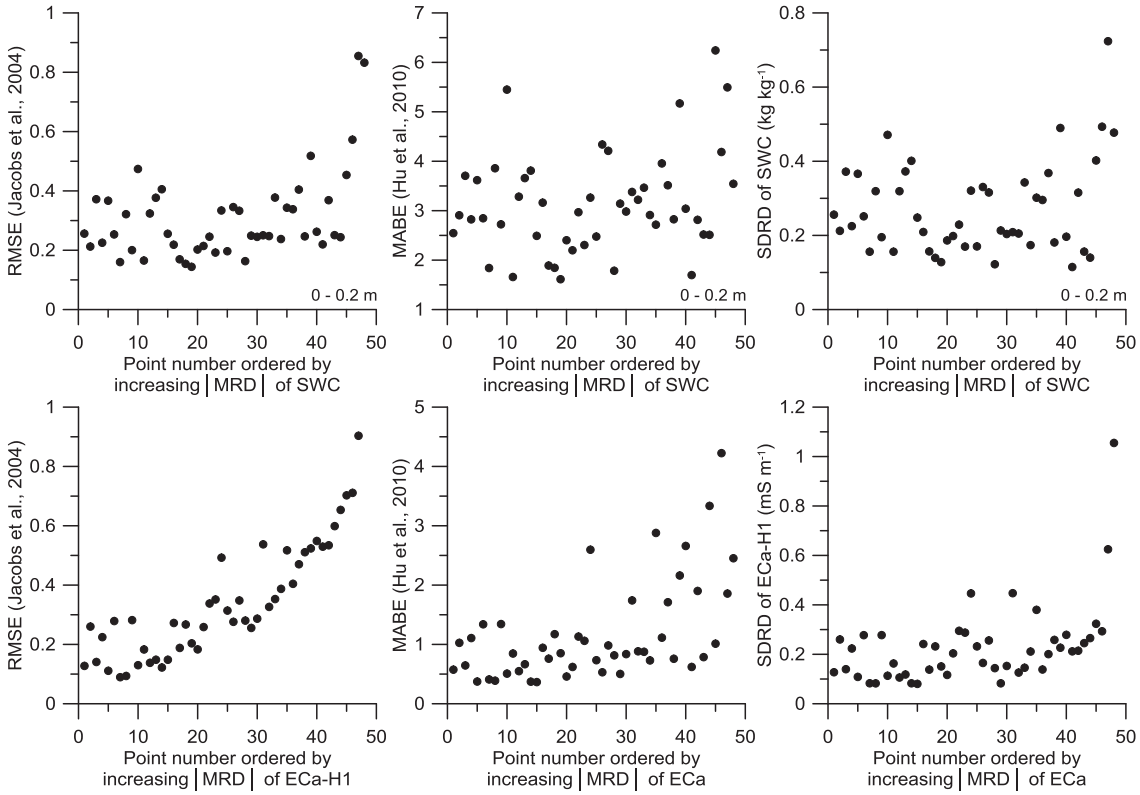

Figure 6. 5 Relationships between the root mean squared error (RMSE), the mean absolute bias error (MABE), and the standard deviation of the relative difference (SDRD) with the ordered values of the absolute mean relative difference (MRD) for soil water content (SWC) and apparent electrical conductivity (ECa-H1) data.

Although the RMSE, MABE and the |MRD| increased with increasing SDRD, locations with lower SDRD values were related to RMSE, MABE and |MRD| values, similar to values from locations with mean SDRD, for SWC and ECa.

The usefulness of traditional TSA is not amended by these relationships nevertheless the identification of representative locations based on these relationships may lead to a large amount of locations which are far from each other.

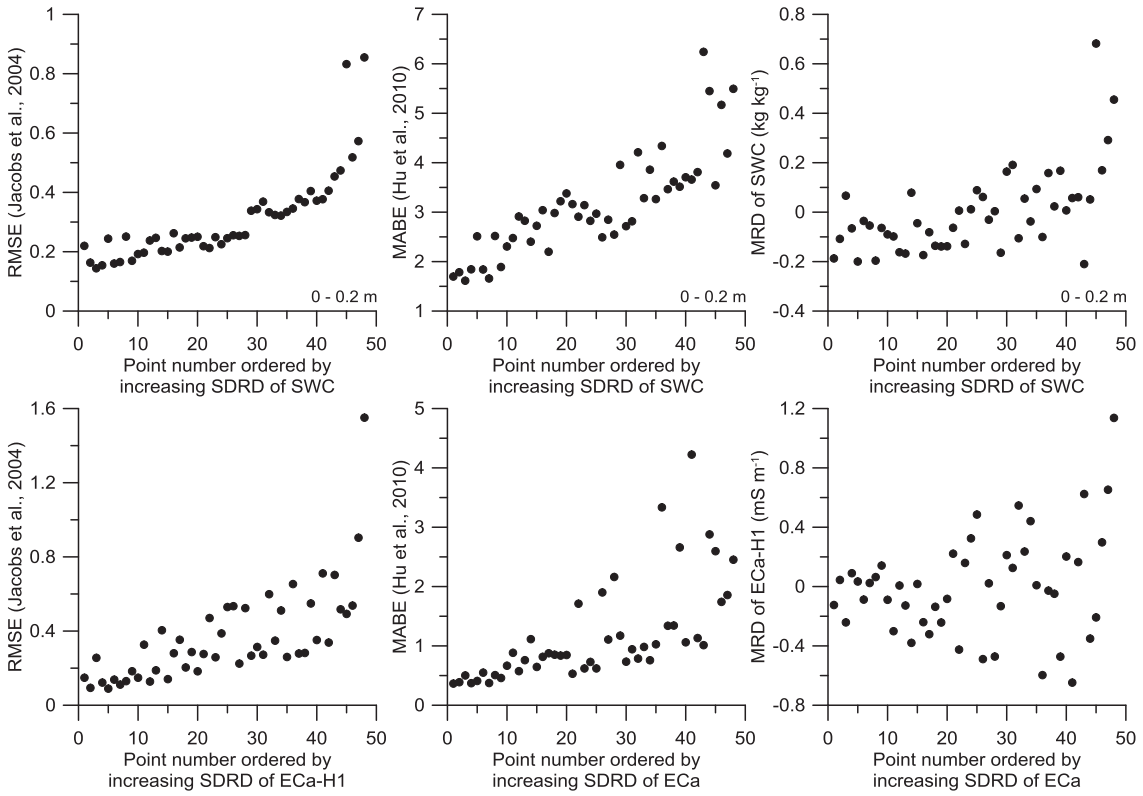

Figure 6. 6 Relationships between the root mean squared error (RMSE), the mean absolute bias error (MABE), and the mean relative difference (MRD) with the standard deviation of the relative difference (SDRD) for soil water content (SWC) and apparent electrical conductivity (ECa-H1).

Temporal stability analysis as proposed by Vachaud et al. (1985), implicitly relies on the assumption of linear relations at all sampling locations, between the observed SWC and the spatial mean SWC. Therefore, the R between both was calculated at each sampling location and related to the MRD, SDRD, RMSE and MABE (Figure 6.7). The R ranged from 0.92 to 1, indicating that all locations represent the spatial mean SWC relatively well. R values higher than 0.98 showed MRD ranging from -0.2 to 0.7, SDRD from 0.1 to 0.7, RMSE from 0.1 to 0.9 and MABE from 0.5 to 6.51. Approximately the entire range of MRD, SDRD, RMSE and MABE is covered by locations with R values greater than 0.98 (strong linear relationships), indicating that the R value is not useful to identify representative locations with temporal stability. The same relationships were calculated for ECa data (Figure 6.8). The R coefficient ranged from 0.94 to 1, and R values higher than 0.98 showed MRD ranging from -0.6 to 0.6, SDRD from 0.1 to 0.6, RMSE from 0.1 to 0.9 and MABE from 0.5 to 4.5[1].

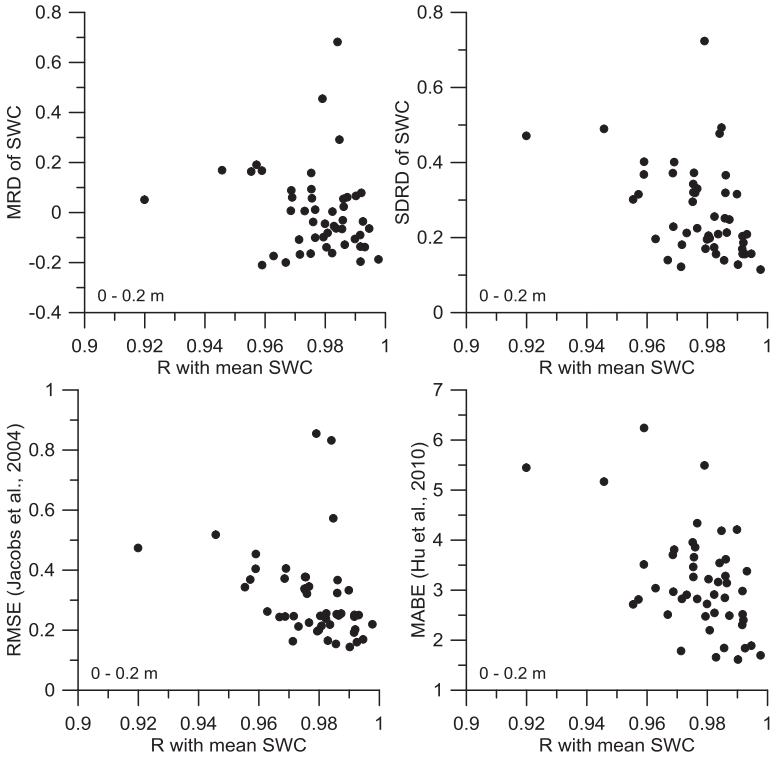

Figure 6. 7 Relationships between the root mean squared error (RMSE), the mean absolute bias error (MABE), the mean relative difference (MRD) and the standard deviation of the relative difference (SDRD) versus the correlation coefficient (R) with the mean soil water content (SWC, kg kg-1).

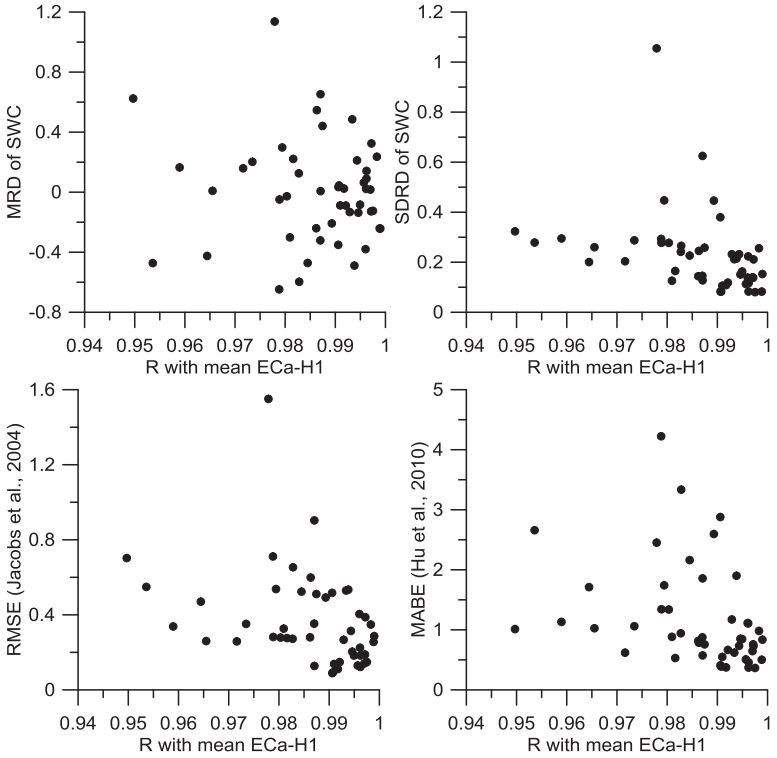

Figure 6. 8 Relationships between the root mean squared error (RMSE), the mean absolute bias error (MABE), the mean relative difference (MRD) and the standard deviation of the relative difference (SDRD) versus the correlation coefficient (R) with the apparent electrical conductivity (ECa-H1, mS m^{-1}).

Relationship between the R with the mean SWC and the R with the mean ECa (Figure 6.9) showed that some locations with higher R values for ECa had lower R values for SWC, and viceversa. In the light of the presented results, each sampling location was individually studied.

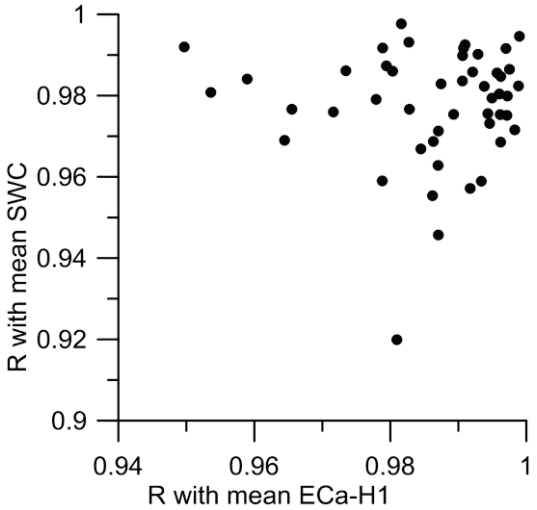

Figure 6. 9 Relationship between the R with the mean soil water content (SWC, kg kg-1) and the mean apparent electrical conductivity (ECa-H1,mS m-1).

6.3.5 Fitted models for SWC and ECa measurements

Linear, exponential and power law models

At each sampling location, three different models (linear (Eq. 6.6), exponential (Eq. 6.7) and power law (Eq. 6.8)) were fitted to the point and spatially averaged SWC and ECa data. We start from the initial hypothesis that a linear model describes best the relationship between point SWC and ECa and their spatial means at each location. The criterion used to reject this hypothesis and adopt the exponential or the power law model was an increment in R^2 greater than 0.01. For SWC 25% of the 48 locations were better modeled with the exponential relationship. In the case of ECa 33% was better modeled with the exponential relationship and 25% with the power law.

Locations 37, 44 and 33 are representative of the different patterns found for ECa and SWC (Figure 6.10). For location 37 a linear relationship suited best for SWC and ECa. Location 44 showed an exponential relationship for SWC and ECa, indicative of an upper limit for the spatial average and point values that still increase beyond this threshold. Location 33 presented a power law relationship for ECa and a linear relationship for SWC, with the $m< 1$. In terms of ECa, locations that follow an exponential model show lower point values than the spatial mean,

while locations that follow a power law model show higher point values than the spatial mean, for each survey.

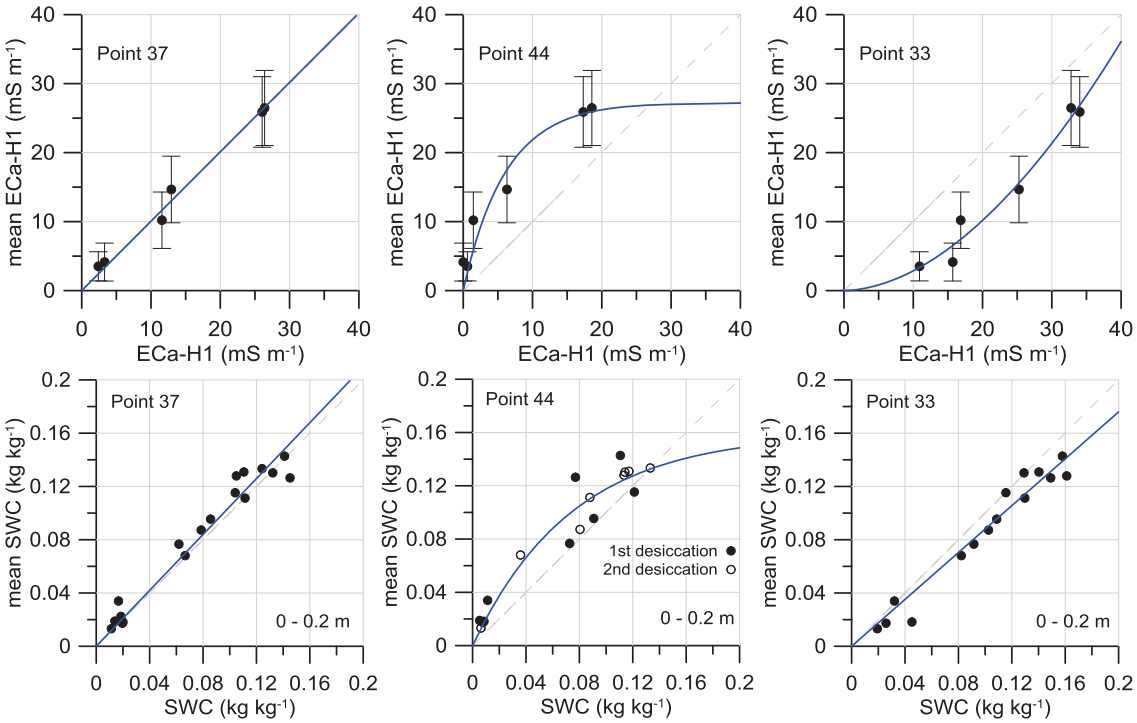

Figure 6. 10 Relationships between the spatial mean and point values of apparent electrical conductivity (ECa-H1) and soil water content (SWC) for each survey at locations 37, 44 and 33. These locations are representative for the different patterns found.

In terms of SWC, locations with an exponential model showed lower point values than the spatial mean of SWC, in contrast to locations with a linear model where point values are similar to the spatial mean, for all the surveys. Fitted linear models showed *m* values ranging from 0.7 to 1.2. *m* values lower than 1 indicated locations with steadily lower SWC than the spatial mean and *m* values higher than 1 are indicative of locations with SWC above the spatial mean. Approximately half (47%) of the locations that followed the linear pattern showed a tendency towards the exponential model for the highest SWCs (e.g. point 30, Figure 6.11). However, since only a small number of points caused this apparent trend, the R^2 did not improve when using the exponential model instead of the linear model. This indicates that at some locations a maximum SWC is reached which is higher than the spatial mean SWC, possibly as a result of combined effects of soil texture and topography.

Overall, 70% of the locations showed a linear behavior for SWC and 40% for ECa. 92% of the locations with a power-law behavior for ECa followed a linear behavior for SWC. One third of the locations with an exponential model for ECa showed also an exponential behavior of SWC. The latter is probably due to locations that behaved similar to point 30 (Figure 6.11) where the

lack of measurements at higher SWCs masks the visualization of the exponential behavior. This indicates that ECa data are more useful to identify sampling locations with linear behavior in these semi-arid environments, even though three times less surveys were available for ECa as compared to SWC. Locations with a linear behavior are indicative of temporal stability in SWC.

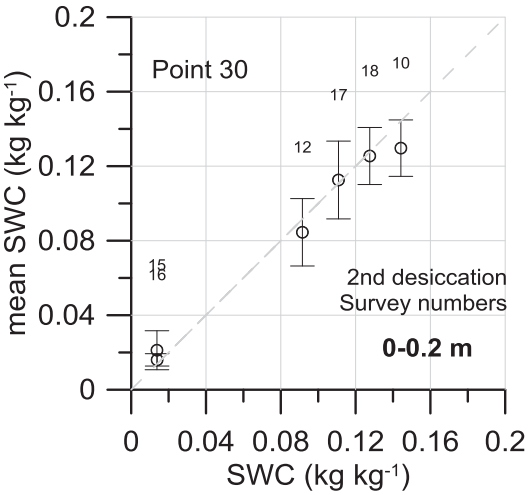

Figure 6. 11 Relationship between point and spatial mean SWC for six survey dates at location 30.

Relationship between clay content and parameters from the models

The influence of clay content on the different relationships between point and spatial mean SWC and ECa were explored at the 48 locations. Relationships between profile mean clay content and the fitted parameters from the linear (m) and exponential (A_0, C) models that best fitted SWC (Figure 6.12) at each location, showed that: 1) clay content decreased with m value, with higher clay contents for $m<1$ and lower clay contents for $m>1$; 2) clay content decreased with A_0, indicating that the higher the clay content the smaller the point SWC value at which the mean SWC reaches its maximum; and 3) clay content increases with C, indicating that the higher the clay content the higher the maximum mean SWC.

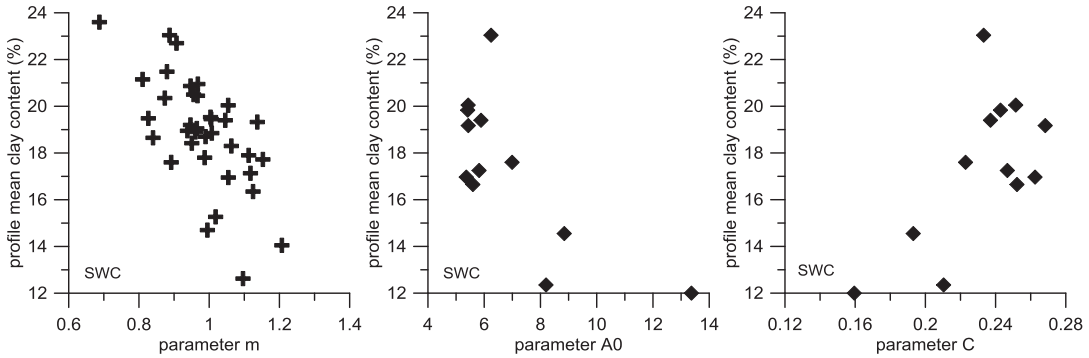

Figure 6. 12 Relationships between profile mean clay content (%) and parameters from the fitted linear (m) and exponential (A0, C) models to the relationship between point and spatial mean soil water content (SWC).

Relationships between profile mean clay content (%) and parameters from the fitted linear (*m*), exponential (A_0, *C*) and power-law (*a*, *b*) models to the relationships between point and mean ECa (Figure 6.13) were similar to those found for SWC. The power-law model was mainly found at locations with higher clay contents (from 17 to 24%).

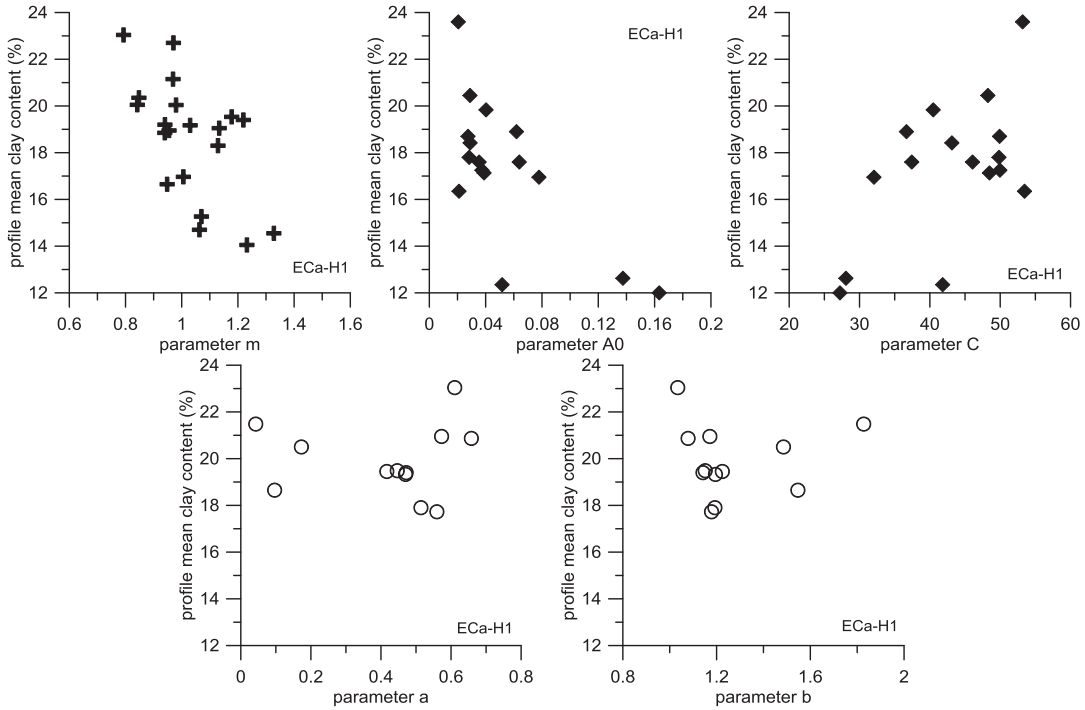

Figure 6. 13 Relationships between profile mean clay content (%) and parameters from the linear (m), exponential (A0, C) and power law (a, b) models fitted to the relationship between point and mean apparent electrical conductivity (ECa-H1).

Most of the locations with a linear behavior showed R^2 values higher than 0.95 for SWC and ECa (Figure 6.14). Those locations are most appropriate in terms of temporal stability and representativeness of the spatial mean SWC. ECa was more helpful (Figure 6.10) than SWC to identify such locations. From ECa data it was possible to discriminate locations with nonlinear behavior (exponential or power law), while from SWC data the power law behavior cannot be determined.

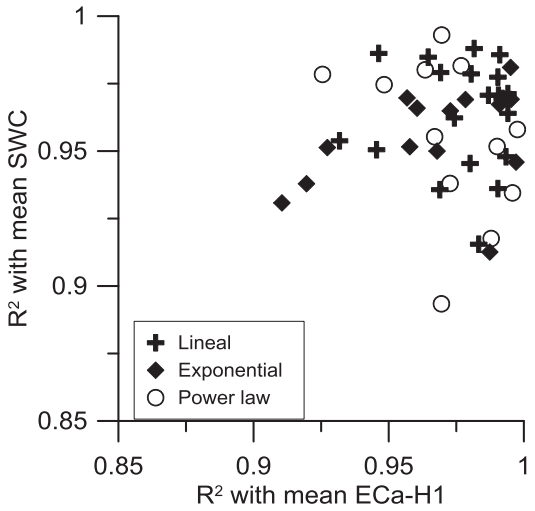

Figure 6. 14 Relationship between the R^2 with the mean soil water content (SWC, kg kg-1) and the mean apparent electrical conductivity (ECa-H1) calculated from the best adjusted models (linear, exponential and power law) for each sampling point.

TSA of ECa surveys

Figure 6.15 shows a map of the MRD obtained from the interpolated ECa maps. Negative MRD values (MRD < - 0.2), in blue, delimited areas with steadily lower ECa values as compared to the spatial mean. Positive MRD values (MRD< + 0.2), in red, delimited areas with steadily higher ECa values as compared to the spatial mean. Intermediate to low MRD values (-0.2>MRD>0.2) delimited areas that generally showed ECa values close to the spatial mean. Areas with intermediate to low MRD corresponded to what we defined in this work as "linear behavior" (Figure 6.10), being most appropriate for TSA. As pointed out for figure 6.13 the different behavior of different points was related to clay content. Here this is corroborated by the spatial distribution of these areas, which is similar to the pattern found for clay content (Figure 6.4). The spatial distribution of MRD showed the lowest MRD in the northern part of the catchment, while the highest values were found the southwestern area, near the border of the catchment. Also a N-S fringe in the central part of the catchment showed high MRD.

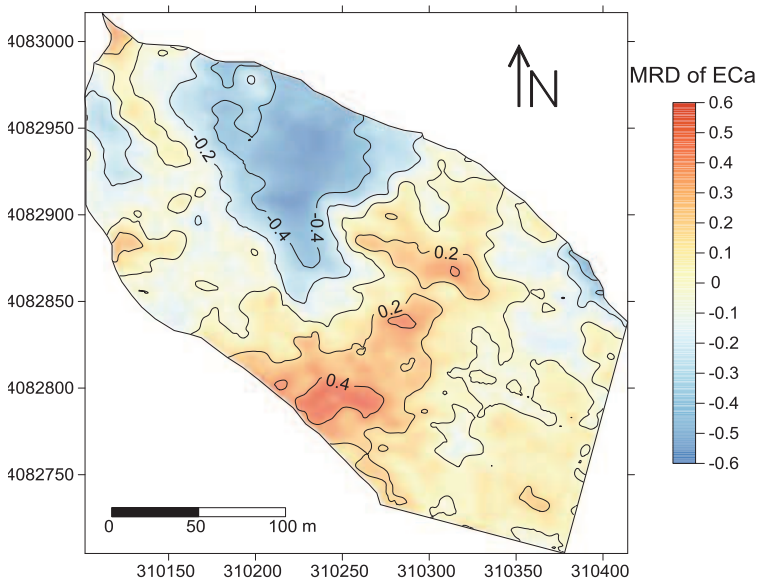

Figure 6. 15 Mean relative difference (MRD) of apparent electrical conductivity (ECa, mS m^{-1}), overlying contour lines of the MRD of ECa.

6.4 Conclusions

Representative areas for spatial mean SWC estimation were identified in the field based on the search of zones with a "linear behavior". Using temporal stability analysis for SWC and ECa, MRD, SDRD, RMSE and MABE were compared in their ability to identify representative locations. For both, SWC (18 soil surveys) and ECa (6 soil surveys), locations with MRDs close to zero and small SDRDs showed RMSE and MABE values close to those found at other locations. Since temporal stability analysis (Vachaud et al. 1985) relies on the assumption of a linear relationship between point observations and the spatial mean of SWC, this relationship was evaluated for each location. At some locations an exponential relationship was found more appropriate in terms of a higher R^2 as compared to the linear relationship. For ECa, also a power law was found more appropriate at certain locations. Those locations showed generally a linear behavior for SWC. The different behaviors found for SWC and ECa could be explained by differences in soil texture (*i.e.* clay content), which is directly related to soil water content. Since the non-linear behavior could be more easily identified from ECa, for which only six surveys were available, as compared to the eighteen SWC surveys, a TSA from the interpolated ECa maps was performed to identify zones in the field with "linear behavior". Locations with linear behavior showed greater R^2 values as compared with the exponential and power law relationships for ECa and SWC data. The results suggest that the identified zones are preferential to estimate the spatial mean ECa or SWC of the catchment.

REFERENCES

Brevik E.C., Fenton T.E., Lazari A. 2006. Soil electrical conductivity as a function of soil water content and implications for soil mapping. Precis. Agric.. 10.1007/s11119-006-9021-x.

Brevik E.C., Fenton T.E. 2002. Influence of soil water content, clay, temperature, and carbonate mineral son electrical conductivity readings taken with an EM-38. Soil Survey Horizons, 43(1): 9-13.

Calamita G., Brocca L., Perrone A., Piscitelli S., Lapenna V., Melone F., Moramarco T. 2012. Electrical resistivity and TDR methods for soil moisture estimation in central Italy test-sites. J. Hydrol., 454-455 (2012) 101-112.

Corwin D.L., Lesch, S.M. 2003. Application of soil electrical conductivity to precision agriculture: Theory, principle and guidelines. Agron. J., 95:455-471.

Corwin D.L., Lesch S.M. 2005. Characterizing soil spatial variability with apparent soil electrical conductivity: I. Survey protocols. Comp. Electron. Agric., 46:103-133.

Espejo A., Giráldez J.V., Vanderlinden K., Taguas E.V., Pedrera A. 2014. A method for estimating soil water diffusivity from moisture profiles and its applications across an experimental catchment. J. Hydrol., 516:161-168.

Friedman S.P. 2005. Soil properties influencing apparent electrical conductivity: a review. Comput. Electron. Agric., 46:45–70.

García del Barrio I., Malvárez L., González J.I. 1971. Mapas provinciales de suelos. Cádiz. Ministerio de Agricultura. Madrid.

Grayson R.B., Western A.W. 1998. Towards areal estimation of soil water content from point measurements: Time and space stability of mean response. J. Hydrol., 207:68-82.

Grossman R.B., Reinsch T.G. 2002. The solid phase, in: Dane, J. H., Topp, G. C. (Eds.), SSSA Book Series: 5. Methods of Soil Analysis. Part 4 – Physical Methods. Soil Science Society of America, Madison, Wisconsin, USA, pp. 201-415.

Hu W., Shao M.A., Reichardt K. 2010. Using a new criterion to identify sites for mean soil water storage evaluation. Soil Sci. Soc. Am. J., 74:762-773.

Jacobs J.M., Mohanty E., Hsu E., Miller D. 2004. SMEX02: Field scale variability, time stability and similarity of soil moisture. Remote Sens. Environ. 92:436-446.

James I.T., Waine T.W., Bradley R.I., Taylor J.C., Godwin R.J. 2003. Determination of soil type boundaries using electromagnetic induction scanning techniques. Biosyst. Eng., 86:421–430.

Martínez G., Vanderlinden K., Espejo A.J., Giráldez J.V., Muriel J.L. 2010. Field-scale soil moisture pattern mapping using electromagnetic induction. Vadose Zone J., 9:871–881.

Martinez G., Vanderlinden K., Ordoñez R., Muriel J.L. 2009. Can apparent electrical conductivity improve the spatial characterization of soil organic carbon?. Vadose Zone J., DOI: 10.2136/vzj2008.0123.

McCutcheon M.C., Faharani H.J., Stednick J.D., Buchleiter G.W., Green T.R. 2006. Effect of soil water on apparent soil electrical conductivity and texture relationships in a dryland field. Biosyst. Eng., 94:19-32.

McNeill J.D. 1980. Electromagnetic terrain conductivity measurement at low induction numbers.Technical Note TN-6.Geonics Limited, Missisauga, Ontario, Canada.

Mualem Y., Friedman S.P. 1991. Theoretical prediction of electrical conductivity in saturated and unsaturated soil. Water Resour. Res., 27:2771–2777.

Núñez-Maderal E. 2008. Calculadora geodésica edición especial para la Península Ibérica, Cartesia.org, Spain.http://www.cartesia.org/download.php?op=viewdownloaddetails&lid=172&ttitle=Calculadora_UTM-Geogr%E1ficas_Espa%F1a. Accessed 11 July 2014.

Rhoades J.D., Raats P.C.A., Prather R.J. 1976. Effects of liquid-phase electrical conductivity, water content, and surface conductivity on bulk soil electrical conductivity. Soil Sci. Soc. Am. J., 40:652-655.

Robinson D.A., Abdu H., Lebron I., Jones S. 2012. Imaging of hill-slope soil moisture wetting patterns in a semi-arid oak savanna catchment using time-lapse electromagnetic induction. J. Hydrol., DOI: 10.1016/j.jhydrol.2011.11.034.

Saey T., Simpson D., Vitharana U.W.A., Vermeersch H., Vermang J., van Meirvenne M. 2008. Reconstructing the paleotopography beneath the loess cover with the aid of an electromagnetic induction sensor. Catena 74 (2008) 58–64.

Seneviratne S.I., Corti T., Davin E.L., Hirschi M., Jaeger E.B., Lehner I., Orlowsky B., Teuling A.J. 2010. Investigating soil moisture climate interactions in a changing climate: A review. Earth Sci. Rev., 99: 125-161.

Sheets K.R., Hendrickx J.M.H. 1995. Noninvasive soil water content measurement using electromagnetic induction. Water Resour. Res., 31:2401-2409.

Soil Survey Staff. 1999. Soil taxonomy: A basic system of soil classification for making and interpreting soil surveys. 2nd ed. NRCS USDA Agr. Hbk. 436

Vachaud G., Passerat De Silans A., Balabanis P., Vauclin M. 1985. Temporal stability of spatially measured soil water probability density function. Soil Sci. Soc. Am. J., 49:822-828.

Vanderlinden K., Verrecken H., Hardelauf H., Herbst M., Martinez G., Cosh M.H., Pachepsky Y.A. 2012. Temporal stability of soil water contents: a review of data and analyses. Vadose Zone J., doi:10.2136/vzj2011.0178.

Vereecken H., Huisman J.A., Bogena H., Vanderborght J., Vrugt J.A., Hopmans J.W. 2008. On the value of soil moisture measurements in vadose zone hydrology: A review. Water Resour. Res., 44, W00D06, doi:10.1029/2008WR006829.

Vitharana U.W.A., van Meirvenne M., Cockx L., Bourgeois J. 2006 Identifying potential management zones in a layered soil using several sources of ancillary information. Soil Use Manage. 22:405-413

Whelan B.M., McBratney A.B., Minasny B. 2002. Vesper 1.5 – spatial prediction software for precision agriculture. In: Robert PC, Rust RH, Larson WE. (eds.) Precision Agriculture, Proceedings of the 6th International Conference on Precision Agriculture, ASA/CSSA/SSSA, Madison, Wisconsin.

Chapter 7. General Conclusions and Future Research Directions

7.1 General conclusions

A mobile platform was developed to acquire efficiently high resolution apparent electrical conductivity (ECa) data in traditional olive orchards. This mobile platform is described in Chapter 2 and it consists of a sled made of non-metallic pieces that hosts an electromagnetic induction (EMI) soil sensor, the DUALEM-21S (D21S). The design of the sled avoids overturning of the sensor, mechanical damages and sensor warming. The D21S does not need direct soil contact. Within the sled it is operated at 0.075 m above the soil surface. An all-terrain vehicle (ATV) pulls the sled via a non-metallic articulated arm of two 2 meter length. This articulation is designed to avoid interferences from the metallic pieces of the ATV and to turn the sled easily between tree rows. Additional equipment such as a field PC, a RTK-GPS receiver and a guidance system was also included. Using this mobile configuration, simultaneous measurements of ECa, apparent magnetic susceptibility, coordinates and elevation are acquired at the desired spatial resolution in each studied field.

Soil moisture conditions close to field capacity are generally recommended for ECa surveys, but are not met during long periods of the year in the study region. Results from Chapter 4 showed that field capacity is not an absolute requisite for EMI surveys. Relative spatial variations in ECa were stable in time and independent of the general soil water status, as a result of the dominant relationship between ECa and time-invariant soil properties, such as clay content. However, repeated ECa surveys in time add information of time-dependent variables, such as soil water content.

Soil properties influence ECa in different ways. The spatial relationships between soil properties and ECa improved when the study area was classified according to ECa. In chapters 3 and 5 two catchments (La Conchuela and La Manga) were classified using this approach in three and four areas, respectively.

Impaired tree development and die-off was observed at the "La Conchuela" catchment (Chapter 3). After two EMI surveys three management areas were delimited in terms of ECa. The three areas were related to tree development. The area with the lowest average ECa (zone A) showed

optimal tree growth, the area with the highest ECa values (zone C) showed acceptable tree development, but in the area with intermediate ECa values (zone B) tree-growth and die-off were observed. Spatial variations in soil properties (soil water content (SWC), clay content, stone content...) were related to the spatial variation in measured ECa. The downslope position of area B in combination with the spatial relative values of measured soil properties caused deficient drainage conditions, which led to saturation and water logging conditions during wet periods. The better drainage conditions in zone A were confirmed by the relationship between soil water content and ECa increments. Based on this information, management practices, such as removing infested trees or not replanting dead trees, can be proposed within zone B to reduce inputs and to prevent further spreading of the disease.

In Chapter 5, soil ECa values were used to delimit four areas in an olive orchard, based on the spatial distribution of the first principal component of seven ECa surveys. Soil properties (SWC, profile soil data and ECa) were studied within each area, and using analysis of the variance (ANOVA) significant differences were detected between classes for organic matter, pH, clay content and bulk density. Relationships between soil profile data and ECa were also studied. Soil texture (clay content) was the single soil property that showed positive and significant correlations for all survey dates. Temporal relationships between ECa and SWC were modeled using an exponential relationship, and parameters from the model showed significant differences between classes and were related to the time stable clay content. Results indicated a strong influence of clay contents on the relationship between SWC and ECa.

Finally, in Chapter 6, ECa-based representative zones for field-average soil moisture estimation were delimited. The assumed linear relationships between point SWC and ECa, and their spatial means were evaluated at each sampling location. At some locations the use of exponential relationships increased the coefficient of determination (R^2), as compared to the linear relationships. For ECa also power law relationships increased the R^2 at some locations. All locations with a linear behavior showed the greatest R^2 values as compared with the exponential or power law relationships for ECa and SWC. The different behaviors were all related to the state variable soil texture. Therefore, because from ECa data the non-lineal patterns were more easily discriminated, a temporal stability analysis from interpolated ECa maps was computed to identify zones in the field with this pattern. Those zones are preferred for field-average soil moisture estimation.

7.2 Future research

A single proximal soil sensor measurement cannot reflect all soil properties. Different sets of advantages and inconveniences are inherent to each proximal soil sensing technique. Ideally

simultaneous measurements can be made with complementary proximal soil sensors. Therefore, a future research avenue could be the integration of ground penetration radar (GPR) and EMI technologies in a single measurement platform. The GPR provides a very precise depth approximation of the interfaces between different underground features while EMI provides volumetric measurements of ECa for different soil volumes.

Another line for future research could focus on the integration of proximal and remote sensing techniques. Remote sensors record data above the soil surface, measuring only topsoil properties which might be different form subsoil properties. Also the identification of *Verticillium* wilt in olive orchards of different agronomic characteristics has been possible through remote sensing. Data from remote sensing techniques in addition to data obtained with the D21S on a mobile configuration (Chapter 2) will allow, not only the identification of physiological stress caused by *Verticillium* wilt, but also the delineation of different management zones and the possible explanation for *Verticillium dahliae* infestation, based on topographic indexes and soil properties.

Another line for future research can focus on the practical field applications. During the last decades the traditional olive orchards have been transformed due to the increasing market demand, with the adoption of high plantation densities, the introduction of drip irrigation, the occupation of more fertile soils in the valleys... Higher yields and lower inputs are the prime characteristics of Precision Agriculture techniques, but to apply these techniques management zones have to be delimited. This spatial classification could be based on apparent electrical conductivity surveys. The soil properties that directly or indirectly affect ECa can provide information on limiting soil conditions for yield, which can be compared to expected optimal yields obtained under normal weather conditions.

APPENDIX

- Pedrera-Parrilla A., Martínez G., Espejo-Pérez A.J., Gómez J.A., Giráldez J.V., Vanderlinden K. Mapping impaired olive tree development using lectromagnetic induction surveys. 2014. Plant and Soil, DOI 10.1007/s11104-014-2207-5.

- Currículum vítae.

Mapping impaired olive tree development using electromagnetic induction surveys

Aura Pedrera-Parrilla, Gonzalo Martínez, Antonio Jesús Espejo-Pérez, José Alfonso Gómez, Juan Vicente Giráldez & Karl Vanderlinden

Plant and Soil
An International Journal on Plant-Soil Relationships

ISSN 0032-079X

Plant Soil
DOI 10.1007/s11104-014-2207-5

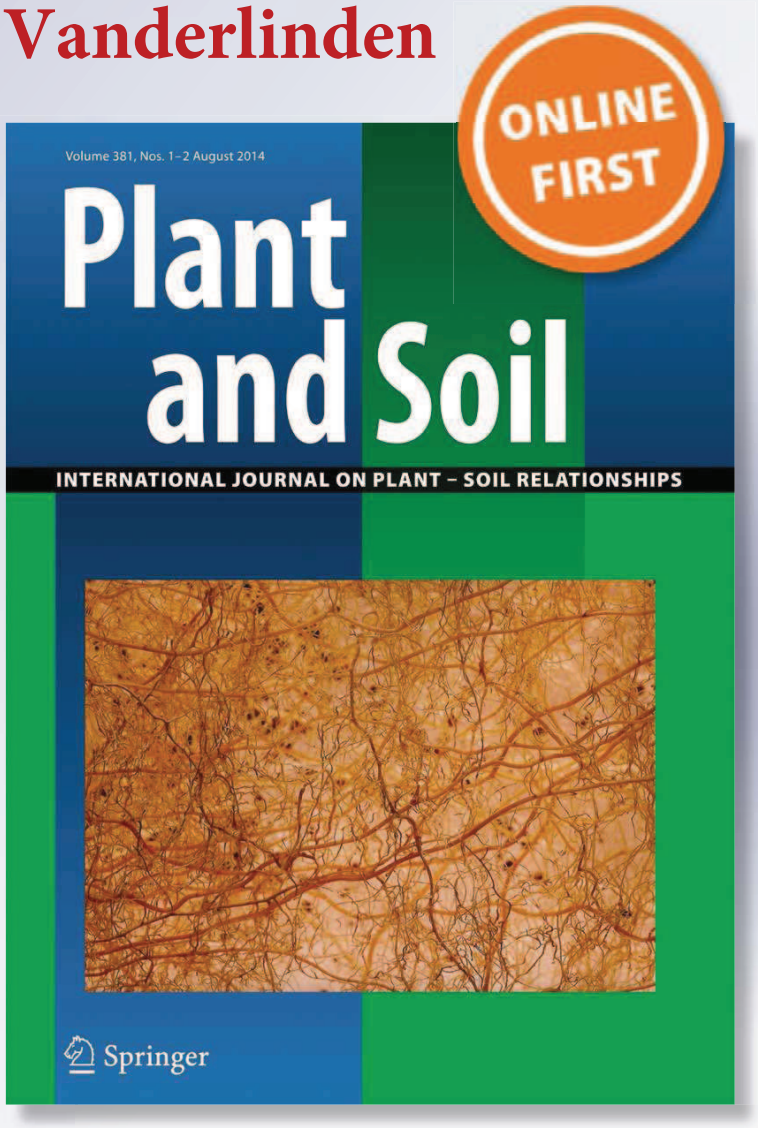

Springer

Plant Soil
DOI 10.1007/s11104-014-2207-5

REGULAR ARTICLE

Mapping impaired olive tree development using electromagnetic induction surveys

Aura Pedrera-Parrilla · Gonzalo Martínez · Antonio Jesús Espejo-Pérez · José Alfonso Gómez · Juan Vicente Giráldez · Karl Vanderlinden

Received: 4 March 2014 / Accepted: 17 July 2014

Abstract
Background and aims Future success of olive cropping in the Mediterranean depends critically on improving yield, reducing production costs, and preventing infestation by soil-borne pathogens. In order to put forward adequate soil management practices accurate knowledge of the spatial distribution of soil properties is required. The aims of this study were to delimit areas with constrained tree development in an olive orchard using electromagnetic induction (EMI), and to identify the causal relationships between apparent electrical conductivity (ECa) and soil properties.
Methods The experimental field was exhaustively sampled for different soil properties and ECa was measured in 2011 and 2012 under dry and wetter soil conditions, respectively.
Results The spatial ECa distribution matched the observed canopy coverage pattern well. Three zones were delimited according to ECa values from 0 to 27.5, from 27.5 to 57.5, and greater than 57.5 mS m^{-1}. All ECa signals, regardless of soil-water status, exhibited a common dominant ECa pattern. The area with the lowest ECa values (0–27.5 mS m^{-1}) showed optimal tree growth (45 % canopy coverage) and presented significantly lower average clay contents than the other two areas. Intermediate ECa values (27.5–57.5 mS m^{-1}) identified accurately the area with deficient tree development and tree die-off (12 % canopy coverage), and corresponded with an area along the drainage pathway where profile-averaged soil-water, clay, stone and organic matter content were highest.
Conclusions EMI surveys detected subtle differences in soil properties and provided useful information to delimit areas with constrained tree development. The approach can be used as a screening technique before installing tree plantations.

Keywords Olive · Soil-borne pathogens · Apparent electrical conductivity · Soil management · Vertisol · Soil water content

Abbreviations

ANOVA	analysis of variance
CA	projected canopy area
CV	coefficient of variation
DOE	depth of exploration

Responsible Editor: Hans Lambers.

A. Pedrera-Parrilla · K. Vanderlinden (✉)
IFAPA, Centro Las Torres-Tomejil, Ctra. Sevilla-Cazalla km 12.2, 41200 Alcalá del Río, Sevilla, Spain
e-mail: karl.vanderlinden@juntadeandalucia.es

A. J. Espejo-Pérez · J. V. Giráldez
Departamento de Agronomía, Universidad de Córdoba, Campus de Rabanales, Edificio da Vinci. Ctra. km 396 Madrid 14071 Córdoba, Spain

J. A. Gómez · J. V. Giráldez
Instituto de Agricultura Sostenible, CSIC, Apartado 4084, 14080 Córdoba, Spain

G. Martínez
IFAPA, Centro Alameda del obispo. Avda. Menéndez Pidal s/n, 14004 Córdoba, Spain

Published online: 03 August 2014

ECa	apparent electrical conductivity
EMI	electromagnetic induction
H	horizontal co-planar coil orientation
KC	kurtosis coefficient
OM	organic matter
P	perpendicular coil orientation
s	standard deviation
SC	skewness coefficient
SWC	soil water content
WI	wetness index
Z	elevation

Introduction

Olives (*Olea europaea* L.) have supported Mediterranean civilizations for thousands of years. Nowadays olives remain important for their social and economic implications, e.g. in sustaining rural communities (Loumou and Giourga 2003) and for the health benefits of olive oil (de Backer et al. 1997; Clodoveo et al. 2014). Today, a total area of about 2.6 Mha is dedicated to olive cultivation in Spain, representing more than one fourth of the total world acreage of this crop (FAOSTAT 2012, MAGRAMA 2012). Spanish olive oil production represents 62 % of the total EU production (European Commission 2012). The largest olive cultivation area is situated in Andalusia, with approximately 60 % of the national acreage and 82 % of the national olive production (CAP 2012). Olive cultivation and associated industries contribute for 40 % to the rural employment in Andalusia and for almost one third of the region's agricultural production value.

Olives were traditionally cultivated on marginal, often sloping land, and poor soils (e.g., Semple 1931 chapter XIV). The increasing market demand and the introduction of drip irrigation improved the crop's profitability and promoted olive cultivation in the more fertile soils in the valleys. More olive production coincided with the adoption of high plantation densities and the development of high yield varieties, but resulted in an increasing appearance of soil borne diseases, such as Verticillium wilt, caused by the fungus *Verticillium dahliae* Kleb. (Sánchez-Hernández et al. 1998, Navas-Cortés et al. 2008, López-Escudero and Mercado-Blanco 2011). During four cropping seasons Navas-Cortés et al. (2008) found the largest infection rates from late winter to early spring, corresponding roughly to the wettest period of the year. Propagation within the field is possibly caused by the transport of infested plant material (e.g. leafs or fruits) or soil particles by runoff water, wind or tillage. Diseases are often associated with temporary waterlogging conditions, while soil properties, tree age and cultivar contribute to the risk of infestation (López-Escudero and Mercado-Blanco 2011). Despite recent advances in remote-sensing techniques for the early detection of *Verticillium* wilt (Calderón et al. 2013), the disease causes important losses to the farmers who need to reestablish their plantations. Other fungi such as *Phytophtora* spp cause root rot, and are often associated with deficient drainage and soil aeration conditions, which if persisting in time cause also root asphyxia. Optimal growing conditions for olive trees are generally found in non-stratified, moderately fine textured soils, with good aeration and permeability, and high water-holding capacity. Such conditions are often not found in the generally more clayey valley soils. Despite the obvious effects of terrain and soil characteristics on olive growth and susceptibility to soil-borne diseases, little attention is generally paid to the within-field variability of these factors when establishing new plantations.

Conventional soil surveying to determine spatial patterns of soil properties is in general prohibitive at commercial farms. Soil sampling is time consuming, expensive and provides only a limited spatial coverage. Electromagnetic induction (EMI) sensors provide a suitable alternative (Minasny et al. 2013; Doolittle and Brevik 2014; and references therein), providing simultaneously apparent electrical conductivity (ECa) values of different soil volumes with varying depths. Under non-saline conditions ECa depends in theory only on soil water content and temperature (Keller and Frischknecht, 1966). However, it is indirectly also affected by other factors. Therefore, Friedman (2005) suggested to group the factors that affect ECa into three categories, corresponding to the bulk soil (e.g. porositiy, water content, structure), the solid particles (e.g. particle shape and orientation, particle-size distribution), and the soil solution (e.g. conductivity of the aqueous solution, cation composition, temperature).

Traditionally, EMI surveys have been used to identify management zones in the context of precision agriculture (Johnson et al. 2003; Corwin and Lesch 2003; Corwin and Plant 2005; Vitharana et al. 2006; 2008). The inference of the horizontal and vertical distribution of clay from EMI surveys has received considerable

attention (Triantafilis and Lesch 2005; Kitchen et al. 2005; Jung et al. 2005; Saey et al. 2008, 2009; Rodriguez-Perez et al. 2011) as a result of its relevance for water dynamics across fields or catchments.

Periodical surveys with EMI sensors under contrasting soil moisture conditions can be used to identify hydrological patterns in watersheds (Sherlock and McDonnell 2003; Abdu et al. 2008; Martínez et al. 2010, 2012; Robinson et al. 2012). Such patterns (e.g. soil water content, water table depth) have been shown to be related to the spatial distribution of vegetation (Robinson et al. 2008, 2010; Atwell et al. 2013). Robinson et al. (2010) studied the adequacy of EMI surveys for assessing soil spatial resource heterogeneity in a savanna tree-grass ecosystem. In order to evaluate the dominance of trees over grasses and vice versa, the ECa histogram was divided into four sections. Higher ECa values occurred under grass dominance while lower ECa values were found in zones with tree dominance, corresponding to lower clay contents.

The objectives of this work were (1) to delimit areas with impaired tree development using electromagnetic induction surveys, and (2) to identify the underlying relationships between ECa and soil properties causing the spatial patterns in the tree development.

Materials and methods

Site description

The study was performed in an experimental catchment at the "La Conchuela" farm (37°48′54′ N, 4°53′53′W), 10 km west of Córdoba, Spain (Fig. 1). The mean elevation is 93 m a.m.s.l. and the mean slope is 9 %. The soil is a deep Vertisol formed on Miocene marls, characterized by Soil Survey Staff (1999) as a Chromic Haploxerert. For similar clay soils in the region, water retention at field capacity and wilting point was near 0.3 and 0.15 kg kg^{-1}. The catchment is intersected by a gully from south-east to north-east (Fig. 1). The catchment covers approximately 8 ha of an irrigated olive orchard which was planted in 1993 with a tree density of 240 trees ha^{-1}. Approximately 40 % of the trees were replanted as a result of water logging and a subsequent severe infestation by *Verticillium dahliae* and possibly other soil borne pathogens during the wet spring of 1996 (Gómez et al. 2009). Generally, in these soils, diseases and root asphyxia appear during extremely wet winters, throughout which the soil remains in near saturated conditions for prolonged periods. The climate is Mediterranean, with monthly average daily temperatures of 9.3 °C and 28 °C, in January and July, respectively. The mean annual precipitation is 650 mm, of which 75 % occurs from October to March, and occasional precipitation between June and September. Testi et al. (2006) found modeled average annual evapotranspiration for a 300 trees ha^{-1} mature orchard in Córdoba of 1,025 mm. Earlier experimental work by Palomo et al. (2002) showed that water supplies near 400 mm during the irrigation seasons of 1997 and 1998 were adequate.

Soil profile description and soil sampling strategy

Based on a preceding EMI survey, seven locations were selected (Fig. 1) where soil profile pits were dug to a depth of 2 m. The soil profile was described according to Soil Survey Staff (1993). Soil samples were collected from the center of each horizon and later analyzed in the laboratory for soil texture, cation exchange capacity (CEC), exchangeable Na, carbonates (CO_3), and organic matter (OM).

During the spring of 2010 soil profile samples were collected down to 0.9 m at 45 locations on a pseudo-regular grid using a 0.093-m diameter cylinder auger (Eijkelkamp Agrisearch Equipment, Giesbeek, The Netherlands)[1] and a percussion drill. The profile samples were divided in three 0.3-m long subsamples and analyzed in the laboratory for soil OM, pH, texture, electrical conductivity of the saturated paste (1:5) filtrate (EC), bulk density (ρ_b) and stone content. In order to obtain more detailed information, at nine locations along a SW-NE-oriented transect (see Fig. 1) profile samples down to a depth of 1 m were divided in five 0.2-m long subsamples and analyzed in the laboratory for the same properties. The transect was chosen to cover the entire range of measured ECa values.

In 2011 and 2012 (under dry and wetter soil conditions, respectively) the catchment was sampled at the same 45 locations for gravimetric soil water content. As a result of excessive soil hardness in 2011, samples were only taken down to a depth of 0.3 m, with 0.1-m intervals. At certain locations, only topsoil samples could be taken as a result of excessive soil hardness. In 2012, several days after the first rainfall event in

[1] Manufacturer's names are provided for information and its use does not constitute endorsement.

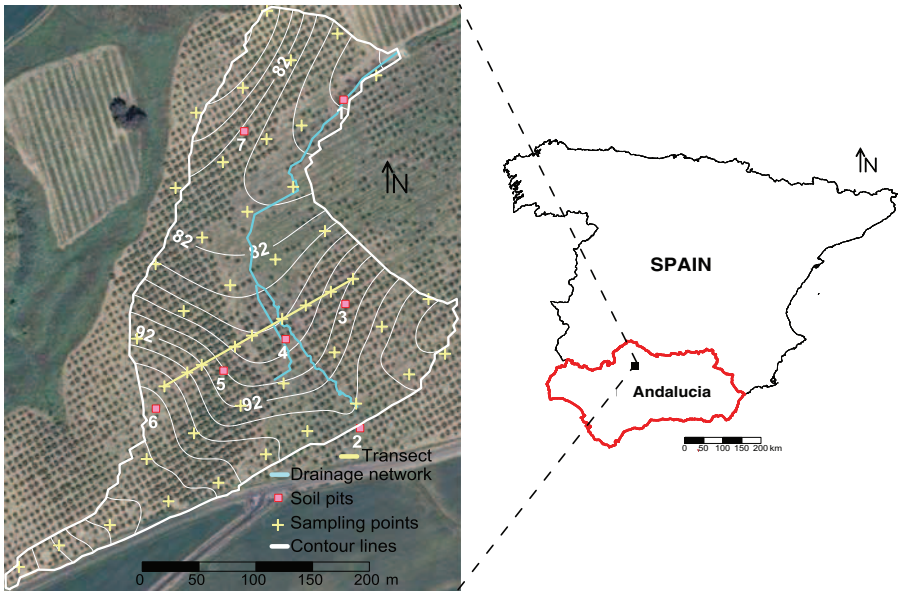

Fig. 1 Location and orthophotograph of the experimental catchment, with topography, catchment boundaries, and position of soil sampling points and pits superposed

autumn, after the prolonged dry summer period, samples were taken down to a depth of 0.6 m, with increments of 0.2 m. A larger sampling interval was chosen in 2012 to reduce the number of samples and associated workload. Samples were taken using a 0.05-m diameter. Fresh sample weight was approximately 300 g.

Apparent electrical conductivity surveys and post-processing

Catchment-wide apparent electrical conductivity surveys were conducted in-between the tree lines in September 2011 and October 2012, simultaneously with the gravimetric water content and point ECa measurements at the 45 locations. Catchment-wide ECa data were used to delimit areas with different tree development, while point ECa measurements and measured soil properties were used to infer relationships between the studied variables.

ECa measurements were made using a Dualem-21S (DUALEM, Milton, Canada) sensor, accommodated in a customized polyvinyl chloride sled and pulled by an all-terrain vehicle, equipped with a real time kinematic-differential global positioning system (Trimble, Sunnyvale, CA) and a rugged Allegro-TK6000 field computer (Juniper Systems, Logan, UT) to log measurements, coordinates, and elevation (Z). The GPS antenna was positioned on the sled, 1.5 m above the center of the inter-coil spacing corresponding to the H1 signal. As a result of the sled configuration, the sensor was operated at a height of 0.075 m above the soil surface.

The sensor works at a fixed frequency of 9 kHz and consists of a transmitter coil at one end and four receiver coils separated 1, 1.1, 2, and 2.1 m from the transmitter coil. Receiver coils are oriented, with respect to the transmitter coil, in a perpendicular (P) or in a horizontal co-planar (H) configuration. Each transmitter-receiver combination provides integrated ECa values for the corresponding explored soil volumes (Table 1). Traditionally a varying sensitivity with depth has been considered (McNeill 1980; Rhoades and Corwin, 1981; Saey et al., 2009). The effective depth of exploration (DOE)

Table 1 Intercoil distance (*ID*, m), coil configuration and depth of exploration (*DOE*, m) for each signal measured by the DUALEM-21S

Signal	ID	Coil configuration	DOE
P1.1	1.1	Perpendicular	0.5
P2.1	2.1	Perpendicular	1
H1	1	Horizontal co-planar	1.5
H2	2	Horizontal co-planar	3

is the depth at which 70 % of the sensor response is obtained. However, work by Callegary et al. (2007) showed that the depth of exploration depends strongly on the soil's ECa. In addition, Callegary et al. (2012) found that variations of the electrical conductivity within the explored soil volume can compromise the measurements and lead to irregular explored soil volumes.

The ECa data were filtered and interpolated (Whelan et al. 2002) on a 1x1-m grid to create maps for the four ECa signals. Also elevation was interpolated on a 1×1-m grid to provide a digital elevation model from which topographic indices, (Vitharana et al. 2008) a slope map, the stream network and the watershed limits were derived.

Data analysis

Analysis of variance (ANOVA) and Pearson correlation coefficients were calculated using point ECa and soil profile data, measured at exactly the same position. Although the explored soil volumes by the ECa and soil measurements differ in several orders of magnitude and no strong correlations are expected, the significance of potential relationships can be tested. Also differences in point ECa and SWC for both surveys were analyzed.

Canopy coverage and projected canopy area of individual trees

The fraction of canopy coverage was calculated by evaluating the color range of the orthophotograph (in bit map protocol) for each delimited zone. First the color range of the canopies was determined, then the total area occupied by canopies was calculated as the sum of the number of pixels with values within that color range, and, finally, the total area covered by canopy was calculated as the sum of pixels, from which the percentage of canopy coverage was calculated. Projected canopy area (CA) of each olive was calculated after transforming the raster to polygons for the selected canopy color range, and filtering canopy areas automatically ($CA \leq 3$ m^2) and manually where necessary. The projected canopy area of each olive tree and the mean ECa for the same area were calculated and analyzed.

Results

Soil properties

Profile pits

Four horizons (A, B, BC and C) were distinguished at pits 1, 2, 3, 5 and 7 (see Fig. 1). Pit 4 showed no BC horizon, while only an A and a C horizon were found at pit 6 (Table 2). In general, depth to the C horizon increased downslope (pits 3–6). The C horizon (marl) appeared in most pits at 1–1.5 m depth, except for pit 5 where the C horizon was found at 1.9 m depth and pit 4 where no C horizon was found. The relatively shallow C horizons found at pits 2 and 6 (at 1.1 and 0.8 m, respectively) were possibly a result of soil loss from the overlaying soil horizons towards the lower elevation positions, e.g. pit 4 where the C horizon was not reached at 2 m depth.

Clay content decreased with depth at pits 1, 3 and 5, and remained approximately constant throughout the profile at the other locations. Pits 5 and 7, located within the area with the best tree development (Fig. 1) showed substantially lower clay contents in the C horizon as compared to the other soil profiles. The highest clay content was observed at pit 4, which was located in the area with significant tree growth and die-off problems. Organic matter content decreased with depth at all pits. Carbonate content increased with depth at pits 1, 3, 5 and 7, and remained constant at the other pits, while Na increased only at pits 1, 2, 4 and 6.

Profile samples

The profile-averaged clay, sand and silt contents calculated for samples from 45 locations throughout the catchment were 48, 6 and 46 %, respectively (Table 3a). The coefficient of variation (CV) also increased with depth, being largest for the sand content (0–0.9 m) as compared to silt and clay content (50, 9, 12 %, respectively). Sand content showed positively skewed distributions, especially for the deeper layers, while clay content was negatively skewed. The kurtosis coefficient (KC) was found to be greater than 3 for sand content in the deeper layers. This indicates the presence of areas with intrusions of coarser sandy material in the dominantly fine textured clay soil.

Table 2 Summary of the profile description of the seven soil pits shown in Fig. 1 and values of selected soil properties. Indexes refer to subdivisions of the same horizon. CEC: Cation exchange capacity and OM: Organic matter content

Soil properties	Soil pit						
	1	2	3	4	5	6	7
A Horizon							
Layer extent (m)	0–0.39	0–0.30	0–0.30[1] 0.30–0.65[2]	0–0.40[1] 0.40–0.80[2] 0.80–1.15[3]	0–0.32[1] 0.32–0.87[2]	0–0.80	0–0.10[1] 0.10–0.32[2] 0.32–0.60[3]
Clay (%)	50.2	50.0	50.3[1] 54.3[2]	55.6[1] 57.1[2] 55.6[3]	48.8[1] 51.6[2]	50.4[1] 52.7[2] 52.2[3]	44.4[1] 46.5[2] 48.9[3]
Na ($mol_c\ kg^{-1}$)	0.71	0.48	0.5[1] 0.6[2]	0.4[1] 0.6[2] 1.2[3]	0.4[1] 0.5[2]	0.5[1] 0.9[2] 1.4[3]	0.4[1] 0.5[2] 0.8[3]
CEC ($mol_c\ kg^{-1}$)	30.8	26.52	27.4[1] 28.9[2]	28.9[1] 29.6[2] 28.3[3]	23.7[1] 27.0[2]	24.1[1] 23.9[2] 22.0[3]	22.4[1] 24.3[2] 25.2[3]
Carbonates (%)	18.34	24.66	30.7[1] 27.0[2]	23.6[1] 22.8[2] 25.6[3]	24.7[1] 24.5[2]	25.8[1] 25.5[2] 27.7[3]	26.2[1] 27.2[2] 28.7[3]
OM (%)	1.22	1.09	1.3[1] 1.1[2]	1.2[1] 1.1[2] 0.6[3]	1.0[1] 0.7[2]	0.8[1] 0.6[2] 0.4[3]	1.2[1] 0.9[2] 0.7[3]
B Horizon							
Layer extent (m)	0.39-0.69[1] 0.69–1.09[2]	0.30–0.77	0.65–0.88	1.15–1.50[1] >1.50[2]	0.87–1.47	–	0.60–0.91
Clay (%)	53.0[1] 53.4[2]	52.5	43.9	55.6[1] 53.5[2]	53.0	–	48.1
Na ($mol_c\ kg^{-1}$)	3.1[1] 3.7[2]	0.8	0.5	1.2[1] 1.2[2]	0.5	–	1.0
CEC ($mol_c\ kg^{-1}$)	33.2[1] 31.1[2]	26.3	20.9	29.8[1] 26.3[2]	28.5	–	25.9
Carbonates (%)	16.3[1] 18.3[2]	26.1	49.8	23.9[1] 29.7[2]	25.6	–	29.2
OM (%)	0.8[1] 0.8[2]	0.7	0.6	0.7[1] 0.5[2]	0.6	–	0.7
BC Horizon							
Layer extent (m)	1.09–1.52	0.77–1.10	0.88–1.24	–	1.47–1.90	–	0.91–1.37
Clay (%)	52.4	52.9	45.1	–	35.6	–	47
Na ($mol_c\ kg^{-1}$)	3.0	1.5	0.7	–	0.4	–	1.1
CEC($mol_c\ kg^{-1}$)	30.3	24.8	22.2	–	15.9	–	26.1
Carbonates (%)	20.1	26.9	41.1	–	44.8	–	31.1
OM (%)	0.7	0.4	0.4	–	0.2	–	0.5

Table 2 (continued)

Soil properties	Soil pit						
	1	2	3	4	5	6	7
C Horizon							
Layer extent (m)	>1.52	>1.10	>1.24	–	>1.90	>0.80	1.37–1.90[1] >1.90[2]
Clay (%)	43.7	52.0	47.7	–	32.8	50.1	46.5[1] 23.4[2]
Na ($mol_c\ kg^{-1}$)	5.0	2.4	0.6	–	0.4	2.6	1.1[1] 0.6[2]
CEC ($mol_c\ kg^{-1}$)	20.2	21.1	21.3	–	13.7	19.1	25.0[1] 13.7[2]
Carbonates (%)	35.9	26.4	35.6	–	46.4	27.7	32.1[1] 23.8[2]
OM (%)	0.2	0.3	0.2	–	0.3	0.2	0.3[1] 0.1[2]

The mean OM content found for the topsoil (0–0.3 m) was 1.0 % (Table 3b), roughly 1.5 and 2 times larger than the mean OM content found for the 0.3–0.6 and 0.6–0.9 m layers. The corresponding CV increased with depth, from 27 % in the topsoil to 53 % in the deepest layer. Electrical conductivity was similar in the upper 0.6 m of soil profile, with an average of 0.18 dS m^{-1} for the two upper horizons, maximum values of 0.38 and 0.31 dS m^{-1}, and a CV of 25 and 28 %, respectively (Table 3b). In the 0.6–0.9 m layer the mean EC value and corresponding CV roughly doubled those found in the upper layers.

In general, similar pH values were observed throughout the soil profiles, while stone content decreased and bulk density increased with depth (Table 3c). Profile-averaged pH was 8.7 indicating alkaline soil conditions. Mean stone content ranged from 3.8 % in the deepest layer to 5.9 % in the top layer. Bulk density ranged from 1.4 to 1.5 Mg cm^{-3}, which are common values for non-compacted clay soils.

Significant ($p<0.05$) positive Pearson correlation coefficients were found between clay and OM content (0.30), and stone and OM content (0.57), while significant negative correlation coefficients were found between sand and clay content (−0.68), elevation and OM content (−0.54), and elevation and stone content (−0.56).

Soil water content

Average SWCs for the dry 2011 survey were 0.05, 0.07 and 0.09 kg kg^{-1} for the 0–0.1, 0.1–0.2 and 0.2–0.3 m layers. Differences were significant at $p<0.05$. Profile mean SWC and standard deviation were 0.06 and 0.02 kg kg^{-1}, while maximum and minimum values were 0.04 and 0.12 kg kg^{-1}, respectively. Overall, distributions were positively skewed.

Data from the wetter 2012 survey showed uniform SWC distributions across the soil profile. Also standard deviation and CV were similar for the top 0.4-m layer, but were half the value found for the 0.4–0.6-m interval. Profile-averaged mean and standard deviation were 0.22 and 0.03 kg kg^{-1}, while maximum and minimum values were 0.14 kg kg^{-1} and 37 kg kg^{-1}, respectively. Only the top 0–0.2 m layer was significantly wetter ($p<0.05$) in 2012 than in 2011.

Table 3 Descriptive statistics of **a**) soil texture (%), **b**) organic matter content (OM, %) and electrical conductivity (EC, dS m^{-1}), and **c**) pH, stone content (%) and bulk density (ρ_b, Mg cm^{-3}), for different depth intervals

	0–0.3 m			0.3–0.6 m			0.6–0.9 m			0–0.9 m		
a)	sand	silt	clay	sand	silt	clay	sand	silt	clay	sand	silt	clay
N*	45	45	45	45	45	45	44	44	44	44	44	44
m	5.8	46.0	48.2	5.8	45.6	48.6	6.0	46.2	47.8	5.9	45.9	48.1
med	6.1	45.8	48.7	5.7	44.9	50.3	5.9	44.8	50.0	6.4	45.3	49.6
min	1.5	38.7	34.6	1.1	36.3	31.3	1	35.9	25.3	1.6	37.3	33.2
max	14.5	55.2	54.2	22.9	58.1	57.2	21.8	62.2	57.8	14.6	58.0	56.4
s	2.7	3.1	4.1	3.6	4.9	6.2	3.8	5.6	7.6	3.0	4.2	5.6
CV	46.9	6.7	8.5	61.5	10.7	12.6	63.3	12.1	15.9	49.8	9.1	11.6
skew	0.8	0.3	−0.7	2.3	0.6	−1.3	1.7	0.9	−1.3	0.8	0.8	−1.2
kurt	1.3	1.1	0.9	9.5	0.7	1.1	4.9	0.8	1.1	0.8	1.0	0.8
b	OM	EC		OM	EC		OM	EC		OM	EC	
N*	44	45		45	45		45	45		44	45	
m	0.97	0.18		0.65	0.18		0.50	0.34		0.71	0.23	
med	0.99	0.16		0.64	0.16		0.42	0.19		0.70	0.17	
min	0.47	0.13		0.19	0.12		0.05	0.12		0.24	0.13	
max	1.48	0.38		1.4	0.31		1.07	2.82		1.15	1.09	
s	0.26	0.04		0.29	0.05		0.27	0.54		0.26	0.19	
CV	27.2	25.35		44.79	28.26		53.21	155.96		36.87	80.94	
skew	-0.07	2.82		0.43	1.22		0.30	4.00		0.10	3.80	
kurt	-1.05	8.69		-0.63	0.31		-1.09	15.06		-1.28	13.99	
c)	pH	stone	ρ_b	pH	stone	ρ_b	pH	stone	ρ_b	pH	stone	ρ_b
N*	45	14	45	45	15	45	45	14	45	45	23	45
m	8.6	5.9	1.39	8.7	5.5	1.46	8.7	3.8	1.51	8.7	3.1	1.45
med	8.6	4.1	1.42	8.8	3.7	1.49	8.8	3.3	1.52	8.7	2.2	1.48
min	8.0	2.5	0.45	8.2	2.7	1.06	7.9	2.6	1.25	8.3	0.9	1.02
max	8.6	19.3	1.75	9.1	13.3	1.67	9.2	6.5	1.77	9.1	8.6	1.66
s	0.19	4.7	0.21	0.2	3.6	0.11	0.3	1.1	0.08	0.2	2.5	0.11
CV	2.2	79.7	15.5	2.3	65.0	7.45	3.2	29.5	5.51	1.9	81.3	7.83
skew	-0.7	2.0	-2.1	-1.0	1.4	-1.3	-1.4	1.3	-0.2	-0.4	1.2	-1.44
kurt	2.0	3.0	6.8	0.6	0.2	2.5	1.7	0.5	2.5	-0.1	0.4	3.42

**N* number of measurements, *m* mean, *med* median, *min* minimum, *max* maximum, *s* standard deviation, *CV* coefficient of variation (%), *skew* skewness, *kurt* kurtosis

Terrain attributes

Slope map

Figure 2 shows the slope map of the entire catchment, with values ranging from 0 to 22 %. The steepest slopes are located near the north-western edge of the catchment, and in the western and eastern part of the catchment. Flatter high elevation zones are found near the southern edge, while flatter low elevation zones appear in the central part of the catchment.

Aspect map

The eastern part of the catchment is predominantly north-facing (Fig. 2), resulting in higher SWC and subsequently higher ECa values, while the north-western and western part of the catchment, with

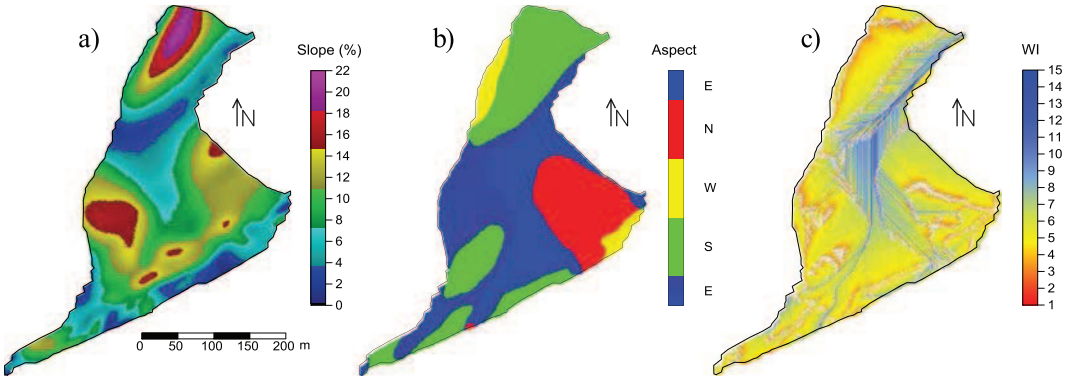

Fig. 2 Maps of **a**) slope, **b**) aspect and **c**) wetness index (*WI*) for the experimental catchment

the steepest slopes, is south-facing. East-facing areas are found in the central part of the catchment, while west-facing slopes are only found in two small areas near the north-western and south-eastern edges of the catchment.

Wetness index (WI) map

The topographic wetness index, $WI = \ln(a/\tan\beta)$, where a is the upslope contributing area and β the local slope angle in radians, was calculated using the D-8 procedure to identify areas with potential concentration of runoff water, possibly resulting in higher soil water contents (Fig. 2). The parallel lines in the derived wetness index were an artefact of the method used to calculate the upslope contributing area. The highest values, $7.5<WI<15$, correspond to flatter low elevation areas of high flow accumulation, mainly in the central part of the catchment, while the lowest values, $WI<7.5$, are found in areas with a small flow accumulation on steep slopes.

ECa measurements and patterns

Point ECa increased from 2011 to 2012 as a result of the larger soil water content in 2012 (Table 4 a). Overall the different signals provided ECa values that increased with increasing DOE, yielding the smallest and highest values for the P1.1 and H2 signals, respectively, indicating the presence of more conductive material at deeper horizons. Average values ranged from 18.7 mS m^{-1} for P1.1 (2011) to 74.9 mS m^{-1} for H1 (2012). The values in 2012 roughly doubled those observed in 2011 for the P1.1, P2.1, and H1 coil configurations, while for H2 only a 10 % increment was observed. The CV was similar across the four signals for 2011 and about 20 (H2) to 50 % (P1.1) smaller in 2012 as compared to 2011, which is generally an effect of the higher mean ECa in 2012 and the increased soil water content in the topsoil. Skewness coefficients ranged from 0.3 (H2) to 1.1 (P1.1) in 2011, and close to 0.45 for all signals in 2012, except for H2 (.52). This shows the tendency to reduce skewness and overall variability as a result of increased soil water content, especially in the top layers where soil moisture increments were largest.

Spatially measured ECa in 2011 (Table 4b) showed average values ranging from 19.7 (P1.1) to 60.6 (H2), similar to those observed for the point ECa measurements, and indicating the representativeness of the 45 samples locations in terms of ECa. The CV ranged from 43 (H2) to 61 (P1.1) and was slightly higher for the P1.1 signal as compared to the point measurements, while the skewness increment, with respect to the point measurements, decreased with smaller DOEs.

The largest area of low ECa values was observed near the western edge of the catchment (Fig. 3), while a smaller area could be identified in the eastern part. Both areas corresponded roughly to zones with steep slopes. The highest ECa values were generally observed in areas with high elevation, in the south and southeastern part of the catchment, characterized by a flatter topography. An area of intermediate ECa values extended from north to south across the catchment, roughly following the course of the main gully.

Correlations between point ECa measured in 2011 and 2012 were significant at $p<0.01$ (Table 5) and increased with increasing DOE, ranging from

Table 4 **a**) Descriptive statistics of point apparent electrical conductivity (ECa, mS m^{-1}), for the 2011 and 2012 surveys, and **b**) descriptive statistics of spatially measured ECa (mS m^{-1}), for the 2011survey See Table 1 for explanation of the four signals

a)	2011				2012			
	P1.1	P2.1	H1	H2	P1.1	P2.1	H1	H2
N*	45	45	45	45	45	45	45	45
m	18.7	36.1	42.3	59.9	53.4	62.4	74.9	63.9
med	15.2	31.1	36.9	55.2	52.6	60.7	73.4	61.8
min	5.7	13.0	14.7	9.0	27.0	27.6	39.8	27.9
max	46.4	76.6	94.2	117.5	95.5	122.7	140.8	127.9
s	9.5	18.1	21.5	29.5	13.9	19.9	21.8	25.1
CV	50.8	50.0	50.8	49.3	26.0	31.8	29.0	39.2
skew	1.08	0.56	0.60	0.31	0.45	0.44	0.43	0.52
kurt	0.90	−0.83	−0.56	−1.01	1.33	0.51	0.34	−0.19

b)	2011			
	P1.1	P2.1	H1	H2
N*	11,102	10,736	11,040	10,707
m	19.7	35.9	43.1	60.6
med	17.2	34.9	41.8	62.7
min	2.6	2.4	7.1	0.7
max	113.5	89.6	134.2	132.5
s	12.1	17.2	21.7	26.2
CV	61.5	47.9	50.4	43.3
skew	2.6	0.7	0.9	0.3
kurt	10.4	0.1	0.9	−0.6

**N* number of measurements, *m* mean, *med* median, *min* minimum, *max* maximum, *s* standard deviation, *CV* coefficient of variation (%), *skew* skewness, *kurt* kurtosis

0.78 (P1.1) to 0.94 (H2). This shows that the increased topsoil water content caused the smallest correlation between both surveys for the signal with the smallest DOE. This smaller correlation, as compared to signals with higher DOE, indicate the potential usefulness of the P1.1 signal to evaluate spatially the topsoil moisture increment across the catchment. Patterns were also similar among the different signals (Table 5) for the same survey. Correlations between ECa signals for the wetter survey (2012) ranged from 0.79 (P1.1×H2) to 0.98 (P2.1×H1) and were generally somewhat smaller than for the dry survey (2011), ranging from 0.92 (P2.1×H2) to 0.99 (P1.1×P2.1 and P2.1×H1). For the P1.1×H2 combination the largest difference in correlation between 2011 (0.95) and 2012 (0.79) was observed, as a result of topsoil wetting in 2012.

Spatial classification of ECa

Given the strong correlation between different ECa signals and surveys the spatial classification was based on a single signal. The ECa maps for 2011 showed the best correspondence with the canopy coverage pattern of the orthophotograph. The P2.1 signal was chosen since its DOE (1 m) corresponds roughly to the analyzed soil profile depth (0.9 m) in this study. The probability density function of the interpolated 2011 P2.1 ECa measurements exhibited a bimodal distribution (Fig. 4a). A sum of two Gaussian pdfs was fitted to the histogram and the parameters of both pdfs were estimated. For the first component, corresponding to the local maximum at the left-hand side of the pdf (Fig. 4a), a mean value of 17.5 mS m^{-1} and a standard deviation of 4 mS m^{-1} was obtained. The second component, corresponding to the local maximum in the center of pdf, a

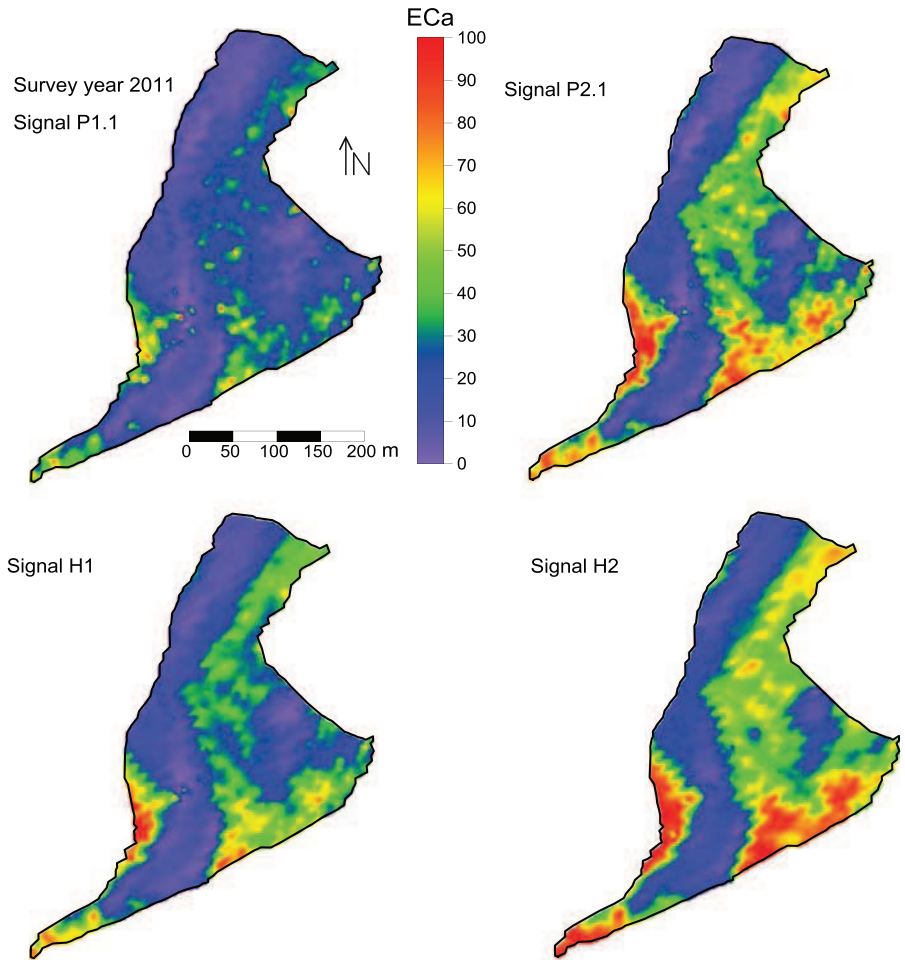

Fig. 3 Apparent electrical conductivity (ECa, mS m^{-1}) maps, corresponding to the four measured signals in 2011. See Table 1 for details on each signal

Table 5 Correlation coefficients between point measurements of apparent electrical conductivity (*ECa*), for different coil configurations and for the 2011 and 2012 surveys. All coefficients are significant at $p<0.01$. See Table 1 for explanation of the four signals

		2011				2012		
		P1.1	P2.1	H1	H2	P1.1	P2.1	H1
2011	P2.1	0.99						
	H1	0.97	0.99					
	H2	0.95	0.92	0.93				
2012	P1.1	0.78	0.77	0.77	0.76			
	P2.1	0.85	0.85	0.86	0.88	0.96		
	H1	0.90	0.89	0.90	0.93	0.92	0.98	
	H2	0.85	0.86	0.88	0.94	0.79	0.91	0.96

mean value of 42.5 mS m^{-1} and a standard deviation of 15 mS m^{-1} was found. The mean±the standard deviation of the second component was used to classify the ECa data. The highest ECa values, representing about 25 % of the total population, were classified as a third group. As a result, the ECa data were classified according to ECa ≤. 27.5 mS m^{-1} (zone A), 27.5<ECa<57.5 mS m^{-1} (zone B), and ECa>57.5 mS m^{-1} (zone C). This classification resulted in the map shown in Fig. 4b. Small intrusions of higher or lower ECa values inside the three delimited areas were disregarded. Descriptive statistics for ECa (P2.1), corresponding to the three zones are shown in Table 6. Mean ECa values and corresponding standard deviations were 20.7, 44.2, 55.3 mS m^{-1}, and 5.6, 8.2 and 13.9 mS m^{-1}, for zones A, B, and C, respectively. From the comparison of the

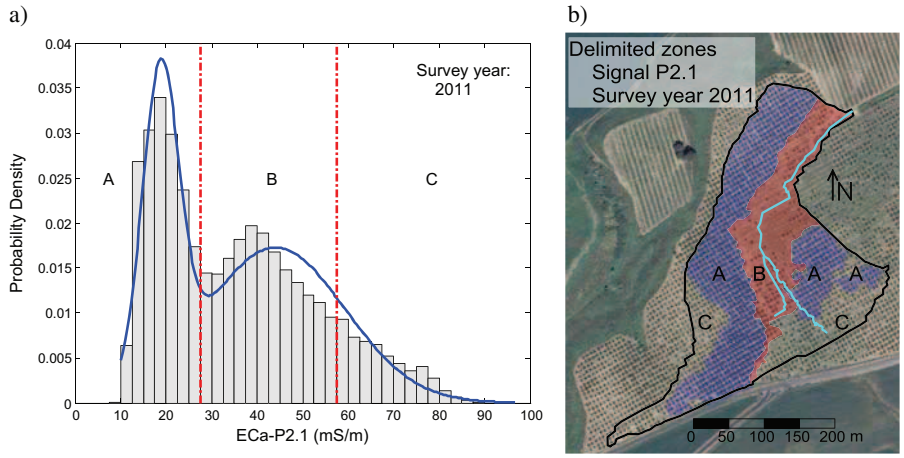

Fig. 4 **a**) Histogram and fitted probability density function of interpolated apparent electrical conductivity (ECa) corresponding to signal P2.1 (survey 2011). The dashed lines represent the limits between the three ECa classes (ECa≤27.5; 27.5≤ECa≤57.5; ECa>57.5 mS m^{-1}) used to delimit the three zones. **b**) Orthophotograph with the three delimited zones (A, B and C) superposed

means and medians it can be deduced that near-normal ECa distributions were obtained for the three classes.

Correspondence between ECa and canopy coverage

A strong correspondence existed between the spatial ECa patterns (Figs. 3 and 4) and canopy coverage as observed from the orthophotograph (Fig. 1). Canopy coverage was 45, 12 and 23 % in areas A, B, and C, respectively (Fig. 5). Zone A, with an area of 3.8 ha and 903 trees, showed the best developed canopies. Only 5 % of the trees were missing within this area. Therefore, a canopy coverage of 45 % was considered as optimal for this catchment.

Table 6 Descriptive statistics for the three delimited zones of interpolated apparent electrical conductivity (ECa, mS m^{-1}) corresponding to signal P2.1 for the 2011 survey

	2011		
	Zone A	Zone B	Zone C
N*	37,526	20,372	18,874
m	20.7	44.2	55.3
med	20.0	42.9	55.4
min	9.2	13.6	20.7
max	60.3	80.6	87.9
s	5.6	8.2	13.9
CV	26.9	18.5	25.1
skew	0.6	0.6	0.1
kurt	0.1	0.3	−1.0

*N number of measurements, *m* mean, *med* median, *min* minimum, *max* maximum, *s* standard deviation, *CV* coefficient of variation (%), *skew* skewness, *kurt* kurtosis

Table 7 shows the descriptive statistics of projected canopy area of individual trees for the three zones. The number of trees in zone A doubled those found in zone C and quadrupled the number of trees found in zone B. The percentage of missing trees in zones A, B and C was 5, 63 and 23 %, respectively. Mean CA in zones A, B and C was 19, 12 and 10 m^2, respectively. Maximum values ranged from 21 m^2, in zones B and C, to 33 m^2 in zone A. Standard deviation ranged from 3 m^2, in zones B and C, to 5 m^2 in zone A. The small skewness and kurtosis values indicated near-normal distributions for CA in the three zones. A one-way ANOVA showed that the means of the three zones were significantly different ($p<0.05$).

For each tree, mean ECa was calculated from the interpolated ECa data within the CA. Figure 6 shows the relationship between CA and the corresponding mean ECa for the three different zones. Although small CAs were found over the entire ECa range, CAs larger than 20 m^2 only occurred below a threshold ECa of 30 ms m^{-1}. The smallest CAs occurred mostly at ECa values ranging from 60 to 80 mS m^{-1}, corresponding to zone C. Slightly larger CAs were found for ECa values ranging roughly from 30 to 60 mS m^{-1}, corresponding to zone B.

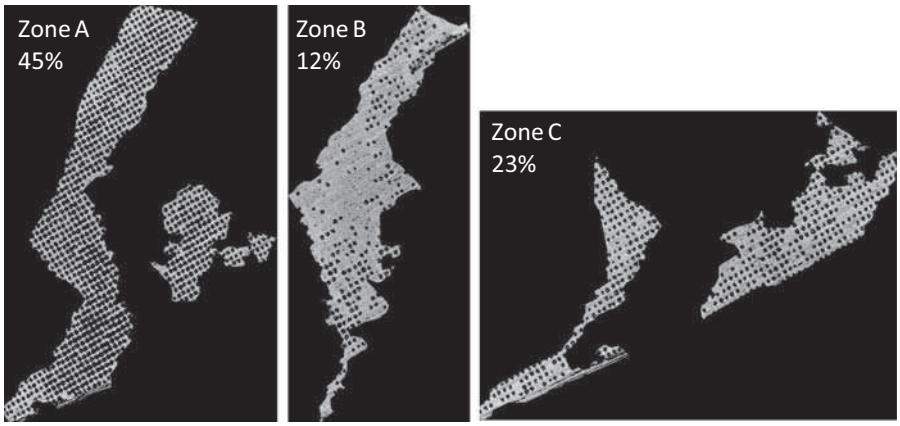

Fig. 5 Classified images used for calculating the total tree canopy coverage in the three delimited areas

Spatial ECa and tree development patterns

Transect data

Data from the nine soil profiles along the transect (see Fig. 1) indicated high ECa, Z, clay and SWC values at the SW end of the transect (point 18), while at the central, low elevation section of the transect intermediate to high ECa values were observed, and the highest clay and SWC (Fig. 7). Lower ECa values and high Z, clay and stone content were found at the NE end (point 26). Soil and terrain conditions in the surroundings of the gully (near point 23) result in wetter soil conditions and might lead to saturation and water logging under persisting extremely wet weather conditions. As a result of the shallow C horizon (Table 2), similar conditions were found at the SW end of the transect, although the higher elevation of this location would prevent water logging.

Table 7 Number of missing trees and descriptive statistics of projected canopy area (*CA*) for the three delimited zones

	CA (m^2)		
	Zone A	Zone B	Zone C
Missing trees (%)	1.6	73.3	13
N*	858	181	349
m	19	12	10
med	19	11	10
min	5	5	4
max	33	21	21
s	5	3	3
CV	27	28	31
skew	0.1	0.4	0.4
kurt	−0.1	−0.1	0.2

**N* number of trees, *m* mean, *med* median, *min* minimum, *max* maximum, *s* standard deviation, *CV* coefficient of variation (%), *skew* skewness, *kurt* kurtosis

Spatial soil profile data set

Findings from the transect (Fig. 7) were then evaluated for the entire field by comparing soil profile properties in the three zones (Table 8). A one-way ANOVA showed that clay content in zone A was significantly

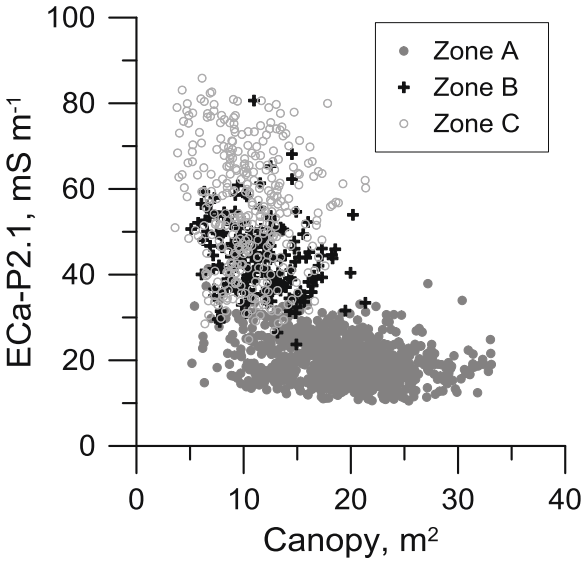

Fig. 6 Relationship between projected canopy area (m^2) and apparent electrical conductivity (ECa) for signal P2.1, distinguishing data from the three delimited zones

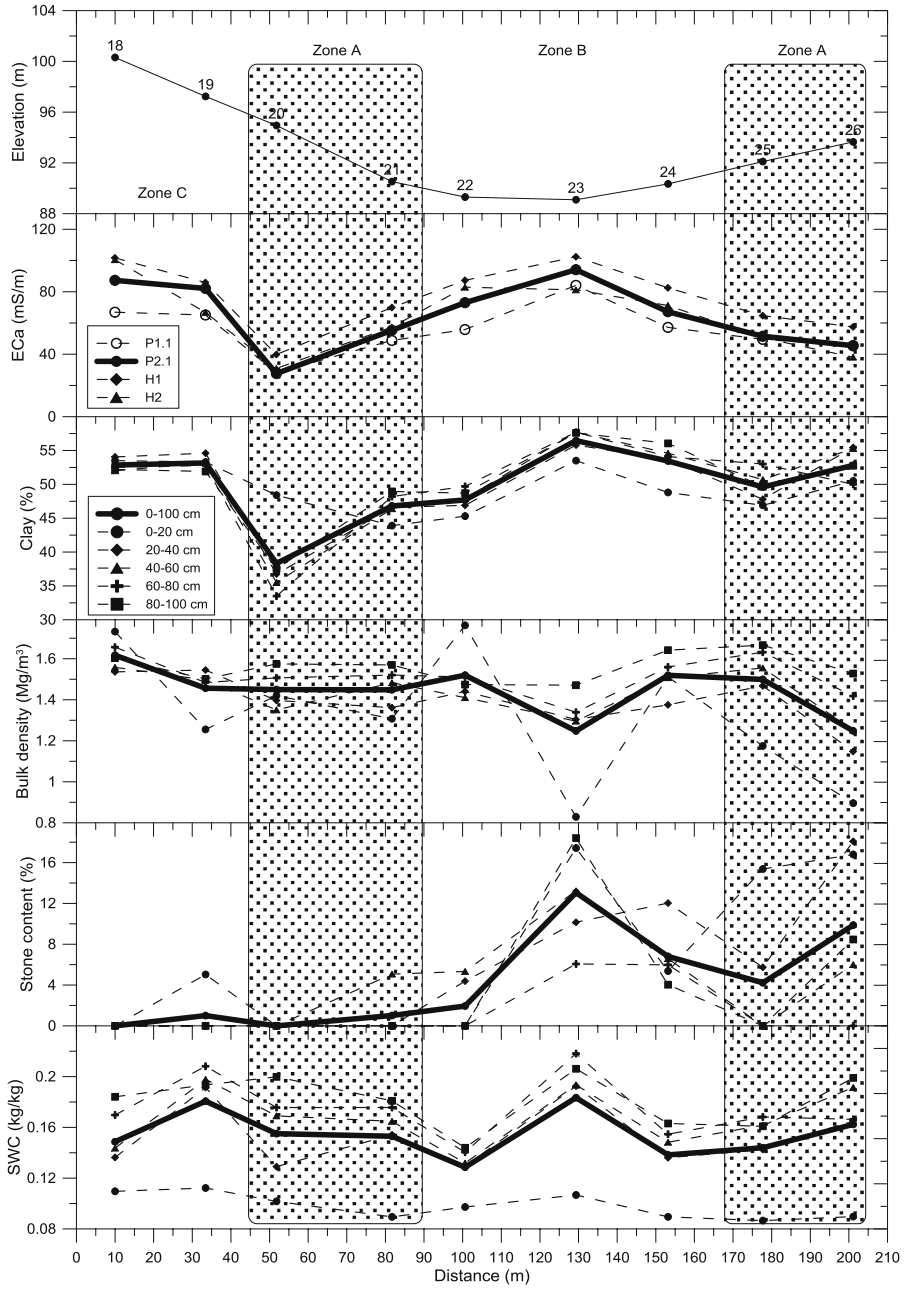

Fig. 7 Elevation, apparent electrical conductivity (*ECa*), clay content, bulk density, stone content and soil water content (*SWC*) for different horizons at nine locations along the transect shown in Fig. 1

($p<0.05$) lower than in zones B and C, with an increasing significance for deeper soil layers (results not shown). Zone B presented a significantly higher soil OM content at all depths as compared to the other two zones, and the highest profile-averaged soil water and stone content, while all soil horizons in zone C contained significantly less sand than the other zones. Silt, EC, pH and bulk density did not show significant differences between the three delimited areas. This means that the observed variations in ECa along the transect are not caused by EC, but are rather a result of soil water content variations and changes in the amount of adsorbed cations of the solid phase (Rhoades et al. 1976; Mualem and Friedman

Table 8 Mean of soil profile-averaged (0–0.9 m) soil water content (*SWC*, %), measured during the 2012 survey, stone content (%), clay and sand contents (%) and organic matter content (*OM*, %) for the different zones. Different letters indicate significant differences ($p<0.05$)

Zone	SWC	Stone content	Clay content	Sand content	OM
A	21.6 (b)	2.0 (b)	46 (b)	6.7 (a)	0.7 (b)
B	23.4 (a)	5.7 (a)	50 (a)	6.8 (a)	0.97 (a)
C	22.7 (ab)	1.7 (b)	47.5 (a)	3 (b)	0.53 (b)

1991). As a result of the significant differences in clay and sand content, significant differences in bulk density would be expected. Figure 7 shows that the variations in bulk density along the profile and the transect do not reflect clearly the variations in clay content. The bulk density of these expansive clay soils depends also on soil water content, which might obscure the expected relationships with texture.

The correlations of SWC and soil texture with ECa were higher for the wetter than for the dry survey, as expected (Table 9). Under dry soil conditions a significant relationship between OM content and ECa-P1.1 was found, probably as a result of the accumulation of organic residues in downslope areas, leading to higher soil water retention, and as a result of the indirect relationship with clay content. A strong positive correlation between ECa and stone content was found for the 2011 survey. This could be an indirect effect of the downslope accumulation of stones (zone B), where also water accumulates and where clay content is highest. In dry environments, Nobel et al. (1992) and Sauer and Logsdon (2002) found that rock fragments protected the soil underneath from evaporation, leading to wetter soil conditions as compared to bare soil.

The point ECa and topsoil (0–0.2-m) SWC data showed positive increments from 2011 to 2012, except for the H2 signal (Fig. 8), with decreasing ECa increments for increasing DOEs. No general relationships were found between the ECa and the SWC increments. However, when considering separately the three zones, relationships between ECa and SWC increments appeared for zone A, especially for the signals with the shallowest DOE (P1.1 and P2.1), although with considerable dispersion ($R^2<0.26$),. In contrast to zones B and C, positive ECa increments were obtained for the H2 signal in zone A. This indicates that, as a result of better infiltration and water transmission conditions in this zone, SWC also increased in deeper layers, resulting in a positive ECa H2 increment. For the same signal negative ECa increments were found in zone C. Topsoil SWC increments were highest in this zone since water did not move towards deeper layers, as a result of the rather shallow C horizon in this area. Zone B showed an intermediate behavior with a general lack of relationship between ECa and SWC increments for all signals.

Discussion

Under non-saline conditions, ECa is mainly influenced by the time-variable water content, and subsequently, by soil texture. According to Friedman (2005) the EMI signals in non-saline soils are related to soil moisture, soil texture and soil depth. McCutccheon et al. (2006) found that volumetric soil water content was the

Table 9 Correlation coefficients between point-measured apparent electrical conductivity (*ECa*) corresponding to signals P1.1 and P2.1, and profile averaged (0–0.9 m) clay, organic matter (*OM*), and stone content for the dry 2011 survey, and soil water content (*SWC*), sand and clay content for the wetter 2012 survey

	2011			2012		
ECa	Clay content	OM	Stone content	SWC	Sand content	Clay content
P1.1	0.50*	0.54*	0.61*	0.65*	−0.46*	0.60*
P2.1	0.51*	0.38	0.75*	0.51*	−0.47*	0.58*

*Significant at $p<0.05$

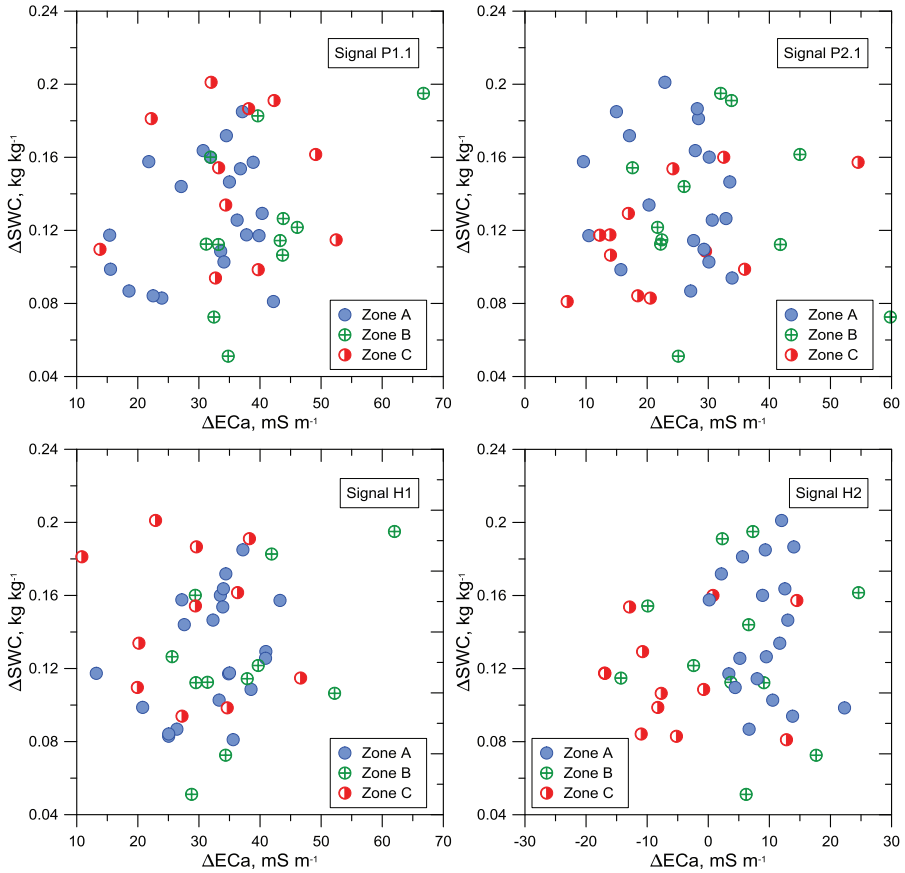

Fig. 8 Relationship between soil water content increments (ΔSWC) and apparent electrical conductivity increments (ΔECa) for the four different signals, from the dry to wetter survey of 2011 and 2012, respectively

dominant factor affecting the spatial and temporal ECa variability, while Harvey and Morgan (2009) found the clay content as the dominant factor. Abdu et al. (2008) made a calibration between ECa and clay content to estimate the soil water holding capacity.

The approach presented here is based on the hypothesis that in this olive-planted catchment with a Vertisol, ECa measurements can be used to assess tree growth problems or die-off, even in advance of plantation establishment, taking also into account SWC, soil properties and topographic attributes. Deficient tree growth and die-off were obvious from field observations and from the orthophotography. Soil profile samples were taken to understand the orchard-growth variability and EMI surveys were conducted in order to delimit areas with unsatisfactory tee development.

Summary statistics and Pearson's correlation coefficients were calculated from all measured soil properties. Positive correlations between clay and OM content were expected, as both were higher in downslope areas. The negative correlation between Z and stone content was possibly a result of relative stone enrichment in the central part of the transect, near the gully (point 23 in Fig. 7), as a consequence of the loss of the smaller soil particles. The negative correlation between Z and OM can be explained by the downslope movement of OM and soil particles, and the poor drainage conditions along the downslope area of the field, resulting in limited carbon mineralization.

Soil water content for the 2012 survey was significantly larger than in 2011. Soil water content increased with depth in the 2011 survey, while it decreased with depth in 2012 as a result of the immediacy of the measurements to the last rainfall event.

Measured ECa values were higher in 2012 than in 2011 as a result of the larger SWC in 2012. Also ECa increased with increasing depth of exploration, indicating the presence of more conductive material in deeper soil layers. The spatial ECa pattern was similar for the

four measured signal. Maps of topographic attributes such as slope, aspect and wetness index reflected partially the ECa patterns and confirmed the underlying relationships between soil properties and ECa. A spatial classification based on the bimodal P2.1 ECa (DOE= 1 m) distribution was performed to delimit areas with impaired tree development conditions. The ECa data were grouped into three classes, based on the decomposition of the bimodal pdf and resulting in the delimitation of three different areas (A, B, and C). Estimated canopy coverage, projected canopy area and percentage of missing trees supported the validity of this classification.

To identify the underlying relationships between ECa and soil properties causing the spatial patterns in the tree development, a preliminary analysis of point ECa, Z, clay, ρ_b ,and stone and soil water content on a transect was made before exploring the entire catchment. Detailed data from the transect (Fig. 7) provided insight into the relationships between ECa, soil properties, and olive development. Elevation ranged from101 m a.m.s.l. at the SW end of the transect (point 18) to 89 m a.m.s.l. near the gully (point 23). Apparent electrical conductivity for the four signals was highest at the SW end of the transect, as a result of the high and homogeneously distributed clay content across the soil profile in this area. This homogeneous soil profile reveals the Vertic character of this soil. Moving down the slope intrusions of coarser material are found in deeper layers (e.g. location 20), as a result of Quaternary and possibly Holocene reworking of the fluvial terrace deposits inside the valley. The presence of stones and coarse fragments was even more prominent along the eastern slope of the transect (Fig. 7, points 24–26), resulting in overall lower ECa values despite the high clay contents observed throughout the soil profile. The highest profile-averaged clay content was observed at location 23, in the lowest part of the transect, corresponding to the area where tree development was deficient. At this location clay content was especially high in the deeper layers, resulting in poor drainage conditions which possibly led to root asphyxia and to diseases such as Verticilium wilt. Figure 7 shows also the high profile-averaged gravimetric water content observed at this location at the moment of the sampling. High clay contents and a shallow C horizon were found at the SW end of the transect and can also cause tree development-limiting conditions (see Fig. 1). Overall, ECa at the NE end of the transect was smaller than the values observed at the SW end, despite the high clay contents found in both areas. The lower ECa values are a result of the higher stone contents observed at locations 23–26, modulated at least partially by higher soil water contents. Bulk density was found not to affect ECa significantly in this study.

The entire catchment was then explored, in accordance to the three delimited zones (Fig. 4). Pearson's correlation coefficients were calculated between ECa for the P2.1 signal and measured soil properties. Significant correlations were found for clay, sand, OM, stone and SWC. Each of these soil properties were then classified according the zone to which they belonged. Zone A, with the low ECa values, covered an area of high elevation and steep slopes, and showed a significantly lower water and clay content, as compared to zones B and C, while it doubled sand content of zone C, and showed significantly lower stone contents than in zone B. These results suggested that optimal tree development in zone A, with a canopy coverage of 45 % (Fig. 5), might be a result of satisfactory drainage conditions. Zone B, with intermediate ECa values, a flatter downslope area and showed significantly higher water and clay content than in zone A, with significantly higher stone contents than in zones A and C. Unsatisfactory tree development from zone B, with a canopy coverage of 12 %, might be a consequence of poor drainage conditions, leading to wetter soil conditions and possibly temporal waterlogging during extremely wet spells, possibly resulting in root asphyxia and infestation by soil-borne pathogens with the consequent wilting effects, especially on young trees. Zone C, with high ECa values, corresponded to a rather flat upslope area, showing intermediate canopy coverage and intermediate water content with respect to zones A and B, and with a significantly higher clay content than in zone A and half of the sand content than in zones A and B. This zone also showed significantly lower stone content than zone B. This zone showed a canopy coverage of 23 %, corresponding to intermediate growing conditions.

Results from the entire catchment support those found along the transect. Relationships between soil properties and ECa found along the transect can be used to interpret the observed ECa variations across the entire catchment, and to delimit the most suitable zones for successful development of the olive trees.

Overall, the proposed methodology enabled us to identify the causative variables for deficient tree development or die-off found in this field by using EMI surveys and soil properties measured at eight points along a transect. The zone where the problem was manifested could be accurately delimited using ECa data. Based on this information management practices, such as removing infested trees or not replanting dead trees, can be proposed within the delimited area to reduce inputs and to prevent further spreading of the disease by installing soil management practices (e.g. no-till and cover crops) that limit the transport of soil particles and vegetative material by tillage or runoff water. Moreover, the proposed method can be implemented before the establishment of plantations, to identify and delimit areas with potential unsatisfactory olive tree development and/or areas with appropriate conditions for infestation by soil-borne pathogens.

Conclusions

Tree growth problems and die-off are important constraints for profitable olive growing in soils with deficient drainage conditions. In this work zones with impaired olive tree development were detected and delimited, based on ECa measurements. Topographic attributes and soil properties (elevation, soil texture, SWC, OM and stone content) were related with tree development. Also relationships between soil properties and ECa under dry and wetter soil conditions were evaluated to identify the key drivers behind the constrained tree development. The results showed that variations in ECa were mainly related with variations in water, clay, sand, and stone content. The area with the lowest average ECa (zone A) showed optimal tree growth and the highest elevation range, while in the downslope area with intermediate ECa values (zone B) tree-growth and die-off problems ocurred. Also the area with the highest ECa values (zone C) showed acceptable tree development. The downslope position of zone B, in combination with its high clay, OM, stone and water contents possibly cause deficient drainage conditions and can lead to saturation and water logging during extremely wet spells. Such conditions promote root asphyxia and the spread of soil-borne diseases. The relationships between SWC and ECa increments for different signals after rainfall confirmed the better drainage conditions in zone A. Correlations between ECa and soil properties were significant but small, possibly as a result of the large differences in explored soil volumes by both measurements and the non-uniform contribution of the different soil layers to the ECa signal. However the relationships found between ECa and soil properties under different SWCs were useful for assessing soil–olive tree development interactions in this heavy clay soil. In addition, the potential of time-lapse ECa maps, corresponding to the different signals, was explored by analyzing the relationship between ECa and SWC increments across the catchment. Time-lapse ECa mapping constitutes a promising avenue for further analysis of the soil water dynamics across this olive-cultivated catchment, and assessment of its relationship with olive tree development, using measurements corresponding to different SWC situations.

Acknowledgments Funding for this work came from the Spanish Ministry of Economy and Competitiveness and FEDER (Grants AGL2009-12936-C03-03, AGL2009-12936-C03-01 and AGL2012-40128-C03-03), and from the Junta de Andalucía (AGR-4782). Also support through PhD grant n° 8 (Res. 15/04/10) by IFAPA is acknowledged. Special thanks to M. Morón, J. García, M.A. Ayala, A. Jardúo and E. Rodríguez of IFAPA Centro Las Torres-Tomejil for their assistance with the field and laboratory work and to Tom Van walleghem for revising this manuscript thoroughly. We are also very grateful to Francisco Natera, the owner of the "La Conchuela" farm, and the staff for their continuous support.

References

Abdu H, Robinson DA, Seyfried M, Jones SB (2008) Geophysical imaging of watershed subsurface patterns and prediction of soil texture and water holding capacity. WaterResour Res 44: W00D18. doi: 10.1029/2008WR007043

Atwell MM, Wuddivira M, Gobin J, Robinson DA (2013) Edaphic controls on sedge invasion in a tropical wetland assessed with electromagnetic induction. Soil SciSoc Am J 77:1865–1874

Calderón R, Navas-Cortés JA, Lucena C, Zarco-Tejada PJ (2013) High-resolution airborne hyperspectral and thermal imagery for early detection of Verticillium wilt of olive using fluorescence, temperature and narrow-band spectral indices. Remote Sens Environ 139:231–245

Callegary J, Ferré TPA, Groom R (2007) Vertical spatial sensitivity and exploration depth of low-induction-number electromagnetic-induction instruments. Vadose Zone J 6:158–167

Callegary J, Ferré TPA, Groom R (2012) Three-dimensional sensitivity distribution and sample volume of low-induction-number electromagnetic-induction instruments. Soil Sci Soc Am J 76:85–91

CAP (2012) Estudios y estadísticas de superficies y producciones agrarias. Available at: http://www.juntadeandalucia.es/agriculturaypesca/portal/servicios/estadisticas/estadisticas/agrarias/superficies-y-producciones.html Accessed 12February 2014

Clodoveo ML, Camposeo S, De Gennaro B, Pascuzzi S, Roselli L (2014) In the ancient world virgin olive oil has been called "liquid gold" by Homer and the "great healer" by Hippocrates. Why is this mythic image forgotten? Food Res Int (Accepted manuscript)

Corwin DL, Lesch SM (2003) Application of soil electrical conductivity to precision agriculture: theory, principle and guidelines. Agron J 95:455–471

Corwin DL, Plant RE (2005) Applications of apparent soil electrical conductivity in precision agriculture. Comput Electron Agric 46:1–10

de Backer G, Bagnara S, Crepaldi G, Fernandez-Cruz A, Godtfredsen J, Jacotot B, Paoletti R, Renaud S, Ricci G, Rocha E, Trautwein E, Urbinati GC, Varela G, Williams C (1997) International consensus statement on olive oil and the Mediterranean diet: implications for health in Europe. Eur J Cancer Prev 6:418–421

Doolittle JA, Brevik EC (2014) The use of electromagnetic induction techniques in soil studies. Geoderma 223–225:33–45

European Commision. (2012) EU agriculture - Statistical and economic information – 2012. Available at: http://ec.europa.eu/agriculture/statistics/agricultural/2012/index_en.htm Accessed 12 February 2014

FAOSTAT (2012) Agricultural statistics. http://faostat.fao.org Accessed 3 November 2014

Friedman SP (2005) Soil properties influencing apparent electrical conductivity: a review. Comput Electron Agric 46:45–70

Gómez JA, Sobrinho TA, Giráldez JV, Fereres E (2009) Soil management effects on runoff, erosion and soil properties in an olive grove of southern Spain. Soil Tillage Res 102:5–13

Harvey OR, Morgan CL (2009) Predicting regional-scale soil variability using a single calibrated apparent soil electrical conductivity model. Soil Sc Soc Am J 73:164–169

Johnson CK, Mortensen DA, Wienhold BJ, Shanahan JF, Doran JW (2003) Site-specific management zones based on soil electrical conductivity in a semiarid cropping system. Agron J 95:303–315

Jung WK, Kitchen NR, Sudduth KA, Kremer RJ, Motavalli PP (2005) Relationship of apparent soil electrical conductivity to claypan soil properties. Soil Sci Soc Am J 69:883–892

Keller GV, Frischknecht FC (1966) Electrical methods in geophysical prospecting. Pergamon Press, New York

Kitchen NR, Sudduth KA, Myers DB, Drummond ST, Hong SY (2005) Delineating productivity zones on claypan soil fields using apparent soil electrical conductivity. Comput Electron Agric 46:285–308

López-Escudero FJ, Mercado-Blanco J (2011) Verticillium wilt of olive: a case study to implement an integrated strategy to control a soil-borne pathogen. Plant Soil 344:1–50

Loumou A, Giourga C (2003) Olive groves: 'The life and identity of the Mediterranean'. Agric Human Values 20:87–95

MAGRAMA(2012) Encuesta sobre superficies y rendimientos de cultivos. 2012. Available at: http://www.magrama.gob.es/es/estadistica/temas/novedades/Olivar2012_tcm7-262578.pdf Accessed 12 February 2014

Martínez G, Vanderlinden K, Espejo AJ, Giráldez JV, Muriel JL (2010) Field-scale soil moisture pattern mapping using electromagnetic induction. Vadose Zone J 9:871–881

Martínez G, Vanderlinden K, Pachepsky Y, Espejo AJ, Giráldez JV (2012) Estimating topsoil water content of clay soils with data from time-lapse electrical conductivity surveys. Soil Sci 177:369–376

McCutccheon MC, Farahani HJ, Stednick JD, Buchleiter GW, Green TR (2006) Effect of soil water on apparent soil electrical conductivity and texture relationships in a dryland field. Biosyst Eng. doi: 10.1016/j.biosystemseng.2006.01.002

McNeill JD (1980) Electromagnetic terrain conductivity measurement at low induction numbers. Technical Note TN-6.Geonics Limited, Missisauga

Minasny B, Whelan BM, Triantafilis J, McBratney AB (2013) Pedometrics research in the vadose zone – review and perspectives. Vadose Zone J. doi: 10.2136/vzj2012.0141

Mualem Y, Friedman SP (1991) Theoretical prediction of electrical conductivity in saturated and unsaturated soil. Water Resour Res 27:2771–2777

Navas-Cortés JA, Landa BB, Mercado-Blanco J, Trapero-Casas JL, Rodríguez-Jurado D, Jiménez-Díaz RM (2008) Spatiotemporal analysis of spread of infections by Verticillium dahliae pathotypes within a high tree density olive orchard in southern Spain. Phytopathology 98:167–180

Nobel PS, Miller PM, Graham EA (1992) Influence of rocks on soil temperature, soil water potential, and rooting patterns for desert succulents. Oecologia 92:90–96

Palomo MJ, Moreno F, Fernández JE, Dıaz-Espejo A, Girón IF (2002) Determining water consumption in olive orchards using the water balance approach. Agr Water Manage 55:15–35

Rhoades JD, Corwin DL (1981) Determining soil electrical conductivity-depth relations using an inductive electromagnetic soil conductivity meter. Soil Sci Soc Am J 45:255–260

Rhoades JD, Raats PAC, Prather RJ (1976) Effects of liquid-phase electrical conductivity, water content, and surface conductivity on bulk soil electrical conductivity. Soil Sci Soc Am J 40:651–655

Robinson DA, Abdu H, Jones SB, Seyfried M, Lebron I, Knight R (2008) Ecogeophysical imaging of watershed-scale soil patterns links with plant community spatial patterns. Vadose Zone J 7:1132–1138

Robinson DA, Lebron I, Quejereta JI (2010) Determining soil-tree-grass relationships in a California oak savanna using eco-geophysics. Vadose Zone J 9:528–536

Robinson DA, Abdu H, Lebron I, Scott J (2012) Imaging of hillslope soil moisture wetting patterns in a semi-arid oak savanna catchment using time-lapse electromagnetic induction. J Hydrol 416–417:39–49

Rodriguez-Perez JR, Plant RE, Lambert JJ, Smart DR (2011) Using apparent soil electrical conductivity (ECa) to characterize vineyard soils of high clay content. Precis Agric 12:775–794

Saey T, Simpson D, Vitharana UW, Vermeersch H, Vermang J, Van Meirvenne M (2008) Reconstructing the paleotopography beneath the loess cover with the aid of an electromagnetic induction sensor. Catena 74:58–64

Saey T, Simpson D, Vermeersch H, Cockx L, Van Meirvenne M (2009) Comparing the EM38DD and DUALEM-21S sensors for depth-to-clay mapping. Soil Sci Soc Am J 73:7–12

Sánchez-Hernández ME, Ruiz-Dávila A, Pérez de Algaba A, Blanco-López MA, Trapero-Casas A (1998) Occurrence and etiology of death of young olive trees in southern Spain. Eur J Plant Pathol 104:347–357

Sauer TJ, Logsdon SD (2002) Hydraulic and physical properties of stony soils in a small watershed. Soil Sci Soc Am J 66: 1947–1956

Semple EC (1931) The geography of the Mediterranean region: Its relation to ancient history. AMS Press, New York

Sherlock M, McDonnell JJ (2003) A new tool for hillslope hydrologists: spatially distributed measurements of groundwater and soil water using electromagnetic induction. Hydrol Proc 17:1965–1978

Soil Survey Staff (1993) Soil Survey Manual. Soil Conservation Service. USDA Ag. Hbk. 18, Washington

Soil Survey Staff (1999) Soil taxonomy: A basic system of soil classification for making and interpreting soil surveys. 2nd ed. NRCS USDA Hbk 436

Testi L, Villalobos FJ, Orgaz F, Fereres E (2006) Water requirements of olive orchards: I simulation of daily evapotranspiration for scenario analysis. Irrigation Sci 24:69–76

Triantafilis J, Lesch SM (2005) Mapping clay content variation using electromagnetic induction techniques. Comput Electron Agric 46:203–237

Vitharana UWA, Van Meirvenne M, Cockx L, Bourgeois J (2006) Identifying potential management zones in a layered soil using several sources of ancillary information. Soil Use Manage 22:405–413

Vitharana U, Van Meirvenne M, Simpson D, Cockx L, De Baerdemaeker J (2008) Key soil and topographic properties to delineate potential management classes for precision agriculture in the European loess area. Geoderma 143:206–215

Whelan BM, McBratney AB, Minasny B (2002) Vesper 1.5 – spatial prediction software for precision agriculture. In: Robert PC, Rust RH, Larson WE (eds) Precision Agriculture, Proceedings of the 6th International Conference on Precision Agriculture. ASA/CSSA/SSSA, Madison

A. Pedrera-Parrilla

PhD Student en IFAPA

aura.pedrera@hotmail.com

Extracto

Research Interests:
Agriculture; Soil; Water; Soil Physics; Hydrology; Soil and Water Conservation; Spatial Variability of Soil Properties; Precision Agriculture; Near Surface Geophysics; Electromagnetic Induction (EMI); Electrical Conductivity; Geostatistics;

Experiencia

Estudiante de doctorado (PhD Student) at IFAPA
noviembre de 2010 - Actualidad (4 años)

PhD Stay (Department of Soil Management) at Ghent University
junio de 2014 - junio de 2014 (1 mes)

PhD Stay (Department of Soil Management) at Ghent University
agosto de 2011 - septiembre de 2011 (2 meses)

Prácticas tutoradas por PhD A. De Haro at Instituto Agricultura Sostenible (CSIC)
julio de 2007 - septiembre de 2007 (3 meses)

Proyectos

Evaluación y mejora del manejo de conservación en fincas de olivar intensivo o usando herramientas hidrogeofísicas y modelos ecohidrológicos probabilísticos.
2012 a Actualidad
Miembros:A. Pedrera-Parrilla, G.Martínez, I. Llanos, K. Vanderlinden, V. H. Durán, J. L. Muriel, A. Pedrera-León

Investigador principal: K. Vanderlinden
AGL2012-40128-C03-03

Publicaciones

Mapping impaired olive tree development using electromagnetic inductionsurveys
Plant and Soil, Springer julio de 2014
Autores: A. Pedrera-Parrilla, G. Martínez, A. J. Espejo, J. A. Gómez, J. V. Giráldez, K. Vanderlinden

DOI 10.1007/s11104-014-2207-5

Assessing soil moisture dynamics to characterize hydrological patterns in an olive tree planted catchment
Florisa Melone Book Conference 2014
Autores: A. J. Espejo, J. V. Giráldez, K. Vanderlinden, L. Brocca, A. Pedrera-Parrilla, G. Martínez

Use of electromagnetic induction surveys to delimit zones of contrasting tree development in an irrigated olive orchard in Southern Spain
Geophysical Research Abstracts Vol. 16, EGU2014-952, 2014 mayo de 2014
Autores: A. Pedrera-Parrilla, K. Vanderlinden, A. J. Espejo, J. A. Gómez, J. V. Giráldez

Influence of Soil Management on Water Retention from Saturation to Oven Dryness and Dominant Soil Water States in a Vertisol under Crop Rotation
Geophysical Research Abstracts Vol. 16, EGU2014-3684, 2014 mayo de 2014
Autores: K. Vanderlinden, Y. Pachepsky, A. Pedrera-Parrilla, G. Martínez, A. J. Espejo, J. V. Giráldez

Detection of subsurface runoff flow with soil water sensor network in an experimental catchment
Geophysical Research Abstracts Vol. 16, EGU2014-4966, 2014 mayo de 2014
Autores: A. Espejo, J. V. Giráldez, K. Vanderlinden, A. Pedrera-Parrilla, G. Martínez

A method for estimating soil water diffusivity from moisture profiles and its applications across an experimental catchment
Journal of Hydrology, Elsevier 14 de febrero de 2014
Autores: A. J. Espejo, J. V. Giráldez, K. Vanderlinden, E. V. Taguas, A. Pedrera-Parrilla
DOI: 10.1016/j.jhydrol.2014.01.072

Seminario "Usos de un sensor de inducción electromagnética en estudios de conservación de suelo y agua en olivar"
Máster de Hidráulica Ambiental, con Mención de Calidad MCD2006-00361, en el curso 2012-2013. junio de 2013
Autores: A. Pedrera-Parrilla

Effectiveness of apparent electrical conductivity surveys at varying soil water contents for assessing soil and water dynamics across a rainfed mountain olive orchard in SW Spain
Geophysical Research Abstracts Vol. 15, EGU2013-1008-2, 2013 abril de 2013
Autores: A. Pedrera-Parrilla, E. Van De Vijver, K. Vanderlinden, S. Martos, M. Van Meirvenne, A. J. Espejo, E. V. Taguas, J. V. Giráldez

Below-canopy versus inter-row soil water content dynamics across a rainfed olive orchard in SW Spain
Geophysical Research Abstracts Vol. 15, EGU2013-700, 2013 abril de 2013
Autores: A. J. Espejo, K. Vanderlinden, J. V. Giráldez, A. Pedrera-Parrilla, E. V. Taguas

Soil Organic Carbon distribution in three contrasting olive orchards in Southern Spain
Geophysical Research Abstracts Vol. 15, EGU2013-6392, 2013 abril de 2013
Autores: E. V. Taguas, María Burguet, G. Guzmán, A. Pedrera-Parrilla, K. Vanderlinden, T. Vanwalleghem, R. Pérez, J. L. Ayuso, J. A. Gómez

Simulation of Soil Water Content Variability in a Heavy Clay Soil under Contrasting Soil Managements

Geophysical Research Abstracts Vol. 14, EGU2012-8363, 2012 2012
Autores: A. Pedrera-Parrilla, K. Vanderlinden, G. Martínez, A. J. Espejo, J. V. Giráldez

Effect of Soil Management and Topography On the Spatial and Temporal Organization of Soil Moisture.
ASA-CSSA-SSSA International Annual Meetings octubre de 2011
Autores: K. Vanderlinden, A. Pedrera-Parrilla, A.J. Espejo, J.V. Giráldez

Efecto del manejo del suelo sobre la variabilidad espacial y temporal de la humedad del suelo a escala de parcela
X Jornadas de Investigación de la Zona No Saturada del suelo, Salamanca (España), 2011 I.S.B.N.: 978-84-694-6642-1 octubre de 2011
Autores: A. Pedrera-Parrilla, K. Vanderlinden, A. J. Espejo, J. V. Giráldez, J. L. Muriel

Influence of soil management on soil moisture variability. Implications for field monitoring.
Universidad Internacional de Andalucía - Optimizing and Integrating Predictions of Agricultural Soil and Water Conservation Models at Different Scales. septiembre de 2010
Autores: A. Pedrera-Parrilla, K. Vanderlinden, J. V. Giráldez, A. J. Espejo

Spatial and temporal organization of soil moisture at the #eld scale as affected by soil management
Geophysical Research Abstracts Vol. 12, EGU2010-8823, 2010 mayo de 2010
Autores: A. Pedrera-Parrilla, K. Vanderlinden, J. V. Giráldez, A. J. Espejo

SOIL WATER MODELLING IN A RAINFED OLIVE ORCHARD CATCHMENT OF SPAIN TO IDENTIFY SPATIAL AND TEMPORAL HYDROLOGICAL PATTERNS
Florisa Melone Memorial Conference octubre de 2013
Autores: A. J. Espejo, L. Brocca, T. Moramarco, K. Vanderlinden, A. Pedrera-Parrilla, J. V. Giráldez

MÉTODOS PARA EVALUAR LA HUMEDAD DEL SUELO A ESCALA DE PARCELA Y CUENCA
VI Simposio del agua en Andalucía 2012
Autores: A. J. Espejo, A. Pedrera-Parrilla, G. Martínez, J. V. Giráldez, K. Vanderlinden, K. L. Prados, C. Guardiola

López-Geta, J.R., Ramos, G., Fernández-Rubio, R. y Lorca-Fernández, D. (Ed.). Publicaciones del IGME, serie Hidrológica y aguas subterráneas, 30, 2: 1287-1296.

Spatial and temporal distribution of ground cover and its relationship with SOC distribution and soil loss in two olive grove catchments with contrasting soils
2nd Global Land Project Open Meeting 21 de marzo de 2014
Autores: E. V. Taguas, K. Vanderlinden, A. Pedrera-Parrilla, M. Burguet, T. Vanwalleghem, G: Guzmán

Non-local Controls on Spatial and Temporal Variability of Soil Water Content in Heavy Clay Soils
American Geophysical Union, Fall Meeting 2011, abstract #H31M-02 9 de diciembre de 2011
Autores: K. Vanderlinden, A. Pedrera-Parrilla, G. Martínez, A. J. Espejo, J. V. Giráldez, Y. A. Pachepsky

Soil water diffusivity estimation from distributed water content observations across a rainfed olive orchard
AGU CHAPMAN Conference. Biosphere II, Tucson, Arizona, USA octubre de 2013

Autores: A. J. Espejo, J. V. Giráldez, K. Vanderlinden, A. Pedrera-Parrilla, G. Martínez

Estimating soil water diffusivity across a rainfed olive orchard using measurements from a sensor network
XI Jornadas de Investigación de la Zona No Saturada del suelo, Lugo (España), 2013 ISBN: 978-84-616-6234-0 noviembre de 2013
Autores: A. J. Espejo, J. V. Giráldez, K. Vanderlinden, A. Pedrera-Parrilla, G. Martínez, M. Morón, E. V. Taguas

Educación

Universidad de Granada y Universidad de Córdoba
Master of Science (MSc), Hidráulica Ambiental (Environmental Hydraulics), 2010 - 2011

Universidad de Córdoba
Ingeniera Agrónoma (Agronomical Engeneering), 2003 - 2009

Ghent University
Beca ERASMUS (ERASMUS Grant), 2006 - 2007

Certificaciones

Certificado de Aptitud Pedagógica (CAP)
Universidad de Córdoba 2009

Cursos

Beca ERASMUS (ERASMUS Grant)
Ghent University

Francés A2	2007
Inglés B2	2007
Neerlandés para extranjeros	2006

Ingeniera Agrónoma (Agronomical Engeneering)
Universidad de Córdoba

Certificado de Aptitud Pedagógica (UCO)	año 2009, 180 horas

Estudiante de doctorado (PhD Student)
IFAPA

Formación de técnicos especialistas. La investigación en el IFAPA	año 2012, 30 horas
La comunicación en la transferencia de tecnología	año 2013
Técnicas de análisis estadístico de datos	año 2013
Alemán B1	año 2012, 80 horas
1st MAC International Workshop of Archaelogical Geophysics	Ullastret, 21-25 May 2012

Cursos independientes

Programación y unidades didácticas: Diseño y elaboración (USTEA)	año 2010, 100 horas
La violencia entre iguales y la mediación escolar (USTEA)	año 2010, 40 horas

Idiomas

Español	(Competencia bilingüe o nativa)
Inglés (B2)	
Francés (A2)	
Alemán (B1)	
Neerlandés	(Competencia básica)

Aptitudes y conocimientos

Microsoft Office
Matlab
Grapher
Surfer
ArcGIS
Vesper
SPSS
Statistix
AutoCAD

Experiencia de voluntariado

Socia en Oxfam Intermón
2003 - Actualidad (11 años)